Titre: Title:	A Numerical Predictive Tool for Long-term Properties of Thermoplastics under Complex Operating Conditions
Auteur: Author:	Lingyu Yue
Date:	2022
Type:	Mémoire ou thèse / Dissertation or Thesis
Référence: Citation:	Yue, L. (2022). A Numerical Predictive Tool for Long-term Properties of Thermoplastics under Complex Operating Conditions [Ph.D. thesis, Polytechnique Montréal]. PolyPublie. https://publications.polymtl.ca/10258/

POLYTECHNIQUE MONTRÉAL
affiliée à l'Université de Montréal

A numerical predictive tool for the long-term properties of thermoplastics under complex operating conditions

LINGYU YUE
Département de génie mécanique

Thèse présentée en vue de l'obtention du diplôme de *Philosophiæ Doctor*
Génie mécanique

Mars 2022

POLYTECHNIQUE MONTRÉAL
affiliée à l'Université de Montréal

Cette thèse intitulée :

A numerical predictive tool for the long-term properties of thermoplastics under complex operating conditions

présentée par **Lingyu YUE**
en vue de l'obtention du diplôme de *Philosophiæ Doctor*
a été dûment acceptée par le jury d'examen constitué de :

Delphine PÉRIÉ-CURNIER, présidente
Martin LÉVESQUE, membre et directeur de recherche
Marie-Claude HEUZEY, membre et codirectrice de recherche
Jonathan JALBERT, membre et codirecteur de recherche
Hongbing LU, membre
Alexander LION, membre externe

DEDICATION

To my parents.

ACKNOWLEDGEMENTS

I would like to thank Prof. Martin Lévesque, Prof. Marie-Claude Heuzey and Prof. Jonathan Jalbert for their guidance throughout this project. Your confidence allowed me to complete this thesis on multidisciplinary intersections, including viscoelasticity, polymers, composites and Bayesian statistics. Your advice and constructive criticism have led to my scientific maturity. Also, I am very grateful for your encouragement during some tough times for me.

I owe special gratitude to the members of Laboratory for Multiscale Mechanics (LM2) research group. I would like to particularly thank Ilyass Tabiai, Anton Trofimov, Mohamadreza Moeini, Shibo Zou, Rui Tao, Vladislav Sushitskii, Pierre Faucheux, Simon Breumier, Patrick Diehl for their contributions and the fruitful discussions all along this project. I also thank the members of the rheology group for their weekly presentations and discussions, which prompted me to revisit this project from a different point of view. The technical support from Isabelle Nowlan, Kambiz Chirazi, Benedict Benser and Fabrice Danet from Department of Mechanical Engineering and Anic Desforges from Department of Chemical Engineering is also grateful acknowledged.

I would like to thank Qingkai Meng, from Lavergne Groupe Inc, for providing polycarbonate and poly(ethylene terephthalate) pellets.

I would like to acknowledge the contributions of the National Science and Engineering Research Council of Canada (NSERC) and the Fonds de Recherche du Québec Nature et Technologies (FRQNT). Their financial support through scholarships made this project possible.

I would like to express my gratitude to my parents for providing an unconditional support. All of this would not have been possible without you. Finally, but certainly not least, I would also like to thank the one who has accompanied me with her patience and support through the years, my beloved Xiao.

RÉSUMÉ

Avec l'utilisation croissante des composites thermoplastiques dans l'ingénierie, il est devenu essentiel d'étudier les performances des matériaux dans diverses conditions de fonctionnement complexes. La température et le vieillissement physique affectent considérablement les propriétés mécaniques des thermoplastiques. Par conséquent, pour améliorer la précision de prédiction de la simulation numérique de composants soumis à des conditions de service réelles, la caractérisation des propriétés tridimensionnelles des thermoplastiques impliquant la température et le vieillissement physique est nécessaire mais a rarement été abordée.

L'estimation des paramètres du modèle de la série de Prony, la loi du comportement viscoélastique thermodynamique la plus utilisée en ingénierie, à partir de données expérimentales est un problème mal posé. Cela signifie que les paramètres identifiés ne sont pas garantis d'être uniques et que les erreurs expérimentales affectent les résultats de l'identification. Pour résoudre ce problème, le nombre de paramètres est généralement fixé arbitrairement, ce qui peut conduire à un déséquilibre entre la précision de la prédiction et le temps de calcul des structures.

Cette thèse propose une méthode robuste et automatisée d'identification des paramètres tridimensionnels pour les thermoplastiques impliquant l'effet de la température et du vieillissement physique. La robustesse signifie que la méthode doit être capable de gérer différents niveaux d'erreurs de mesure; l'automatisation signifie que la méthode ne doit pas nécessiter d'entrée utilisateur pour chaque ensemble de données. Cette méthode pourrait être utilisée comme un outil numérique prédictif pour guider les chercheurs et les ingénieurs à développer efficacement de nouveaux matériaux thermoplastiques pour des composants soumis à des conditions de service complexes.

Tout d'abord, une méthode basée sur un cadre bayésien a été proposée pour déterminer les paramètres viscoélastiques tridimensionnels des thermoplastiques à température ambiante. Cette méthode permet de calculer la distribution des paramètres du modèle à partir des données expérimentales. Dans le cadre du paradigme bayésien, la distribution *a posteriori* peut être calculée en multipliant la fonction de vraisemblance et la fonction antérieure des paramètres. La fonction de vraisemblance a été construite sur la base de l'hypothèse selon laquelle l'erreur expérimentale est distribuée indépendamment de manière gaussienne. La loi a priori des paramètres a été imposée pour éviter les problèmes d'identifiabilité. La loi a posteriori a été estimée par simulation de Monte Carlo à chaîne de Markov (MCMC), ce qui a permis de surmonter le caractère mal posé du problème d'identification pour le modèle

de série de Prony. Le résultat de l'identification était l'estimation du maximum a posteriori (MAP) de la distribution a posteriori des paramètres. Le nombre optimal de paramètres a été déterminé en fonction du critère d'information bayésien (BIC). La méthode a d'abord été appliquée à des données artificielles, montrant que les paramètres peuvent être identifiés avec succès à partir de données présentant différents niveaux d'erreur ajoutée. Ensuite, la méthode a été appliquée à des données expérimentales sur deux thermoplastiques, le polypropylène et le polyméthacrylate de méthyle. Les paramètres ont été identifiés à partir des données d'essais mécaniques sur des spécimens de type-I de la norme ASTM et validés expérimentalement en comparant les mesures de corrélation d'images numériques (DIC) et les simulations de la méthode des éléments finis (FEM) avec les paramètres identifiés pour des spécimens à géométrie complexe. Les résultats ont démontré la robustesse et l'adéquation de la méthode proposée appliquée aux thermoplastiques à température ambiante.

Ensuite, une campagne d'essais de vieillissement physique non isotherme sur du polycarbonate a été réalisée pour caractériser l'effet de la température et du vieillissement physique sur les propriétés mécaniques. Les spécimens ont été fabriqués en moulage par injection. Les essais séquentiels de fluage-récupération ont été réalisés à différentes températures selon la méthodologie classique de Struik. Les essais mécaniques ont été réalisés avec un cadre d'essai de traction équipé d'une chambre environnementale à température ambiante (20 °C), 40 °C, 60 °C, 80 °C, 100 °C and 120 °C. Les déformations axiales et transversales ont été mesurées avec un extensomètre bi-axial. Il a été constaté que la température et le couteau de l'extensomètre peuvent provoquer des dérives de mesure dans l'essai sur des thermoplastiques à des températures élevées. Ainsi, une procédure robuste, simple et facile à suivre a été proposée pour corriger les dérives des mesures de l'extensomètre dans cette étape. Les résultats expérimentaux ont montré leur reproductibilité et leur fiabilité.

Enfin, la méthode bayésienne proposée a été étendue pour identifier simultanément les paramètres du modèle tridimensionnel liés à la viscoélasticité, à la température et au vieillissement physique. Le principe de superposition temps-température (TTS) a été utilisé pour décrire les effets de la température et du vieillissement physique sur les propriétés mécaniques par des facteurs de glissement. Les paramètres viscoélastiques et les facteurs de glissement ont pu être identifiés simultanément à partir des données expérimentales avec la méthode étendue. Le modèle KAHR-t_e a ensuite été utilisé pour évaluer les facteurs de glissement pour les essais de vieillissement non isotherme à différentes températures. Cette méthode étendue a été appliquée aux données expérimentales pour le polycarbonate. Les résultats expérimentaux corroboraient les prédictions effectuées avec les paramètres déterminés.

Cette thèse propose un outil numérique pour prédire les propriétés mécaniques tridimen-

sionnelles à long terme des thermoplastiques impliquant la température et le vieillissement physique. Il pourrait être utilisé pour caractériser et développer des matériaux thermoplastiques dans des conditions de service complexes de manière efficace et précise.

ABSTRACT

With the increasing use of thermoplastic composites in engineering, like aerospace, it has become critical to investigate the performance of materials under various complex operating conditions. Temperature and physical aging significantly affect the mechanical properties of thermoplastics. Therefore, to improve the prediction accuracy of the numerical simulation of components subjected to real service conditions, characterizing the three-dimensional properties of thermoplastics involving temperature and physical aging is required but has rarely been addressed.

Estimating parameters of the Prony series model, the most used thermodynamically based viscoelastic constitutive model in engineering, from experimental data is an ill-posed problem, which means that the identified parameters are not guaranteed to be unique and the experimental errors affect the identification results. To address this issue, the number of parameters is usually required to be fixed artificially, which may lead to an imbalance between the prediction accuracy and the computational cost in the simulation of the response of viscoelastic structures.

This thesis aimed at proposing a robust and automated method to identify the three-dimensional parameters for thermoplastics involving the effect of temperature and physical aging. Robustness means that the method should be able to handle different levels of measurement errors; Automation means that the method should not need user input for each data set. This method could be used as a predictive numerical tool to assist researchers and engineers in efficiently developing novel thermoplastic materials for components subjected to complex service conditions.

First, a Bayesian framework based method was proposed for determining the three-dimensional viscoelastic parameters of thermoplastics at room temperature. This method aimed to compute the posterior distribution of the model parameters from experimental data. Under the Bayesian paradigm, the posterior distribution can be computed by multiplying the likelihood and prior function of parameters. The likelihood function was constructed based on the assumption that the experimental error is independently Gaussian distributed. The prior function was imposed to avoid identifiability issues. The posterior function was estimated by Markov chain Monte Carlo (MCMC) simulation, which could overcome the ill-posedness of the identification problem for Prony series model. The identification result was the maximum a posteriori (MAP) estimate of the posterior distribution of the parameter. The optimal number of parameters was determined according to the Bayesian Information

Criterion (BIC). The method was initially applied to artificial data, showing that the parameters can be successfully identified from data with different levels of added error. Then, the method was applied to experimental data on two thermoplastics, polypropylene and polymethyl methacrylate. Parameters were identified from mechanical test data on ASTM standard type-I specimens and experimentally validated by comparing Digital Image Correlation (DIC) measurements and Finite Element Method (FEM) simulations with the identified parameters for complex geometry specimens. The results demonstrated the robustness and adequacy of the proposed method applied to thermoplastics at room temperature.

Then, a non-isothermal physical aging test campaign on polycarbonate was carried out to characterize the effect of temperature and physical aging on mechanical properties. The specimens were manufactured by injection molding. The sequential creep-recovery tests were performed at various temperatures based on the classical Struik's methodology. The mechanical tests were performed with a tensile testing frame equipped with an environmental chamber at room temperature (20 °C), 40 °C, 60 °C, 80 °C, 100 °C and 120 °C. The axial and transverse strains were measured with a bi-axial extensometer. It was found that the temperature and knife edge of the extensometer can cause measurement drifts in the test of thermoplastics at elevated temperatures. Thus, a robust, straightforward and easy-to-follow procedure was proposed to correct drifts of extensometer measurements in this step. The experimental results showed reproducibility and reliability.

Finally, the proposed Bayesian method was extended to simultaneously identify the viscoelastic, temperature and physical aging related three-dimensional model parameters. The time-temperature superposition (TTS) principle was used to describe the effects of temperature and physical aging on mechanical properties by shift factors. The viscoelastic parameters and shift factors could be simultaneously identified from experimental data with the extended method. The KAHR-t_e model was then used to evaluate the shift factors for non-isothermal aging tests at different temperatures. This extended method was applied to the experimental data on polycarbonate. The experimental results were in good agreement with the predictions of the determined parameters.

This thesis proposes a numerical tool to predict the long-term three-dimensional mechanical properties of thermoplastics involving temperature and physical aging. It could be used to characterize and develop thermoplastic materials under complex operating conditions efficiently and accurately.

TABLE OF CONTENTS

LIST OF TABLES

LIST OF FIGURES

LIST OF SYMBOLS AND ACRONYMS

Latin symbols

a	Horizontal shift factor
a_T	Temperature shift factor
a_{t_e}	Psychical aging shift factor
a_v	Vertical shift factor
a_δ	Structural shift factor
$\mathbf{C}$	Stiffness tensor
f	Probability density function
$\mathcal{J}$	Objective function
M	Number of series
$\mathbf{S}$	Compliance tensor
T	Temperature
t_e	Physical aging time
$\mathbf{x}$	Applied excitation
$\mathbf{y}$	Experimental measurement

Greek symbols

$\boldsymbol{\varepsilon}$	Strain tensor
ε^{I}	Axial strain
$\varepsilon^{\mathrm{II}}$	Transverse strain
$\varepsilon^{\dagger} = \varepsilon^{\mathrm{I}} - \varepsilon^{\mathrm{II}}$	Shear related strain
$\varepsilon^{\ddagger} = \varepsilon^{\mathrm{I}} + 2\varepsilon^{\mathrm{II}}$	Bulk related strain
ϵ	Experimental error
κ	Bulk stiffness
$\tilde{\kappa}$	Bulk compliance
λ	Reciprocal retardation times
μ	Shear stiffness
$\tilde{\mu}$	Shear compliance
Ψ	Helmholtz's free energy
$\boldsymbol{\sigma}$	Stress tensor
σ_ϵ	Variance of experimental error

$\boldsymbol{\theta}$	Model parameter
$\boldsymbol{\Theta}$	Parameters space
ω	Reciprocal relaxation times
$\boldsymbol{\chi}$	Internal variable of material

Abbreviations

1D	One-dimension
3D	Three-dimension
AIC	Akaike Information Criterion
BIC	Bayesian Information Criterion
CTE	Coefficient of thermal expansion
DIC	Digital Image Correlation
FE	Finite element
KAHR model	Kovacs-Aklonis-Hutchinson-Ramos model
MAP	Maximum a posteriori
MCMC	Markov Chain Monte Carlo
NI	National Instruments
PC	Polycarbonate
PMMA	Polymethyl methacrylate
PP	Polypropylene
SA	Simulated annealing
TTS	Time-temperature superposition
WLF model	Williams-Landel-Ferry model

CHAPTER 1 INTRODUCTION

Advanced composites are used in the aerospace industry due to their high strength to weight ratio, as well as their fatigue and corrosion resistance. For example, composites account for 50% of Boeing 787 and Airbus A350 structural mass. Thermoset composites, especially those relying on epoxy, are the mostly used composites. However, high raw material and fabrication costs, restricted storage life, and lack of recyclability are major concerns that force aircraft manufacturer to look for alternatives. Thermoplastic composites have lower constituents costs, rapid and reversible processing, and longer shelf life without refrigeration. Nonetheless, the processing of thermoplastic composites requires high temperature and pressure, which is their most important shortcoming.

Thermoplastics exhibit complex properties due to their intricate microstructure, especially when temperature and physical aging are involved. Thermoplastics are generally viscoelastic, meaning that their response to mechanical loading is time-dependent. Temperature increases the compliance and flexibility of polymers, while physical aging rigidifies and embrittles these materials over time. At elevated temperatures, these effects can occur concurrently and interact.

Therefore, investigating the mechanical properties of thermoplastics under various complex working conditions is one of the essential steps in developing thermoplastic composites. The majority of existing research has been concentrated on uni-dimensional mechanical properties of thermoplastics, assuming that the bulk behavior or Poisson's ratio remain constant throughout the test. This assumption, however, could be violated when investigating the long-term behavior of materials or involving the effect of temperature and physical aging. Therefore, to improve the predictions capabilities in demanding applications for components submitted to actual service conditions, characterizing the long-term three-dimensional properties of thermoplastics is critical but rarely addressed.

The Prony series model is one of the most frequently used thermodynamically based viscoelastic constitutive models. Estimating parameters from experimental data for this model is an ill-posed problem, which means that the results cannot be guaranteed uniquely and that minor errors in the data can result in significant variations. Considering that the computational time involved in the simulation of the response of a viscoelastic material is proportional to the number of viscoelastic parameters, it would be of considerable interest to develop identification strategies that yield a minimum number of parameters.

This thesis aims at developing a numerical tool to predict the long-term mechanical behavior

of thermoplastics under complex operating conditions. The main objectives are: (1) to propose a robust and automated method for identifying the three-dimensional viscoelastic parameters from experimental data on thermoplastic specimens at room temperature and determining the optimal number of parameters, (2) to generate experimental data for non-isothermal physical aging tests of a thermoplastic at elevated temperatures and (3) to extend the proposed method by combining temperature and physical aging effects.

This thesis is organized as follows. Chapter 2 presents a literature survey on viscoelastic constitutive models, parameters identification methods and Bayesian theorem. The specific objectives associated with the main objective are detailed in Chapter 3. The scientific approach to fulfill the specific objectives is presented in Chapter 4. The three articles resulting from this work are presented in Chapters 5 to 7. Chapter 8 discusses the relationships between the articles. Finally, Chapter 9 concludes this work and recommends several topics for future work.

CHAPTER 2 LITERATURE AND REVIEW

Notations

In this thesis, unless otherwise specified, scalars and vectors are respectively denoted by normal letters (e.g., a, T) and boldfaced lower case Latin letters (e.g., $\boldsymbol{x}$, $\boldsymbol{y}$); second and fourth order tensors are respectively represented by boldfaced Greek letters (e.g., $\boldsymbol{\sigma}$, $\boldsymbol{\varepsilon}$) and boldfaced upper case Latin letters (e.g., $\mathbf{S}$, $\mathbf{C}$). In particular, under the statistical paradigm, random variables and their realizations are respectively denoted by upper case letters (e.g., X, Y) and lower case letters (e.g., x, y); statistical model parameters are represented by Greek letters (e.g. α, σ_ϵ).

2.1 Viscoelasticity of polymers

Polymers are very large molecules (macromolecules) whose structure is monomers linked together by covalent bonds (Painter and Coleman, 1994). The monomers composition, as well as their arrangement, drive the resulting properties. Various phases exist in polymers depending on the configuration of the molecular chains. Linear molecular chains packed in a regular three-dimensional pattern in polymers are considered crystalline phases; the phase for which the molecules are random and entangled is referred to as amorphous. Semi-crystalline polymers consist of both crystalline and amorphous phases.

In a polymer, the thermal energy yields the flexible molecular chain to wriggle and writhe, resulting in a continual change in its contour shape. Therefore, temperature generally has a remarkable effect on the mechanical properties of polymers. The glass transition temperature, T_g, is an important characteristic for a polymer. Above this temperature, the amorphous phase of a polymer changes from a solid-like state to a liquid-like state due to the thermal motions of molecular chains increasing, leading to a severe decrease of the mechanical properties.

2.1.1 Linearly viscoelastic constitutive theories

When a polymer is subjected to an external stress, the configuration of the molecular chains in the amorphous phase is rearranged. The rearrangement on the local scale, e.g., the orientation of bonds in the chain backbone, is terminated quickly, while the long-range scale, e.g., the whole molecular chain, is slow. As a result, the polymers' response to the external stress

persists over a wide and continuous time scale (Ferry, 1980). Therefore, unlike pure elastic materials response proportionally with the applied load, polymers exhibit a time-dependent response, i.e., *viscoelasticity*, when submitted to a mechanical load due to amorphous phases in the polymers.

Viscoelasticity manifests itself through strain creep or stress relaxation, as schematized in Figure 2.1. In a creep-recovery test, the strain increases over time while the material is subjected to a constant load. Once the stress is removed, the elastic strain recovers immediately, whereas the viscous strain returns slowly to its initial state. In a relaxation test, when the material is subjected to a constant strain, the stress slowly decreases over time until a steady state is reached.

Thermodynamically based constitutive theories for viscoelasticity have been developed and widely used in the last several decades to describe the mechanical behavior of viscoelastic materials under varying loading and temperature histories (Biot, 1954; Caruthers *et al.*, 2004; Cunat, 2001; Drozdov, 2000; Lévesque *et al.*, 2008; Schapery, 1964). These constitutive

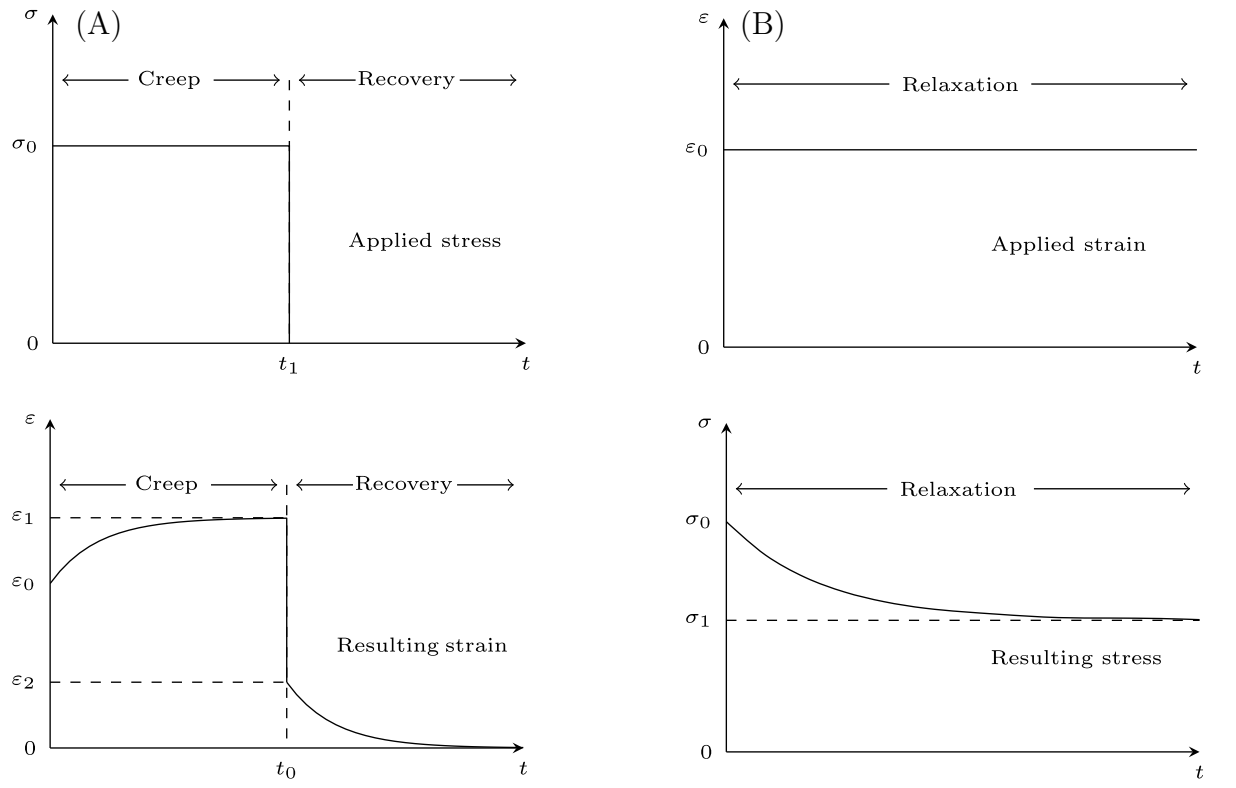

Figure 2.1 Viscoelastic behavior of a material during (A) a strain creep-recovery test; (B) a stress relaxation test (Crochon, 2014).

theories are developed based on the well-known Clausius-Duhem inequality:

$$\boldsymbol{\sigma} : \dot{\boldsymbol{\varepsilon}} - \rho\left(\dot{\Psi} + \eta\dot{T}\right) - \frac{\boldsymbol{q}\cdot\boldsymbol{\nabla}T}{T} \geq 0, \tag{2.1}$$

where $\dot{}$ stands for the time differentiation. $\boldsymbol{\sigma}$ and $\boldsymbol{\varepsilon}$ represent the stress and strain of the material, respectively. ρ is the mass density, η is the entropy density and $\boldsymbol{q}$ is the heat flux. Ψ denotes Helmholtz's free energy, which is assumed to be a function of $\boldsymbol{\varepsilon}$ and the internal variable $\boldsymbol{\chi}$ characterizing the material's thermodynamical state, i.e., $\Psi = \Psi(\boldsymbol{\varepsilon}, \boldsymbol{\chi})$.

In linear viscoelasticity, the thermodynamical forces $\boldsymbol{f}$ and $\boldsymbol{b}$ are assumed as linear functions of the time variation of the state variables (Lévesque *et al.*, 2008; Schapery, 1964), i.e.,

$$\boldsymbol{f} = \mathbf{F} : \dot{\boldsymbol{\varepsilon}}, \tag{2.2a}$$

$$\boldsymbol{b} = \mathbf{B} : \dot{\boldsymbol{\chi}}, \tag{2.2b}$$

with $\mathbf{F}$ and $\mathbf{B}$ being semi-positive tensors. Under an adiabatic and isothermal loading history, i.e., $\dot{T} = 0$ and $\boldsymbol{q} = \mathbf{0}$, Equation (2.1) for the case of the linear viscoelasticity becomes:

$$\left(\boldsymbol{\sigma} - \frac{\partial\Psi}{\partial\boldsymbol{\varepsilon}}\right) : \dot{\boldsymbol{\varepsilon}} - \frac{\partial\Psi}{\partial\boldsymbol{\chi}} : \dot{\boldsymbol{\chi}} = \mathbf{F} : \dot{\boldsymbol{\varepsilon}} + \mathbf{B} : \dot{\boldsymbol{\chi}} \geq 0. \tag{2.3}$$

The free energy Ψ can be assumed as a second order Taylor expansion of the state variable around an equilibrium state Ψ_0 as:

$$\Psi(\boldsymbol{\varepsilon}, \boldsymbol{\chi}) = \Psi_0 + \frac{1}{2}\boldsymbol{\varepsilon} : \mathbf{L}_1 : \boldsymbol{\varepsilon} + \boldsymbol{\varepsilon} : \mathbf{L}_2 : \boldsymbol{\chi} + \frac{1}{2}\boldsymbol{\chi} : \mathbf{L}_3 : \boldsymbol{\chi}, \tag{2.4}$$

where $\mathbf{L}_i$ are semi-definite positive fourth order tensors, which can be expressed as:

$$\mathbf{L}_1 = \frac{\partial\Psi}{\partial\varepsilon_i\partial\varepsilon_j}; \mathbf{L}_2 = \frac{\partial\Psi}{\partial\varepsilon_i\partial\chi_r}; \mathbf{L}_3 = \frac{\partial\Psi}{\partial\chi_r\partial\chi_s}. \tag{2.5}$$

When combining Equations (2.3) and (2.4), the differential form of a three-dimensional linearly viscoelastic constitutive model at constant temperature can be expressed as:

$$\boldsymbol{\sigma}(t) = \mathbf{L}_1 : \boldsymbol{\varepsilon}(t) + \mathbf{L}_2 : \boldsymbol{\chi} \tag{2.6a}$$

$$\mathbf{B} : \dot{\boldsymbol{\chi}} + \mathbf{L}_3 : \boldsymbol{\chi} + \mathbf{L}_2^{\intercal} : \boldsymbol{\varepsilon} = \mathbf{0}. \tag{2.6b}$$

Solving Equation (2.6) yields:

$$\boldsymbol{\sigma}(t) = \int_0^t \mathbf{C}(t-\tau) : \frac{\mathrm{d}\boldsymbol{\varepsilon}}{\mathrm{d}\tau}\mathrm{d}\tau, \tag{2.7}$$

with $\mathbf{C}(t)$ denoting the relaxation kernel that can be expressed as a Prony series as:

$$\mathbf{C}(t) = \mathbf{C}^{(0)} + \sum_{m=1}^{M} \mathbf{C}^{(m)} \exp[-\omega_m t], \tag{2.8}$$

where the relaxation stiffnesses $\mathbf{C}^{(m)}$ are positive semi-definite tensors, ω_m are reciprocal relaxation times associated to $\mathbf{C}^{(m)}$. M is the total number of relaxation times.

The stress-based linearly viscoelastic constitutive model can be obtained through a similar approach (Schapery, 1970) and be expressed as:

$$\boldsymbol{\varepsilon}(t) = \int_0^t \mathbf{S}(t-\tau) : \frac{\mathrm{d}\boldsymbol{\sigma}}{\mathrm{d}\tau}\mathrm{d}\tau, \tag{2.9}$$

with

$$\mathbf{S}(t) = \mathbf{S}^{(0)} + \sum_{m=1}^{M} \mathbf{S}^{(m)}(1 - \exp[-\lambda_m t]), \tag{2.10}$$

where $\mathbf{S}(t)$ denotes the retardation kernel. The creep compliances $\mathbf{S}^{(m)}$ are positive semi-definite tensors and the λ_m are reciprocal creep times associated with $\mathbf{S}^{(m)}$.

To implement the viscoelastic constitutive theory in a finite element (FE) package, solutions of differential or integral equations need to be computed, which can be accomplished through two types of strategy. Taylor *et al.* (1970) has proposed the recursive scheme to compute the solution of hereditary integrals, like that of Equation (2.10). The time derivation of load history is assumed to be constant during each time increment; then, a recursive formula is introduced to relate successive time steps. The differential scheme developed by Crochon *et al.* (2010) solves the differential equations, as Equation (2.6), based on finite differential (FD) methodologies, e.g., Euler, Crank-Nicholson and Runge-Kutta. Both integral and differential schemes can achieve the same level of accuracy and can be easily extended to three-dimensional and non-linear models.

2.1.2 Time-temperature superposition principle

The time-temperature superposition (TTS) principle relates the material's viscoelastic properties under service conditions to its properties in a reference state by a so-called *shift factor* (Andrews and Tobolsky, 1951; Ferry, 1980).

Temperature effect

According to the TTS principle, the creep compliance of a thermorheologically simple material $\mathbf{S}(t)$ at temperature T can be derived by shifting the creep compliance $\mathbf{S}^{\text{ref}}(t)$ at reference temperature T^{ref} as :

$$\mathbf{S}(t;T) = \mathbf{S}^{\text{ref}}\left(\frac{t}{a_T};T^{\text{ref}}\right), \tag{2.11}$$

where a_T is horizontal temperature shift factors.

When the temperature is above T_g, the temperature shift factor a_T is commonly mathematically described by the Williams-Landel-Ferry (WLF) model (Williams *et al.*, 1955) which is expressed as:

$$\log a_T = -\frac{C_0(T-T^{\text{ref}})}{C_1+(T-T^{\text{ref}})}, \tag{2.12}$$

where C_0 and C_1 denote universal constants. While below T_g, the Arrhenius equation (Schapery, 1974) can be used, as:

$$\log a_T = -A_T\left(\frac{1}{T^{\text{ref}}}-\frac{1}{T}\right), \tag{2.13}$$

where A_T represents the material's parameter.

Physical aging effect

Physical aging manifests itself through a variation of viscoelastic properties as a function of time, for temperatures below T_g and under no influence from any other external stimuli (Hutchinson, 1995; McKenna *et al.*, 1995; Struik, 1977; White, 2006). A polymer remains in its equilibrium thermodynamic state above its T_g. When it is quenched from a temperature above its T_g to a temperature below its T_g, the molecular rearrangements that occur rapidly when the sample's temperature is above its T_g are significantly slowed down to a range that the material cannot maintain an equilibrium with the cooling rate. The polymer stays in non-equilibrium state and towards equilibrium. However, when the cooling stops, the thermodynamic state of materials is moved towards equilibrium. A schematic illustration of physical aging at a temperature below T_g is shown in Figure 2.2. Physical aging typically increases thermoplastics brittleness and stiffness.

To evaluate the effect of physical aging on the mechanical properties of polymers, Struik (1977) extended the TTS principle to the case of physical aging. The creep compliance $\mathbf{S}(t)$ of a material aged for a time t_e at temperature T can be obtained by shifting the creep

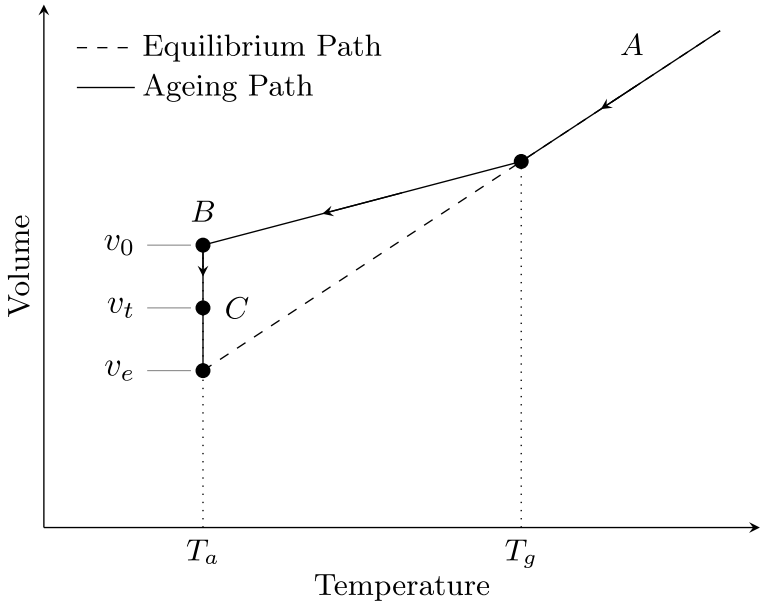

Figure 2.2 Illustration of physical aging for a polymer (adapted from Crochon (2014)). The material is in thermodynamic equilibrium above T_g (A). When quenched, the volume of the polymer decreases toward an out-of-equilibrium volume v_0 (B). Then, while maintaining a constant temperature, the volume gradually approaches equilibrium v_e through the process of physical aging (C).

compliance $\mathbf{S}^{\text{ref}}(t)$ when aged for a reference time t_e^{ref} at reference temperature T^{ref} by:

$$\mathbf{S}(t;T,t_e) = a_v(T,t_e)\ \mathbf{S}^{\text{ref}}\left(\frac{t}{a(T,t_e)};T^{\text{ref}},t_e^{\text{ref}}\right), \tag{2.14}$$

where $a(T,t_e)$ and $a_v(T,t_e)$ respectively denote horizontal and vertical shift factors that depend on temperature and physical aging. The shift factor $a_v(T,t_e)$ is generally found to have little effect, when compared to the horizontal shift factor, and can be considered to be close to unity in most cases (Bradshaw and Brinson, 1999; Crochon *et al.*, 2015; Sullivan *et al.*, 1993). The horizontal shift factor $a(T,t_e)$ can be decomposed into the product of the temperature shift factor a_T and the aging shift factor a_{t_e} (Bradshaw and Brinson, 1997b; Struik, 1977), leading to:

$$a(T,t_e) = a_T a_{t_e}. \tag{2.15}$$

For the case of isothermal physical aging, during which the physical aging occurs at a constant temperature, the aging shift factor a_{t_e} can be evaluated by (Struik, 1977):

$$a_{t_e}(t_e,T) = \left(\frac{t_e}{t_e^{\text{ref}}}\right)^{\mu(T)}, \tag{2.16}$$

where $\mu(T)$ stands for the shift rate depending on temperature T and is assumed constant during aging. However, for complex temperature histories, referred to as non-isothermal physical aging, Equation (2.16) no longer holds because of the accumulation of physical aging at different temperatures (Bradshaw and Brinson, 1997a).

Bradshaw and Brinson (1997a, 1997b) have proposed the continuous shift factor (CSF) to evaluate the effect of physical aging on the mechanical properties during a non-isothermal aging test. Based on the effective time theory (Brinson and Gates, 1995; Knauss and Emri, 1981), the viscoelastic constitutive model becomes

$$\boldsymbol{\varepsilon}(t) = \int_0^t \mathbf{S}\Big(\phi(t) - \phi(\tau)\Big) : \frac{\mathrm{d}\boldsymbol{\sigma}}{\mathrm{d}\tau}\mathrm{d}\tau, \tag{2.17}$$

where the effective time ϕ is utilized in this method to record the accumulative effects of temperature and physical aging throughout the complex thermal history, i.e.,

$$\phi(t) = \int_0^t a_T a_{t_e}(\xi)\mathrm{d}\xi. \tag{2.18}$$

Because of the absence of an analytical form for $\phi(t)$, a reasonable function with unknown parameters must be chosen to model the effective time. The parameters of $\phi(t)$ are then determined by fitting Equation (2.17) to experimental data. This method is able to accurately simulate and predict the long-term mechanical behavior of polymers. However, the choice of fitting function for the effective time is arbitrary and artificial.

Guo and Bradshaw (2009); Guo *et al.* (2009) developed the KAHR-a_{t_e} method to predict the mechanical response of polymers during long-term non-isothermal physical aging. In this method, based on experimental observations (McKenna *et al.*, 1995; Struik, 1977, 1988), the relationship between the aging shift factor a_{t_e} and the structural shift factor a_δ has been assumed as:

$$a_{t_e}(a_\delta)\Big|_T = \left(\frac{c_0}{a_\delta}\right)^{c_1};\ c_0, c_1 > 0, \tag{2.19}$$

where T is the temperature at which the mechanical load is applied, c_0 and c_1 are temperature dependent constants. According to the KAHR model (Kovacs *et al.*, 1979), a_δ can be expressed as:

$$a_\delta = \exp[-\zeta\delta], \tag{2.20}$$

where ζ is a material parameter. δ denotes the specific volume recovery response, which is defined as:

$$\delta(t, T) = \frac{v(t, T) - v_\infty(T)}{v_\infty(T)}, \tag{2.21}$$

where v and v_∞ represent the instantaneous and equilibrium specific volume, respectively. δ is determined by:

$$\delta(z) = -\Delta\alpha \int_0^z R(z-\varsigma)\frac{\mathrm{d}T}{\mathrm{d}\varsigma}\mathrm{d}\varsigma, \tag{2.22}$$

with

$$R(z) = \exp\left[-\left(\frac{z}{\tau_\alpha}\right)^{\beta_\alpha}\right], \tag{2.23}$$

and

$$z(t) = \int_0^t \frac{\mathrm{d}\xi}{a_T a_\delta}, \tag{2.24}$$

where $\Delta\alpha = \alpha_l - \alpha_g$ represents the difference in the coefficient of thermal expansion (CTE) between the liquid and glassy states of the polymer. R is the normalized retardation function of the reduced time z with the material parameters τ_α and β_α. The temperature shift factor is given by (Kovacs *et al.*, 1979):

$$a_T = \exp[-\Delta\alpha\zeta e^b(T - T_r)], \tag{2.25}$$

where T_r is a reference temperature and b is a material constant. Thus, six parameters (ζ, b, c_0, c_1, τ_α, β_α) are required in this model that must be determined through non-isothermal aging tests.

2.1.3 Three-dimensional viscoelastic properties experimental characterization

When modeling or characterizing the three-dimensional mechanical properties of polymers, it is commonly assumed that the bulk modulus or Poisson's ratio of the material is constant. Therefore, the three-dimensional problem can be reduced to a uni-dimensional problem in most cases (Courtois, Marcin, *et al.*, 2019; Crochon *et al.*, 2015). However, this assumption may be violated, especially if the test duration is sufficiently long, or when investigating the effect of temperature on mechanical properties of polymers across glass transition temperature (Emri and Prodan, 2006; Lu *et al.*, 1997; Qvale and Ravi-Chandar, 2004; Sanahuja and Toulemonde, 2011; Tscharnuter *et al.*, 2011b; Tschoegl *et al.*, 2002).

In the context of linear viscoelasticity, the use of any two of four material functions (the elastic modulus, the shear modulus, the bulk modulus and Poisson's ratio) is sufficient to model the mechanical properties of an isotropic material (Lu *et al.*, 1997). These two material functions must be determined simultaneously (Tschoegl *et al.*, 2002), and several methods have been proposed.

To determine the bulk behavior of Poly(methyl methacrylate) (PMMA), Lu *et al.* (1997)

measured the Young's modulus and Poisson's ratio of planar specimens, and the Young's and shear functions of cylindrical specimens. The bulk function of PMMA was then computed using the material functions measured from the two tests, respectively. It was found that the bulk function requires a high level of measurement accuracy; consequently, the bulk function cannot be robustly derived from the other material functions and must be determined directly from the experiments.

Several special experimental configurations have been developed to measure the bulk properties of polymers. For example, an atmospheric pressure chamber was used to measure the dynamic bulk compliance of PMMA and polyvinyl acetate (PVAc) (Sane and Knauss, 2001), and a confined compression set-up was used to determine the bulk and shear relaxation response of PMMA and polycarbonate (PC) (Qvale and Ravi-Chandar, 2004). However, the measurement accuracy of the bulk behavior of polymers is susceptible to errors caused by experimental set-up. For example, it was found that a gap of 1.27×10^{-2} mm between the specimen and the equipment could introduce errors up to 30% in the bulk properties measurement (Qvale and Ravi-Chandar, 2004). In addition, the accessibility of these devices limits their widespread use in engineering.

Temperature and physical aging effects characterization

Aging effects can be measured through Struik's methodology (Struik, 1977), which can be divided in three types:

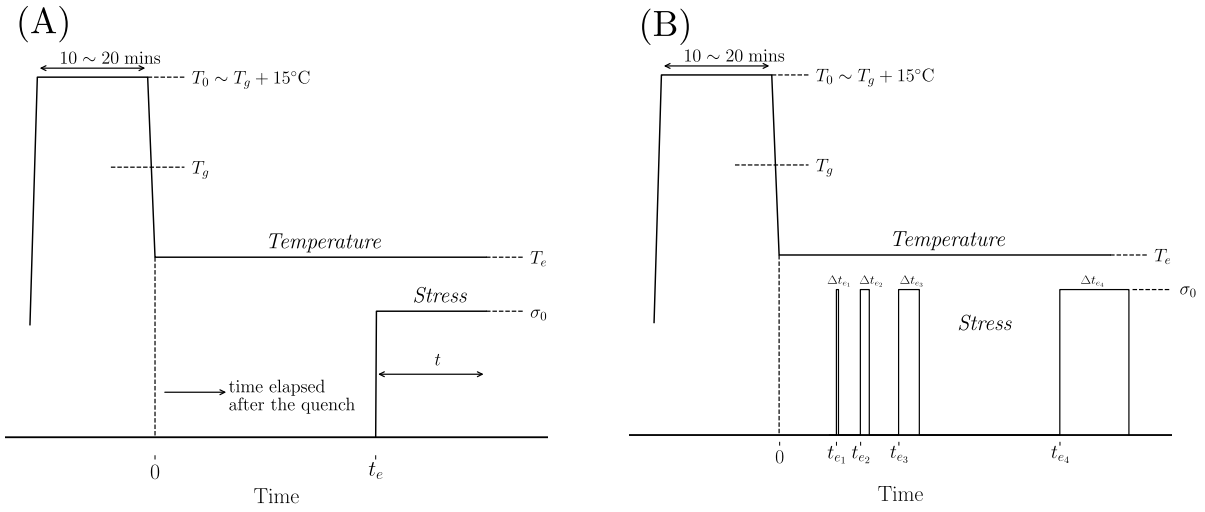

Figure 2.3 Temperature and loading histories of isothermal physical aging tests (Struik, 1977) (A) isothermal long-term aging test; (B) isothermal short-term aging test.

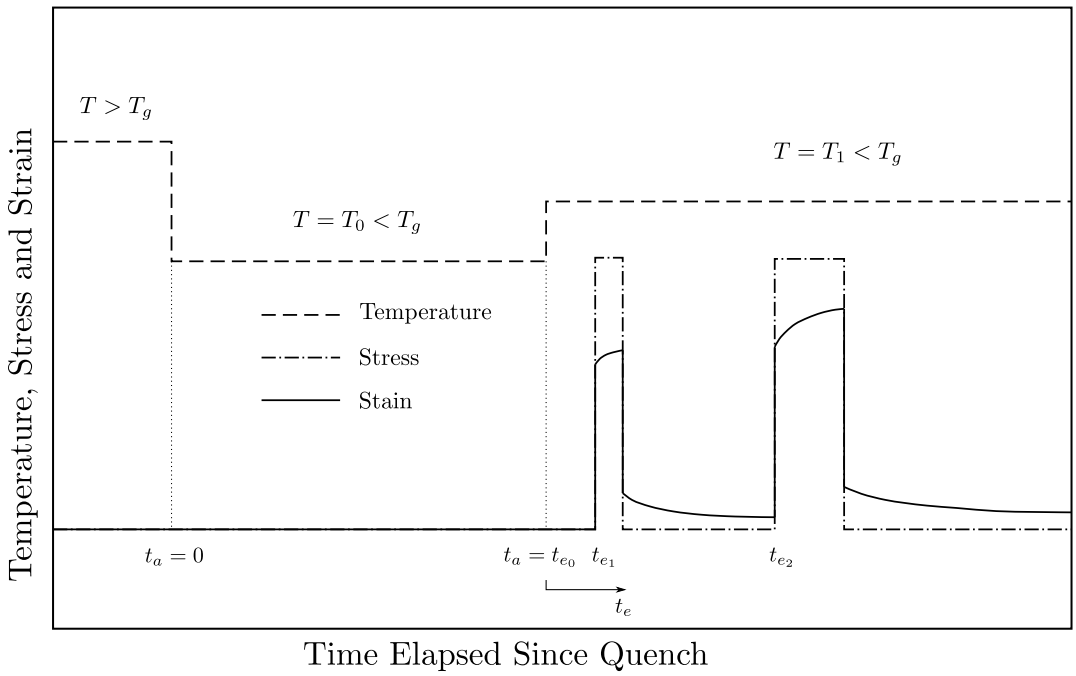

Figure 2.4 Schematic of the single up-jump non-isothermal aging test (adapted from Guo *et al.* (2009)). The specimen is firstly rejuvenated at a temperature above T_g, then quenched to a desired temperature T_0 below T_g and held for a duration t_{e_0}. After that, the temperature is increased ("*up-jump*") to and maintained at the aging temperature T_1. The aging time t_e is counted after this up-jump. Then the sequential creep tests are performed.

- **Isothermal long-term aging test**. This test begins with an annealing period during which the polymer is submitted to a temperature 10°C to 15°C above its T_g for 10 to 20 minutes. This period is used to erase their previous thermal or aging histories. Next, the sample is quenched to a temperature T_e below its T_g and kept at this temperature. Then a creep test (see Section 2.1 for more details on creep tests) is started once a time t_e has elapsed since the quench. The effect of aging can therefore be determined by repeating this test for various t_e. Figure 2.3(A) shows the procedure of long-term aging testing for an aging time t_e at a temperature T_e.

- **Isothermal short-term aging test**. This methodology starts with the same annealing procedures as that of the long-term test. Instead of only one creep test, a sequence of creep and recovery tests is performed on the material. Each creep duration should never exceed 10% of the total aging time in order to ignore the aging effect during testing. Otherwise, a correction is needed. The temperature and loading histories for a typical short-term aging test is illustrated in Figure 2.3(B). t_{e_i} denotes the aging time of material before starting the ith creep-recovery test. Δt_{e_i} represents the creep

period which should satisfy that $\Delta t_{e_i} < 10\%\ t_{e_i}$. In practice, since the amount of time is required for the temperature "up-jump", it is necessary to wait enough time before creep testing to ensure that the specimen reaches its thermal equilibrium state.

- **Non-isothermal aging test**. This methodology is similar to the short-term aging test. After being quenched directly to the aging temperature, the material was submitted to a complex initial temperature history before performing sequential creep-recovery tests. Figure 2.4 schematizes a single temperature variation non-isothermal aging experiment.

The isothermal long-term aging test is easy to be performed, which can be used for polymers submitted to any stress level. However, it consumes more time than a short-term test. The short-term test can be used to investigate the aging effect of a material at a temperature for different aging times in just one experiment. However, this methodology is only valid when the material can be considered as linearly viscoelastic. The non-isothermal aging test takes into account the influence of temperature which exists in the real engineering application, which can be used to investigate if the previous temperature histories have an effect on the aging of the material.

Equipment and strain measurement techniques

Most existing investigations into the mechanical properties of polymers involving temperature and physical aging effects rely mainly on Dynamic Mechanical Analysis (DMA) measurements (Courtois, Hirsekorn, *et al.*, 2019; Guo and Bradshaw, 2009; Kovacs *et al.*, 1963; Meyer *et al.*, 1965; O'connell and McKenna, 1997; O'Connell and McKenna, 2002). The technique, however, features limitations when it comes to measuring the mechanical properties of materials, including the specimen size limitation, the difficulty of aligning the specimen due to the relatively small size of mounts and the fact that only uni-dimensional properties can be investigated during these tests. This last feature limits the application of DMA in characterizing the three-dimensional properties of polymers. When compared to DMA, tensile testing frames allow various experimental set-ups and thus can be used to characterize the three-dimensional properties of materials at elevated temperatures when equipped with an environmental chamber and strain measurement equipment.

Three types of equipment are mostly used to measure strains in mechanical testing. The *strain gauge* is an analog electrical sensor bonded to the specimen surface that is used to measure the strains of solid materials (Knauss *et al.*, 2008). It is well suited for accurately determining specimen strains under various loading conditions and temperatures. However, the high cost, the difficulty of selecting an appropriate bonding agent and the stringent requirements

of the bonding technology make using a strain gauge relatively tedious and expensive. The *extensometer* is a device fixed on the specimen by its knife edge, and the average strain of the gauge section of the specimen during the experiment is computed from the displacement of the knife edge. This measurement method provides the most convenient and cost-efficient way for accurately measuring strains (Knauss *et al.*, 2008). However, measurements with an extensometer are subject to errors caused by its characteristics (Knauss *et al.*, 2008; Womack, 2020b, 2020c), such as temperature sensitivity, the penetration of the knife edge, especially in high-temperature tests. *Digital Image Correlation* (DIC) yields strain fields through analyzing pictures of specimens covered with a speckle pattern. However, the use of DIC with an environmental chamber requires special care and equipment to account for refraction from the chamber's window (Rataj *et al.*, 2015), the image distortions due to the heated air (Valeri *et al.*, 2017), and the black-body radiation of the specimen (Grant *et al.*, 2009). Among the three above-mentioned techniques, the extensometer seems the most convenient, accurate, and easy to use when performing strain measurement at elevated temperature.

However, strain measurements are subject to environmental influences that result in drift, which arises from two primary sources.

Temperature sensitivity Alike most electronic sensors, the transducer in the extensometer is susceptible to temperature, which causes the extensometer's measurement results to drift when the temperature changes. When the extensometer is powered, heat is generated by the current flow, causing a temperature change, and the resulting drift is known as the *warm-up drift* (Womack, 2020c). This drift generally stabilizes after the device has been plugged in for a few minutes. When the ambient temperature changes, the extensometer experiences a *thermal drift* (Womack, 2020b). This drift includes not only the response of the sensor to the temperature change but also records the deformation of the load cell, test machine, or other device subjected to the temperature change. Distinguishing the different factors that cause thermal drift remains a challenge (Womack, 2020b).

Knife edges To hold the extensometer on the specimen, the knife edges are usually rather sharp. Therefore, the knife edge will penetrate into the specimen when the extensometer is mounted and cause the *penetration drift* (Knauss *et al.*, 2008). This drift is particularly noticeable when testing thermoplastic polymers. Since the extensometer is manually mounted on the specimen, the knife-edge position and the contact force (Knauss *et al.*, 2008), i.e., the force applied to attach the knife-edge, may differ between tests, introducing measurement error.

2.2 Viscoelastic parameters identification

Obtaining constitutive theory parameters from experimental data can be cast as a non-linear optimization problem as (Grédiac and Hild, 2012):

$$\hat{\boldsymbol{\theta}}_{LS} \in \underset{\theta \in \Theta}{\arg\min}\ \mathcal{J}(\boldsymbol{\theta}),\ \ \mathcal{J}(\boldsymbol{\theta}) = \|\boldsymbol{g}(\boldsymbol{\theta}, \boldsymbol{x}) - \boldsymbol{y}\|_2, \tag{2.26}$$

where $\hat{\boldsymbol{\theta}}_{LS}$ stands for the least squares estimate of the viscoelastic parameters vector $\boldsymbol{\theta}$, $\boldsymbol{x} = (x_i : i = 1, \ldots, T)$ is the applied excitation vector given T discrete times i, $\boldsymbol{y} = (y_i : i = 1, \ldots, T)$ are the corresponding observed discrete time responses and $g(\boldsymbol{\theta}, \boldsymbol{x})$ represents the response predicted by a physical model using the parameters vector $\boldsymbol{\theta}$ submitted to an excitation $\boldsymbol{x}$. $\|\cdot\|_2$ denotes the l^2-norm. $\mathcal{J}(\boldsymbol{\theta})$ stands for the objective function. For the constitutive theory to meet thermodynamics principles, the parameters space Θ should be defined as $\Theta \in \mathbb{R}^+$. In particular, for the three-dimensional constitutive model, the stiffness and compliance matrices should be positive semi-definite.

2.2.1 Ill-posedness of the problem

Estimating Prony series viscoelastic parameters from static or dynamic mechanical testing data is a well-known *ill-posed problem*, which means that the model parameters identification from testing data is not uniquely assured and small perturbations in the data could induce significant variations in the identified parameters. To the knowledge of the authors, the ill-posedness of this problem comes from two aspects.

First, due to experimental constraints, the measurement of the full compliances or modulus over the whole time domain for the polymer cannot be performed. The mechanical testing is always carried out over a given time window. There may exist infinite numbers of kernel functions that represent experimental data in this experimental time window. As a result, parameters identified from testing data are generally not unique. Therefore, the existence of limited experimental time windows renders the ill-posedness of the identification problem.

Second, the numerical solution of Equation (2.26) for Prony series model is not unique. The Prony series model parameters identification is actually refers to a classical positive exponential sums fitting problem which has been discussed over the past several decades (Holmström and Petersson, 2002; Istratov and Vyvenko, 1999). The ill-posedness of this problem was firstly reported by Lanczos (1988). Lanczos generated data series using three exponentials and fitted them equally well by several different exponentials. Similarly, Ruhe (1980) showed that an arbitrary exponential can be well approximated by a sum of others.

Liu (2001) demonstrated this feature.

2.2.2 Existing identification problem

To overcome the ill-posedness of viscoelastic parameters identification, scores of methods have been proposed since 1960s. Existing viscoelastic parameters identification methods rely on the least square norm and can be divided into three categories.

Fixing a priori characteristic times This is the most used method in which the number and values of characteristics times (ω_m or λ_m) are fixed a priori and the associated moduli or compliances need to be estimated.

The most common method is the collocation method proposed by Schapery (1962), by assuming logarithmic equidistant retardation times. However, this method does not enforce thermodynamics restrictions. Lévesque *et al.* (2008) improved this method by introducing an optimization variable to ensure the non-negativeness of parameters. For example, let the unknown stiffness value be $c = \alpha^2$ and α be the parameters to identify. This variable changes the constrained optimization problem to an unconstrained one, which decreases the difficulties of solving. The iterative multi-data method proposed by Kaschta and Schwarzl (1994a, 1994b) is an extension of the classical collocation method (no thermodynamics restrictions imposed). Instead of fixing the retardation times a priori, this method assumes that the retardation times are logarithmically equidistant with a prescribed spacing and starts with the first retardation time. The parameters to be optimized are therefore the first retardation time and compliances. If one or more parameters are negative, the value of the first retardation time is slightly varied until all obtained parameters are positive. Emri and Tschoegl (1993, 1994, 1995) proposed a recursive identification scheme, using the characteristic properties of the exponential in the kernel . This method is based on the fact that, the contributions of the compliances associated with the retardation times located two decades after a given λ_i can be neglected. With pre-selected relaxation times, this method starts calculating the compliance associated to the largest relaxation time and then calculates other compliances. The obtained negative values are set to zero and computation is restarted. The iteration continues until the difference between the previously found and newly computed parameters is smaller than a preset error. Some others methods can also be found in the literature (Gerlach and Matzenmiller, 2005).

These techniques can tremendously reduce the difficulties of solving Equation (2.26). However, the pre-selection of number and values of relaxation or retardation times might not be optimal and the resulting parameter sets might be unnecessarily large. Defining the most

efficient number of retardation times, and their values, is still an open question.

Iteration free methods These methods can simultaneously obtain the tensorial values as well as the characteristic times by defining dedicated mathematical structures. Yeramian reported a method combining Padé approximation and the Laplace transformation of Prony series, which enables the exact identification of characteristic times (Claverie *et al.*, 1989; Yeramian and Claverie, 1987). Jalocha *et al.* (2015) had constructed a specific mathematical structure based on the Fourier transformation of Prony series and computed characteristic times using the Krein-Nudelman theorem (Krein and Nudelman, 1998) from complex analysis.

However, the accuracy of these methods is strongly influenced by the experimental data uncertainties. Halvorson (1992) reported that these methods could amplify the effect of experimental noise on the identified parameters in an unpredictable way.

Stochastic strategies Stochastic approaches have also been proposed to estimate Prony series model parameters, such as the Simulated Annealing (SA) algorithm (Jensen, 2002; Tscharnuter *et al.*, 2011a) or the Bayesian framework with *Markov Chain Monte Carlo* (MCMC) (Haario *et al.*, 2014; Hansen, 2008; Hernández *et al.*, 2017). Rather than presetting characteristic times, these approaches provide a quantitative means to estimate the optimal number of series. Haario *et al.* (2014) introduced an indicator, called *indeterminacy*, to characterize the parameters identification non-uniqueness. Similarly, Freund and Ewoldt (2015) proposed the *evidence* to determine the most adequate model based on user input model errors parameters.

It should be noted that some stochastic methods are not adequate for solving the Prony series identification problem. For example, the SA algorithm solves the optimization problem directly by the Metropolis algorithm. However, the ill-posedness of the Prony series problem may result in discrepancies with an inappropriate choice of the control values of the SA algorithm, which make it difficult to implement it in an automated way. The existing Bayesian methods used to identify Prony series viscoelastic parameters also still require some clarifications and are non-automated. For instance, the error analysis still depends on the knowledge of user, which can not be realized in a robust way.

2.3 Bayesian framework

2.3.1 Bayes' theorem

Given a set of experimental observation $\boldsymbol{y} = \{\boldsymbol{y}_i : i = 1, \ldots, n\}$ associated to a multi-dimensional parameter vector $\boldsymbol{\theta}$, which is considered as a random vector under the Bayesian paradigm, the inference on $\boldsymbol{\theta}$ can be archived through Bayes' theorem as (Bishop, 2006):

$$f_{(\boldsymbol{\theta}|\boldsymbol{Y}=\boldsymbol{y})}(\boldsymbol{\theta}) = \frac{f_{(\boldsymbol{Y}|\boldsymbol{\theta})}(\boldsymbol{y}) \times f_{\boldsymbol{\theta}}(\boldsymbol{\theta})}{f_{\boldsymbol{Y}}(\boldsymbol{y})}, \tag{2.27}$$

where $f_{(\boldsymbol{\theta}|\boldsymbol{Y}=\boldsymbol{y})}(\boldsymbol{\theta})$ is the posterior distribution of $\boldsymbol{\theta}$ after observing the data $\boldsymbol{y}$, $f_{(\boldsymbol{Y}|\boldsymbol{\theta})}(\boldsymbol{y})$ is the likelihood, $f_{\boldsymbol{\theta}}(\boldsymbol{\theta})$ is the prior distribution of $\boldsymbol{\theta}$ and $f_{\boldsymbol{Y}}(\boldsymbol{y})$ is the normalization constant. The prior distribution represents the knowledge on the model parameters before performing the experimentation and the posterior distribution consists in the updated knowledge when accounting for experimentally observed data. Information from the data is introduced via the likelihood. Non-informative prior distribution can be used when no information is available on $\boldsymbol{\theta}$ before the experimentation. Otherwise, an informative prior on $\boldsymbol{\theta}$ can be used. The normalization constant ensures that the posterior integral to be unity, which can be expressed as:

$$f_{\boldsymbol{Y}}(\boldsymbol{y}) = \int f_{(\boldsymbol{Y}|\boldsymbol{\theta})}(\boldsymbol{y}) f_{\boldsymbol{\theta}}(\boldsymbol{\theta}) \mathrm{d}\boldsymbol{\theta}. \tag{2.28}$$

2.3.2 Markov Chain Monte Carlo

The posterior distribution $f_{(\boldsymbol{\theta}|\boldsymbol{Y}=\boldsymbol{y})}(\boldsymbol{\theta})$ is often unavailable under a closed analytical form. Therefore, numerical methods are needed to perform statistical inference. The *Markov Chain Monte Carlo* (MCMC) simulations are frequently used to generate samples from the posterior distribution (Andrieu *et al.*, 2003).

The core of MCMC simulations is to generate a random sample for the posterior distribution of the parameter and then use this sample for the inference purpose (Gelman *et al.*, 2013). A Markov chain, a model in which the future predictions are assumed independent of all but recent observations, is first constructed; then, a random walk is performed on the Markov chain's state space. The fraction of time spent in each state is proportional to the posterior distribution during this process (Murphy, 2012). The schematic procedure of MCMC is illustrated in Figure 2.5. Several sampling algorithms have been developed based on the MCMC procedure (Gelman *et al.*, 2013; Geman and Geman, 1984; Hastings, 1970; Metropolis *et al.*, 1953; Murphy, 2012).

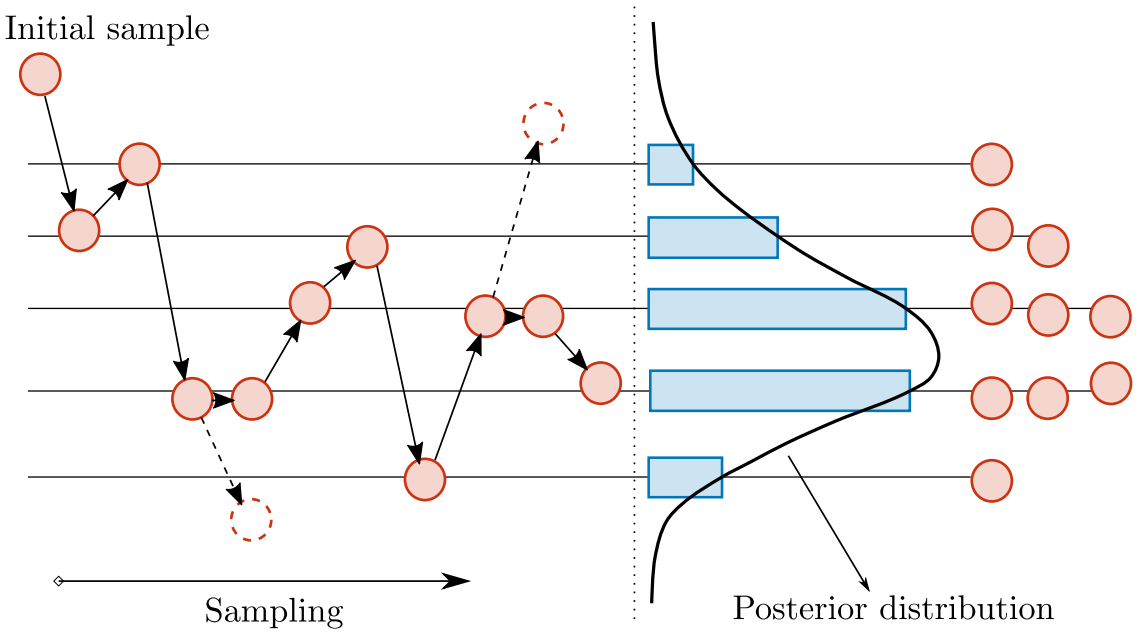

Figure 2.5 Illustration of the MCMC procedure adapted from An *et al.* (2015). A random walk is performed on the state space where a Markov chain is constructed. The fraction of time spent in each state is proportional to the posterior distribution.

Metropolis-Hastings sampling

The basic *Metropolis-Hastings* algorithm is an iterative sampling method, which starts from an initial state of parameters $\boldsymbol{\theta}^0$. Thus, at step s, the state of the parameters is independently determined by the state of the previous step $s-1$. The movement from $\boldsymbol{\theta}^{s-1}$ to $\boldsymbol{\theta}^s$ is drawn from a *proposal distribution* $J(\boldsymbol{\theta}^s|\boldsymbol{\theta}^{s-1})$, which must be constructed so that the Markov chain can reach its unique stationary distribution, which corresponds to the target posterior distribution $f_{(\boldsymbol{\theta}|\boldsymbol{Y}=\boldsymbol{y})}(\boldsymbol{\theta})$. A common choice for the proposal distribution is to use a symmetric distribution, satisfying the condition (Gelman *et al.*, 2013):

$$J(\boldsymbol{\theta}^s|\boldsymbol{\theta}^{s-1}) = J(\boldsymbol{\theta}^{s-1}|\boldsymbol{\theta}^s). \tag{2.29}$$

If the target distribution evaluated with the proposed parameter $\boldsymbol{\theta}^s$ is not less than the current parameter $\boldsymbol{\theta}^s$, this proposed parameter is accepted. Otherwise, the proposed parameter is accepted with a probability

$$\alpha = \frac{f_{(\boldsymbol{\theta}|\boldsymbol{Y}=\boldsymbol{y})}(\boldsymbol{\theta}^s)}{f_{(\boldsymbol{\theta}|\boldsymbol{Y}=\boldsymbol{y})}(\boldsymbol{\theta}^{s-1})}. \tag{2.30}$$

The acceptation rate is defined as $r = \min\{1, \alpha\}$. If the proposed parameter is rejected, the parameter remains the state, i.e., $\boldsymbol{\theta}^s = \boldsymbol{\theta}^{s-1}$. This process is repeated for totally S iterations.

Releasing the symmetric requirement of proposal distribution improves the acceptation rate and accelerate the speed of convergence (Gelman *et al.*, 2013; Hastings, 1970), leading the acceptance rate to:

$$\alpha = \min\left\{1, \frac{f_{(\boldsymbol{\theta};\boldsymbol{Y}=\boldsymbol{y})}(\boldsymbol{\theta}^s)J(\boldsymbol{\theta}^{s-1}|\boldsymbol{\theta}^s)}{f_{(\boldsymbol{\theta};\boldsymbol{Y}=\boldsymbol{y})}(\boldsymbol{\theta}^{s-1})J(\boldsymbol{\theta}^s|\boldsymbol{\theta}^{s-1})}\right\}. \tag{2.31}$$

The specific choice of proposal distribution $J(\boldsymbol{\theta})$ remarkably affects the performance of the algorithm (Bishop, 2006). A common choice is that a Gaussian distribution centered on the previous state. The Metropolis-Hastings sampling is summarized in Algorithm 1.

Gibbs sampling

The existence of an acceptance rate r is responsible for the Metropolis-Hastings algorithms' inefficiency in high-dimensional problems, as r is always less than unity. The Gibbs algorithm is a special case of Metropolis-Hastings sampling, which always yields a probability of acceptance of 100 %. The Gibbs algorithm is based on the principle of sampling each component of the parameter in turn, conditional on the values of all other variables in the distribution (Murphy, 2012). Algorithm 2 summarizes the Gibbs sampling algorithm.

Several sample methods have been developped based on Metropolis-Hastings and Gibbs sampling methods, such as Adaptive Metropolis within Gibbs (AMWG) (Roberts and Rosenthal, 2009), Hamiltonian Monte Carlo (HMC) (Duane *et al.*, 1987), etc.

2.3.3 Application to parameter identification

The parameter identification problem defined in Equation (2.26) can be solved through the Bayesian framework (Kaipio and Somersalo, 2006). Under the Bayesian paradigm, the constitutive model parameters $\boldsymbol{\theta}$ are considered as random variables, and the parameter identification are derived from the posterior distribution which includes the information provided by the experimental data and the prior information of parameters.

In a mechanical experiment, the relation between experimental measurements $\boldsymbol{Y}$ and model predictions $\boldsymbol{g}(\boldsymbol{\theta}, \boldsymbol{x})$ can be drawn by an observation model with an additive error $\boldsymbol{\epsilon}$ as

$$Y_i = g(\boldsymbol{\theta}; x_i) + \epsilon_i,\ i = 1, \ldots, T, \tag{2.32a}$$

$$\epsilon_i \sim \mathcal{N}(0, \sigma_\epsilon^2), \tag{2.32b}$$

where $\mathcal{N}$ denotes the Gaussian distribution. The error ϵ_i of y_i is modeled as a zero mean Gaussian variable with variance σ_ϵ^2, and it is assumed that the errors are independent, i.e., ϵ_i is

Algorithm 1 Metropolis-Hastings sampling algorithm for MCMC simulation.

Initialize $\boldsymbol{\theta}^0$
for $s = 0, 1, 2, \ldots, S$ **do**
  Define $\boldsymbol{\theta} = \boldsymbol{\theta}^s$
  Generate $\boldsymbol{\theta}' \sim J(\boldsymbol{\theta}'|\boldsymbol{\theta})$
  Compute $r = \min\left\{1, \frac{f_{(\boldsymbol{\theta}|\boldsymbol{Y}=\boldsymbol{y})}(\boldsymbol{\theta}')J(\boldsymbol{\theta}|\boldsymbol{\theta}')}{f_{(\boldsymbol{\theta}|\boldsymbol{Y}=\boldsymbol{y})}(\boldsymbol{\theta})J(\boldsymbol{\theta}'|\boldsymbol{\theta})}\right\}$
  Sample $u \sim \mathcal{U}(0,1)$
  if $u < r$ **then**
    $\boldsymbol{\theta}_{s+1} = \boldsymbol{\theta}'$
  else
    $\boldsymbol{\theta}_{s+1} = \boldsymbol{\theta}_s$
  end if
end for

Algorithm 2 Gibbs sampling algorithm for MCMC simulation.

Initialize $\boldsymbol{\theta}^0 = \{\theta_i^0 : i = 1, 2, \ldots, N\}$
for $s = 1, 2, \ldots, S$ **do**
  sample $\theta_1^{s+1} \sim f_{(\theta_1|\theta_2^s, \theta_3^s, \ldots, \theta_N^s, \boldsymbol{y})}(\theta_1)$
  sample $\theta_2^{s+1} \sim f_{(\theta_2|\theta_1^{s+1}, \theta_3^s, \ldots, \theta_N^s, \boldsymbol{y})}(\theta_2)$
  ...
  sample $\theta_j^{s+1} \sim f_{(\theta_j|\theta_1^{s+1}, \ldots, \theta_{j-1}^{s+1}, \theta_{j+1}^s, \ldots, \theta_N^s, \boldsymbol{y})}(\theta_j)$
  ...
  sample $\theta_N^{s+1} \sim f_{(\theta_N|\theta_1^{s+1}, \theta_2^{s+1}, \ldots, \theta_{N-1}^{s+1}, \boldsymbol{y})}(\theta_N)$
end for

independent of ϵ_j, for $i \neq j$. The likelihood function can be constructed from Equation (2.32) (Freund and Ewoldt, 2015; Haario *et al.*, 2014; Hansen, 2008; Hernández *et al.*, 2017), which can be written as:

$$Y_i - g(\boldsymbol{\theta}; x_i) \sim \mathcal{N}(0, \sigma_\epsilon^2), \tag{2.33}$$

then

$$Y_i \sim \mathcal{N}\left\{g(\boldsymbol{\theta}; x_i), \sigma_\epsilon^2\right\}. \tag{2.34}$$

Therefore, the likelihood function, i.e., the joint density of $\boldsymbol{Y}$ given $\boldsymbol{\theta}$, becomes

$$f_{(\boldsymbol{Y}|\boldsymbol{\theta})}(\boldsymbol{y}) \propto \exp\left\{-\frac{1}{2\sigma_\epsilon^2}\left|\left|\, \boldsymbol{y} - \boldsymbol{g}(\boldsymbol{\theta}; \boldsymbol{x}) \,\right|\right|_2\right\}. \tag{2.35}$$

It is interesting to note that the maximum likelihood function (5.27) is formally equivalent to the non-linear least-square optimization problem as Equation (5.16).

Due to the lack of the prior information of the parameter, the non-informative prior are

usually used (Haario *et al.*, 2014; Hernández *et al.*, 2017). Finally, the posterior function of the constitutive model parameters can be computed by:

$$f_{(\boldsymbol{\theta}|\boldsymbol{Y}=\boldsymbol{y})}(\boldsymbol{\theta}) \propto f_{(\boldsymbol{Y}|\boldsymbol{\theta})}(\boldsymbol{y}) \times f_{\boldsymbol{\theta}}(\boldsymbol{\theta}). \tag{2.36}$$

A random sample from this distribution can be obtained with MCMC. Once the posterior distribution of the unknown parameters have been obtained, point estimates could also be defined under the Bayesian paradigm. A common Bayesian point estimate corresponds to the mode of the posterior distribution:

$$\hat{\boldsymbol{\theta}}_{\mathrm{MAP}} = \arg\max_{\boldsymbol{\theta}\in\Theta} f_{(\boldsymbol{\theta}|\boldsymbol{Y}=\boldsymbol{y})}(\boldsymbol{\theta}), \tag{2.37}$$

referred to as the *maximum a posteriori* (MAP) estimate.

2.3.4 Model selection

When fitting a statistical model to the experimental observations, the fit of the model can be improved by increasing the number of parameters. However, the large number of parameters may lead to overfitting and raising the required computation cost and also reduce the prediction accuracy. To balance the model fit and the model complexity, several information criteria for model selection have been proposed in Bayesian analysis (Bishop, 2006).

One of mostly used criterion is the *Bayesian Information Criterion* (BIC), which is expressed as:

$$\mathrm{BIC}(M) = \ln f_{(\boldsymbol{Y}|\hat{\boldsymbol{\theta}}_{\mathrm{MAP}})}(\boldsymbol{y}) - \frac{M}{2}\ln T, \tag{2.38}$$

where M stands for the number of parameters of the model, and T is the total number of data points. The first term of this criterion measures the model fit and the second term penalizes for complexity. A model with a higher BIC is preferable compared to the one with a lower BIC.

Another common model selection criterion also exists, which is the so-called *Akaike Information Criterion* (AIC), having a similar expression to BIC:

$$\mathrm{AIC}(M) = \ln f_{(\boldsymbol{Y}|\hat{\boldsymbol{\theta}}_{\mathrm{MAP}})}(\boldsymbol{y}) - M. \tag{2.39}$$

AIC tends to pick more complex models than BIC, resulting in better predictive accuracy. However, AIC is derived from a frequentist framework and cannot be interpreted as an approximation to the marginal likelihood (Murphy, 2012). As with the BIC, a model a higher AIC is better.

CHAPTER 3 OBJECTIVES AND RATIONALE

3.1 Problem definition

The general objective of this research is to develop a robust and automated numerical tool for predicting the three-dimensional viscoelastic properties of thermoplastic materials under complex loading and temperature histories. In that regard, the literature survey revealed that:

- Obtaining viscoelastic parameters from experiments is still an ill-posed problem. Some methods have been proposed to eliminate the ill-posedness of this problem. However, all the classical methods found in the literature have limitations (e.g., sensitivity to noise, etc.). Statistical methods have an important potential to deliver improved identification methodologies. For example, they can help select the most appropriate models based on experimental and model errors. This overcomes the sensitivity to experimental errors problems encountered in classical methods. However, statistical methodologies have been scarcely applied to viscoelastic properties identification and the proposed methods thus far are still not sufficiently robust and depend on user input.
- Considering that the computational time involved in the simulation of the response of viscoelastic structures scales with the number of viscoelastic coefficients, it would be of considerable interest to devise identification strategies yielding the minimum number of parameters. Several statistical methods have advanced concepts for model selection. However, the optimal parameter count for the Prony series model remains unclear and lacks reliable theory.
- Physical aging influences the long-term mechanical properties of thermoplastic. Most studies concerning this behavior assume that the bulk properties or Poisson's ratio are constant and conducted in a uni-dimensional mode. This assumption, however, can be violated if the testing period is sufficiently long or if high temperatures is involved, resulting in inaccurate predictions of three-dimensional properties.
- The bi-axial extensometer can measure three-dimensional strains in thermo-mechanical tests. However, the extensometer suffers drifts caused by several factors for thermoplastic at elevated temperatures. There is no standard procedure to account for these drifts, and researchers have rarely detailed their approach to address this.

- Most of the works in determining the viscoelastic and aging parameters of polymers have been done in two separate steps, i.e., obtaining the shift factors by constructing the master curve from the experimental data and then fitting the viscoelastic parameters to the constructed master curve. However, this process introduces artificial errors in the master curve, resulting in the inaccuracy in the viscoelastic parameter identification.

3.2 Research objectives

Based on the points raised in the critical evaluation of the scientific literature, three specific objectives have been defined to accomplish the main objective, namely:

1. **Propose a robust and automated method for identifying the three-dimensional viscoelastic constitutive theories for thermoplastic at room temperature**

   A Bayesian framework-based three-dimensional constitutive theory identification method for linearly viscoelastic solids will be proposed to overcome the ill-posedness of the Prony series model identification problem by MCMC simulations. The optimal number of features of the Prony series will be determined according to the information-theoretical criterion. The proposed method will be experimentally validated on different specimens. Poly(methyl methacrylate) (PMMA) and polypropylene (PP) will be investigated.

2. **Generate non-isothermal physical aging experimental data for thermoplastic at different temperatures**

   Non-isothermal physical aging tests at different temperatures will be performed on polycarbonate (PC) specimens. A bi-axial extensometer will measure the axial and transverse strains in specimens. The sources of measurement errors with an extensometer in thermo-mechanical testing will be analyzed. An experimental procedure for three-dimensional mechanical testing at high temperatures will be proposed to account for the drifts of the extensometer at elevated temperature.

3. **Extend the proposed method to simultaneously identify the viscoelastic, temperature and physical aging related model parameters**

   The proposed three-dimensional viscoelastic identification method based on the Bayesian framework will be extended by incorporating temperature and physical aging effects. The viscoelastic parameters and the shift factors will be identified simultane-

ously. The effects of temperature and physical aging on the three-dimensional mechanical properties of PC specimens, i.e., shear and bulk properties, will be investigated.

CHAPTER 4 SCIENTIFIC APPROACH

The specific objectives defined in Chapter 3 are addressed through one published and two submitted journal articles.

4.1 ARTICLE 1: On the tri-dimensional constitutive theory identification of linearly viscoelastic solids based on Bayesian framework

This article proposes a framework based on Bayesian inference to identify the three-dimensional constitutive model parameters for viscoelastic solids. A first contribution of this method is that it overcomes the ill-posedness of the identification problem. A second contribution of the method is that it allows for determining the minimum number of material parameters yielding an optimized accuracy. Finally, this method can be automated and packaged into codes that could be used by other researchers. This article fulfills the first specific objectives, which is to develop a robust and automated way to identify the three-dimensional viscoelastic parameters.

This article was published in the *International Journal of Solids and Structures*, Volumes 230–231, 111157 on July 14, 2021. DOI: 10.1016/j.ijsolstr.2021.111157. This journal publishes original research on mechanics of solids and structures. This article was written almost entirely by the author of this thesis.

4.2 ARTICLE 2: On the strain measurement for thermoplastics with bi-axial extensometer in thermo-mechanical testing: A case of characterizing temperature and physical aging effects on polycarbonate

This article analyzes the source of measurement errors with a bi-axial extensometer in thermo-mechanical testing and proposes a robust, straightforward and easy-to-follow experimental procedure to measure the axial and transverse strains at elevated temperature and to correct for drifts of the extensometer. Furthermore, the methodology proposed in this work can serve as a protocol to guide other types of three-dimensional thermo-mechanical testing with a bi-axial extensometer.

This article was submitted to the journal *Experimental Mechanics* on February 14, 2022. This journal publishes original research and brief technical notes on experimental mechanics. This article was written almost entirely by the author of this thesis.

4.3 ARTICLE 3: On the parameters identification of three-dimensional aging-temperature dependent viscoelastic solids through a Bayesian approach

This article extends the previously proposed Bayesian framework based method to simultaneously identify the viscoelastic, temperature, and physical aging related three-dimensional model parameters. The first contribution of this work is that it demonstrates the extensibility of the Bayesian framework method of parameter identification in complex constitutive models. The second contribution of this work is that the temperature and physical aging effects on the three-dimensional mechanical properties of viscoelastic solids are investigated concurrently, which is critical for the development of composites but rarely addressed.

This article was submitted to the journal *Mechanics of Time-Dependent Materials* on March 1, 2022. This journal publishes original research on the time-dependent behavior of materials and structures. This article was written almost entirely by the author of this thesis.

CHAPTER 5 ARTICLE 1: ON THE TRI-DIMENSIONAL CONSTITUTIVE THEORY IDENTIFICATION OF LINEARLY VISCOELASTIC SOLIDS BASED ON BAYESIAN FRAMEWORK

L. Yue, M. C. Heuzey, J. Jalbert and M. Lévesque (2021). *International Journal of Solids and Structures*, 230, 111157. Published on July 14, 2021. *Minor changes were made following the jury's comments when compared to the published version.*

5.1 Abstract

Linearly viscoelastic constitutive theories are usually expressed as a Prony series involving fourth order tensors and retardation times. Obtaining the numerical values of the terms involved in such constitutive models from experiments is an ill-posed problem in the sense that many parameter sets can adequately fit experimental data. Considering that the computational time involved in the simulation of the response of viscoelastic structures scales with the number of viscoelastic coefficients, it would be of considerable interest to devise identification strategies yielding the minimum number of parameters. We propose in this work a framework based on the Bayesian inference to reach this objective. We have applied our methodology to three-dimensional experimental data and validated the obtained constitutive theory on an independent data set, for two different viscoelastic materials. Our results demonstrated the robustness and adequacy of our method.

5.2 Introduction

Several methods have been proposed to estimate the linearly viscoelastic constitutive theories parameters whose kernels are Prony series. For example, the improved collocation method (Lévesque *et al.*, 2008), the iterative multi-data method (Kaschta and Schwarzl, 1994a, 1994b), the Padé-Laplace method (Claverie *et al.*, 1989; Yeramian and Claverie, 1987), etc., have been proposed to that end.

The computational cost for numerically implementing viscoelastic constitutive theories scales linearly with the number of terms in the Prony series. There is therefore an interest in determining the smallest number of relaxation terms that reproduces experimental results as accurately as possible.

The purpose of this work consists in proposing an *automated* and *robust* tri-dimensional parameters identification method for the linearly viscoelastic constitutive theories under the

Bayesian paradigm and experimentally validating it on two different viscoelastic materials. *Automation* means that the method should not need user input for each data set; *Robustness* means that the method should be able to handle different levels of measurement errors. The proposed method can not only identify viscoelastic parameters in the context of an ill-posed problem, but also is able to determine the smallest number of parameter numbers. Section 5.3 recalls the Prony series viscoelastic constitutive model, discusses existing parameters identification methods and Bayesian inference. The experimental details and methodologies are listed in Section 5.4. Section 5.5 details the proposed Bayesian inference based identification method and its implementation. Section 5.6 applies the proposed method to artificial data, polypropylene and polymethyl methacrylate specimens and compares its performance against the conventional method proposed by Lévesque *et al.* (2008). Section 6 concludes this work.

5.3 Background

5.3.1 Linear viscoelasticity

Thermodynamically based constitutive models

Thermodynamically based linearly viscoelastic constitutive theories were generalized by Biot (1954) and Bouleau (1991, 1999), and were recalled by Lévesque *et al.* (2008). For an adiabatic and isothermal loading history, the Clausius-Duhem inequality classically becomes (Lévesque *et al.*, 2008)

$$\left(\sigma_i - \frac{\partial \Psi}{\partial \varepsilon_i}\right)\dot{\varepsilon}_i - \frac{\partial \Psi}{\partial \chi_r}\dot{\chi}_r = f_i\dot{\varepsilon}_i + b_r\dot{\chi}_r \geq 0, \tag{5.1}$$

where $\boldsymbol{\chi}_r$ are internal variables characterizing the material's thermodynamical state. f_i and b_r are thermodynamic forces and are assumed as linear functions of the time variation of the state variables, i.e. $f_i = F_{ij}\dot{\varepsilon}_j$ and $b_r = B_{rs}\dot{\chi}_s$, with $\mathbf{F}$ and $\mathbf{B}$ being constant semi-positive tensors. $\Psi = \Psi(\boldsymbol{\varepsilon}, \boldsymbol{\chi})$ denotes Helmholtz's free energy. In linear viscoelasticity, Ψ, assumed as a second order Taylor expansion of the state variables around a equilibrium state Ψ_0, becomes

$$\Psi(\boldsymbol{\varepsilon}, \boldsymbol{\chi}) = \Psi_0 + \frac{1}{2}\boldsymbol{\varepsilon} : \mathbf{L}_1 : \boldsymbol{\varepsilon} + \boldsymbol{\varepsilon} : \mathbf{L}_2 : \boldsymbol{\chi} + \frac{1}{2}\boldsymbol{\chi} : \mathbf{L}_3 : \boldsymbol{\chi}, \tag{5.2}$$

where $\mathbf{L}_i$ forms a semi-definite positive fourth order tensor, which can be expressed as:

$$\mathbf{L}_1 = \frac{\partial \Psi}{\partial \varepsilon_i \partial \varepsilon_j}; \mathbf{L}_2 = \frac{\partial \Psi}{\partial \varepsilon_i \partial \chi_r}; \mathbf{L}_3 = \frac{\partial \Psi}{\partial \chi_r \partial \chi_s}. \tag{5.3}$$

When combining Equations (5.1) and (5.2), a three-dimensional linearly viscoelastic constitutive theory can be expressed as:

$$\boldsymbol{\sigma}(t) = \mathbf{L}_1 : \boldsymbol{\varepsilon}(t) + \mathbf{L}_2 : \boldsymbol{\chi} \tag{5.4a}$$

$$\mathbf{B} : \dot{\boldsymbol{\chi}} + \mathbf{L}_3 : \boldsymbol{\chi} + \mathbf{L}_2^{\intercal} : \boldsymbol{\varepsilon} = \mathbf{0}, \tag{5.4b}$$

where $\mathbf{B}$ is the fourth order identity tensor.

Solving differential Equation (5.4) yields

$$\boldsymbol{\sigma}(t) = \int_0^t \mathbf{C}(t-\tau) : \frac{\mathrm{d}\boldsymbol{\varepsilon}}{\mathrm{d}\tau}\mathrm{d}\tau, \tag{5.5}$$

with $\mathbf{C}(t)$ denoting the relaxation kernel that can be expressed as a Prony series as:

$$\mathbf{C}(t) = \mathbf{C}^{(0)} + \sum_{m=1}^{M} \mathbf{C}^{(m)} \exp[-\omega_m t], \tag{5.6}$$

where the relaxation stiffnesses $\mathbf{C}^{(m)}$ are positive semi-definite tensors, ω_m are reciprocal relaxation times associated to the stiffnesses $\mathbf{C}^{(m)}$. M is the total number of relaxation times. It should be noted that Equation (5.5) is a tridimensional form which is quite general. In one dimension, this constitutive law is typically referred to as the generalized Maxwell model, where parameter M represents the number of elements in the model.

Equation (5.4) can also yield the strain history as a function of the stress history as (Luk-Cyr *et al.*, 2013):

$$\boldsymbol{\varepsilon}(t) = \mathbf{A}_1 : \boldsymbol{\sigma}(t) - \mathbf{A}_2 : \boldsymbol{\xi} \tag{5.7a}$$

$$\mathbf{B} : \dot{\boldsymbol{\xi}} + \mathbf{A}_3 : \boldsymbol{\chi} + \mathbf{A}_2^{\intercal} : \boldsymbol{\sigma} = \mathbf{0}, \tag{5.7b}$$

where $\boldsymbol{\xi}$ are internal variables when stresses are applied. $\mathbf{A}_i$ forms a semi-definite positive fourth order tensor. Similarly, the hereditary integral form of Equation (5.7) reads:

$$\boldsymbol{\varepsilon}(t) = \int_0^t \mathbf{S}(t-\tau) : \frac{\mathrm{d}\boldsymbol{\sigma}}{\mathrm{d}\tau}\mathrm{d}\tau, \tag{5.8}$$

with

$$\mathbf{S}(t) = \mathbf{S}^{(0)} + \sum_{m=1}^{M} \mathbf{S}^{(m)}(1 - \exp[-\lambda_m t]), \tag{5.9}$$

where $\mathbf{S}(t)$ denotes the retardation kernel. The creep compliances $\mathbf{S}^{(m)}$ are positive semidefinite tensors and the λ_m are reciprocal creep times associated with the compliances $\mathbf{S}^{(m)}$.

For an isotropic material, the viscoelastic kernel functions have two independent components and can be decomposed as:

$$\mathbf{C}(t) = 3\kappa(t)\mathbf{J} + 2\mu(t)\mathbf{K} \tag{5.10a}$$

$$\mathbf{S}(t) = \frac{1}{3}\tilde{\kappa}(t)\mathbf{J} + \frac{1}{2}\tilde{\mu}(t)\mathbf{K} \tag{5.10b}$$

with

$$J_{ijkl} = \frac{1}{3}\delta_{ij}\delta_{kl} \tag{5.11a}$$

$$K_{ijkl} = \frac{1}{2}\left(\delta_{ik}\delta_{jl} + \delta_{il}\delta_{jk} - \frac{2}{3}\delta_{ij}\delta_{kl}\right), \tag{5.11b}$$

where δ_{ij} is the Kronecker-delta function. $\kappa(t)$ and $\mu(t)$ stand for the bulk and shear relaxation functions while $\tilde{\kappa}(t)$ and $\tilde{\mu}(t)$ represent the bulk and shear creep compliances. These functions can also be expressed as Prony series as

$$c(t) = c_0 + \sum_{m=1}^{M} c_m \exp[-\omega_m^c t], \text{ with } c = \kappa \text{ or } \mu, \tag{5.12a}$$

$$s(t) = \tilde{s}_0 + \sum_{m=1}^{M} \tilde{s}_m(1 - \exp[-\lambda_m^s t]), \text{ with } \tilde{s} = \tilde{\kappa} \text{ or } \tilde{\mu}, \tag{5.12b}$$

Note that ω_m^κ and ω_m^μ (or λ_m^κ and λ_m^μ) do not need to be identical to yield thermodynamically consistent constitutive theories (Lévesque *et al.*, 2007). Consequently, we did not force the equality between ω_m^κ and ω_m^μ , or λ_m^κ and λ_m^μ.

Numerical implementation

In order to implement viscoelastic constitutive equations to Finite Element (FE) packages, the solution of differential or integral equations, e.g. Equations (5.4), (5.5) and (5.8), need to be computed. The recursive scheme proposed by Taylor *et al.* (1970) is one of mostly used algorithm to compute the solution of hereditary integrals, like that of Equation (5.8). Taylor *et al.* (1970) assumed that the time derivative of load history was constant during each time increment and introduced a recursion formula to establish a relationship between successive time steps. Equation (5.8) becomes

$$\varepsilon(t^{n+1}) = \varepsilon^{n+1} = S^{(0)}\sigma^{n+1} + \sum_{m=1}^{M} S^{(m)}\left(\sigma^{n+1} - \sigma^0 - g_m^{n+1}\right). \tag{5.13}$$

The recursion formula g_m^{n+1} can be reduced to

$$g_m^{n+1} = g_m^n \exp[-\lambda_m \Delta t^{n+1}] + (\sigma^{n+1} - \sigma^n) h_m^{h+1}, \tag{5.14}$$

and

$$h_m^{n+1} = \frac{1 - \exp[-\lambda_m \Delta t^{n+1}]}{\lambda_m \Delta t^{n+1}} \text{ with } \Delta t^{n+1} = t^{n+1} - t^n. \tag{5.15}$$

5.3.2 Linearly viscoelastic constitutive theories parameters identification

Obtaining constitutive theory parameters from experimental data can be cast as a non-linear optimization problem as (Grédiac and Hild, 2012):

$$\hat{\boldsymbol{\theta}}_{LS} \in \underset{\theta \in \Theta}{\arg\min}\ \mathcal{J}(\boldsymbol{\theta}), \quad \mathcal{J}(\boldsymbol{\theta}) = \|\boldsymbol{g}(\boldsymbol{\theta}, \boldsymbol{x}) - \boldsymbol{y}\|_2, \tag{5.16}$$

where $\boldsymbol{\theta}$ stands for the viscoelastic parameters vector, for example, $\boldsymbol{\theta} = (c_0, c_1, \ldots, c_M, \omega_1, \ldots, \omega_M)$, $\boldsymbol{x} = (x_i : i = 1, \ldots, T)$ is the applied excitation vector given T discrete times i, $\boldsymbol{y} = (y_i : i = 1, \ldots, T)$ are the corresponding observed discrete times responses and $g(\boldsymbol{\theta}, \boldsymbol{x})$ represents the response predicted by a physical model using the parameters vector $\boldsymbol{\theta}$ submitted to an excitation $\boldsymbol{x}$. $\|\cdot\|_2$ denotes the l^2-norm. $\mathcal{J}(\boldsymbol{\theta})$ stands for the objective function. For the constitutive theory to meet thermodynamics principles, the parameters space Θ should be defined as $\Theta \in \mathbb{R}^+$. In particular, for the tri-dimensional constitutive model, the stiffness and compliance matrices should be positive semi-definite.

Ill-posed nature of the identification problem

Estimating Prony series viscoelastic parameters from static or dynamic mechanical testing data is a well-known *ill-posed problem*, which means that the model parameters identification from testing data is not uniquely assured and small perturbations in the data could induce significant variations in the identified parameters. To the knowledge of the authors, the ill-posedness of this problem comes from two aspects.

First, due to experimental constraints, the measurement of the full compliances or modulus over the whole time domain for the polymer cannot be performed. The mechanical testing is always carried out over a given time window. There may exist infinite numbers of kernel functions that represent experimental data in this experimental time window. As a result, parameters identified from testing data are generally not unique. Figure 5.1 shows an example where three different compliance functions can be very close over the experimental time window, but different outside. Each function can be approximated by a Prony series

model. Therefore, the existence of experimental time windows renders the ill-posedness of the identification problem. Moreover, Davies et al. reported that the relaxation spectra are determinable on a shorter interval than the experimental time window by the concept of sampling localization (Davies and Anderssen, 1997), expressed as:

$$\frac{e^{\pi/2}}{\omega_{\max}} < \omega < \frac{e^{-\pi/2}}{\omega_{\min}}, \tag{5.17}$$

where $\omega_{\min}$ and $\omega_{\max}$ corresponds to the smallest and the longest observations.

Second, the numerical solution of Equation (5.16) for Prony series is not unique. Considering a simple uni-dimensional case where the applied strain history is constant and is set to ε_0, Equation (5.5) becomes

$$\sigma(t) = \sum_{m=0}^{M} c_m^{\star} \exp[-\omega_m t], \tag{5.18}$$

with

$$c_i^{\star} = \varepsilon_0 c_i \text{ and } \omega_0 = 0. \tag{5.19}$$

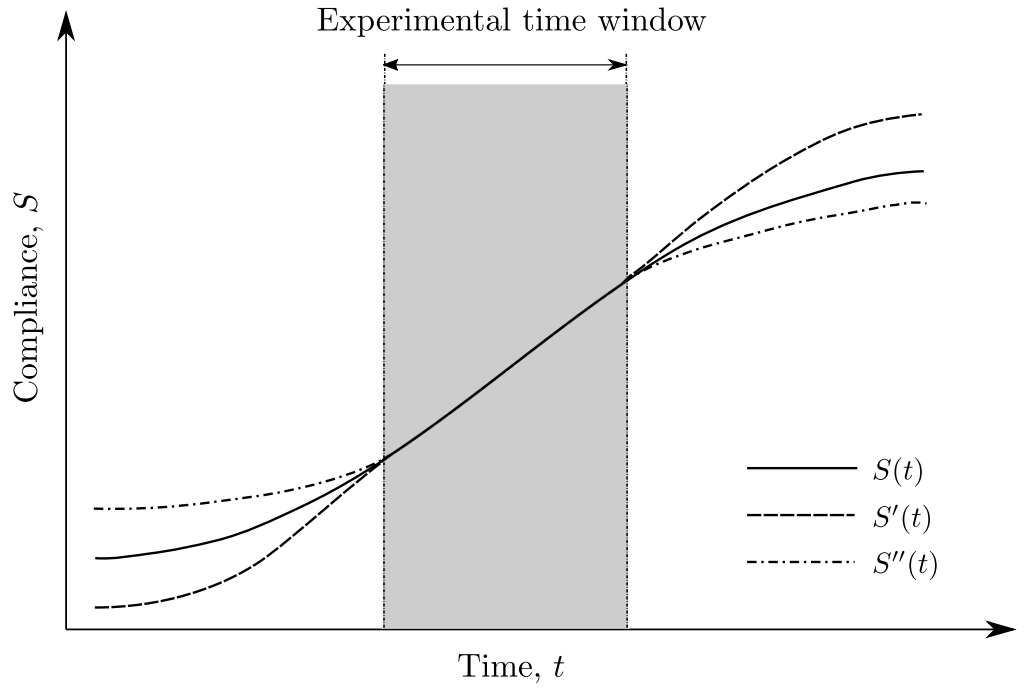

Figure 5.1 Three different compliance in the experimental time window. $S(t)$ represents the *true* compliance function for a given material. Functions $S'(t)$ and $S''(t)$ exhibit very close values only over the experimental time window. Three different functions results in the identical materials behavior in this range.

The associated parameter identification problem of Equation (5.16) is reduced to

$$\underset{\boldsymbol{c},\boldsymbol{\omega}\in\mathbb{R}^{+}}{\arg\min}\ \mathcal{J}(\boldsymbol{c},\boldsymbol{\omega}) = \sum_{i}\left(y_i - \sum_{m=0}^{M} c_m^{\star}\exp[-\omega_m t_i]\right)^2 \equiv \sum_{i} r_i^2, \tag{5.20}$$

where $y_i = \hat{\sigma}_i$ denotes the measured stress data at time t_i. Equation (5.20) refers to a classical positive exponential sums fitting problem which has been discussed over the past several decades (Holmström and Petersson, 2002; Istratov and Vyvenko, 1999). The ill-posedness of this problem was firstly reported by Lanczos (1988). Lanczos generated data series using three exponentials and fitted them equally well by several different exponentials. Similarly, Ruhe (1980) showed that an arbitrary exponential can be well approximated by a sum of others. Liu (2001) demonstrated this feature.

Furthermore, solving Equation (5.20) is difficult, especially when the number of exponential terms M becomes large. Gaussian-Newton or Levenberg-Marquardt algorithms (Gill *et al.*, 2019; Levenberg, 1944; Marquardt, 1963) are conventionally used to solve this nonlinear least-square problem. The Jacobian matrix $\mathbf{D}$ and Hessian matrix $\mathbf{H}$ of the objective function $\mathcal{J}$ are expressed as

$$D_{ij} = \partial r_i/\partial\theta_j,\ \boldsymbol{\theta} = (c_0,\ldots,c_m,\omega_1,\ldots,\omega_m)\,, \tag{5.21a}$$

$$H_{ij} = \frac{1}{2}\frac{\partial^2\mathcal{J}}{\partial\theta_k\partial\theta_j} = \sum_{i}\left(\frac{\partial r_i}{\partial\theta_k}\right)\left(\frac{\partial r_i}{\partial\theta_j}\right) + \sum_{i} r_i\frac{\partial^2 r_i}{\partial\theta_k\partial\theta_j}, \tag{5.21b}$$

with

$$\frac{\partial r_i}{\partial c_m} = -\exp(-\omega_m t_i), \tag{5.22a}$$

$$\frac{\partial r_i}{\partial \omega_m} = -c_m t_i\exp(-\omega_m t_i). \tag{5.22b}$$

Jacobian and Hessian matrices are usually needed to be computed in these algorithms and are sensitive to the variation of parameters ω_m (Ruhe, 1980). Tiny variance in parameters could lead to large perturbations in exponentials. The Hessian matrix may be easily "stuck" within the ill-condition caused by some specific parameters during the optimization process or the empirical data noise (Varah, 1985). Therefore, Equation (5.20) is usually ill-posed, even for a simple problem with small number of exponentials M.

Analysis of existing works on the linearly viscoelastic parameters identification

To overcome the ill-posedness of viscoelastic parameters identification, scores of methods have been proposed since 1960s. Existing viscoelastic parameters identification methods rely on the least square norm and can be divided into three categories.

Fixing a priori characteristic times This is the most used method in which the number and values of characteristics times (ω_m or λ_m) are fixed a priori and the associated moduli or compliances need to be estimated. Schapery (1962) proposed the collocation method by assuming logarithmic equidistant retardation times. However, this method does not enforce thermodynamics restrictions. Lévesque *et al.* (2008) improved this method by introducing an optimization variable to ensure the non-negativeness of parameters. For example, let the unknown stiffness value be $c = \alpha^2$ and α be the parameters to identify. This variable changes the constrained optimization problem to an unconstrained one, which decreases the difficulties of solving. The iterative multi-data method of Kaschta and Schwarzl (1994a, 1994b) is an extension of the classical collocation method (no thermodynamics restrictions imposed). Instead of fixing the retardation times a priori, this method assumes that the retardation times are logarithmically equidistant with a prescribed spacing and starts with the first retardation time. The parameters to be optimized are therefore the first retardation time and compliances. If one or more parameters are negative, the value of the first retardation time is slightly varied until all obtained parameters are positive. Some others methods can also be found in the literature (Gerlach and Matzenmiller, 2005).

These techniques can tremendously reduce the difficulties of solving Equation (5.16). However, the pre-selection of number and values of relaxation or retardation times might not be optimal and the resulting parameter sets might be unnecessarily large. Defining the most efficient number of retardation times, and their values, is still an open question.

Iteration free methods These methods can simultaneously obtain the tensorial values as well as the characteristic times by defining dedicated mathematical structures. Yeramian reported a method combining Padé approximation and the Laplace transformation of Prony series, which enables the exact identification of characteristic times (Claverie *et al.*, 1989; Yeramian and Claverie, 1987). Jalocha et al. have constructed a specific mathematical structure based on the Fourier transformation of Prony series and computed characteristic times using the Krein-Nudelman theorem (Krein and Nudelman, 1998) from complex analysis (Jalocha *et al.*, 2015).

However, the accuracy of these methods is strongly influenced by the experimental data

uncertainties. Halvorson (1992) reported that these methods could amplify the effect of experimental noise on the identified parameters in an unpredictable way.

Stochastic strategies Stochastic approaches have also been proposed to estimate Prony series model parameters, such as the Simulated Annealing (SA) algorithm (Jensen, 2002; Tscharnuter *et al.*, 2011a) or the Bayesian framework with *Markov Chain Monte Carlo* (MCMC) (Haario *et al.*, 2014; Hansen, 2008; Hernández *et al.*, 2017). Rather than presetting characteristic times, these approaches provide a quantitative means to estimate the optimal number of series. Haario *et al.* (2014) introduced an indicator, called *indeterminacy*, to characterize the parameters identification non-uniqueness. Similarly, Freund and Ewoldt (2015) proposed the *evidence* to determine the most adequate model based on user input model errors parameters.

It should be noted that some stochastic methods are not adequate for solving the Prony series identification problem. For example, the SA algorithm solves the optimization problem directly by the Metropolis algorithm. However, the ill-posedness of the Prony series problem may result in discrepancies with an inappropriate choice of the control values of the SA algorithm, which make it difficult to implement it in an automated way. The Maximum Likelihood Estimation (MLE) method constructs a probability distribution based on the cost function, then finds the parameter to maximize the likelihood. Solving the MLE requires the computation of the Hessain matrix, which is the essential difficulty for the Prony series identification problem.

The existing Bayesian methods used to identify Prony series viscoelastic parameters also still require some clarifications and are non-automated. For instance, the error analysis still depends on the artificial choice of user in a arbitrary way. Nevertheless, the Bayesian framework is highly attractive because of its advantages in Prony series parameters identification, when compared to other methods.

First, using a Bayesian framework to estimate parameters does not need computing the derivatives of the objective function, so that the ill-posedness from the ill-conditioned Jacobian and Hessian matrices can be avoided. Second, the MCMC can explore several modes of the model, making the procedure more robust on the non-identifiability issue. Third, the estimation of the experimental errors can be embedded under the Bayesian paradigm, permitting an automated choice of the weighting of the distances in Equation (5.16) based on the data. Fourth, rich information can be drawn from the resulting posterior probabilities of parameters, which allows the uncertainty qualification for the identified model. Moreover, some information criteria can be performed to determine the optimal number of characteristic

times M of the Prony series model.

Therefore, in this work we chose the Bayesian framework to investigate the identification of tri-dimensional Prony series viscoelastic parameter and develop a numerical tool based on it which is robust and automated.

5.3.3 Bayesian framework

For solving the identification problems expressed in Equation (5.16) under the Bayesian paradigm, the constitutive model parameters are modeled as random variables. The randomness characterizes the degree of information concerning the unknown parameters and is modeled with probability distributions. The solution consists in a posterior distribution of the parameters which includes the information provided by the data and the prior information of parameters (Kaipio and Somersalo, 2006).

In a mechanical experiment, the relation between experimental measurements $\boldsymbol{Y}$ and model predictions $\boldsymbol{g}(\boldsymbol{\theta}, \boldsymbol{x})$ can be drawn by an observation model with an additive error $\boldsymbol{\epsilon}$ as

$$Y_i = g(\boldsymbol{\theta}; x_i) + \epsilon_i, \ i = 1, \ldots, T, \tag{5.23a}$$

$$\epsilon_i \sim \mathcal{N}(0, \sigma_\epsilon^2), \tag{5.23b}$$

where $\mathcal{N}$ denotes the Gaussian distribution, $\boldsymbol{\epsilon}$ is modeled as a zero mean Gaussian variable with variance σ_ϵ^2. This model has been used in applications like the relaxation spectrum estimation (Hansen, 2008) or the viscoelastic parameters identification (Haario *et al.*, 2014; Hernández *et al.*, 2017).

Bayesian inference

Bayes' theorem can be expressed as:

$$f_{(\boldsymbol{\theta}|\boldsymbol{Y}=\boldsymbol{y})}(\boldsymbol{\theta}) = \frac{f_{(\boldsymbol{Y}|\boldsymbol{\theta})}(\boldsymbol{y}) \times f_{\boldsymbol{\theta}}(\boldsymbol{\theta})}{f_{\boldsymbol{Y}}(\boldsymbol{y})}, \tag{5.24}$$

where $f_{(\boldsymbol{\theta}|\boldsymbol{Y}=\boldsymbol{y})}(\boldsymbol{\theta})$ is the posterior distribution of $\boldsymbol{\theta}$ after observing the data $\boldsymbol{y}$, $f_{(\boldsymbol{Y}|\boldsymbol{\theta})}(\boldsymbol{y})$ is the likelihood, $f_{\boldsymbol{\theta}}(\boldsymbol{\theta})$ is the prior distribution of $\boldsymbol{\theta}$ and $f_{\boldsymbol{Y}}(\boldsymbol{y})$ is the normalization constant. The prior distribution represents the knowledge on the model parameters before performing the experimentation and the posterior distribution consists in the updated knowledge when accounting for experimentally observed data. Non-informative prior distribution can be used

when no information is available on $\boldsymbol{\theta}$ before the experimentation. Otherwise, an informative prior on $\boldsymbol{\theta}$ can be used.

The likelihood function can be constructed from Equation (5.23), which can be written as:

$$Y_i - g(\boldsymbol{\theta}; x_i) \sim \mathcal{N}(0, \sigma_\epsilon^2), \tag{5.25}$$

then

$$Y_i \sim \mathcal{N}(g(\boldsymbol{\theta}; x_i), \sigma_\epsilon^2). \tag{5.26}$$

Therefore, the likelihood function, i.e. the probability distribution of $\boldsymbol{Y}$ for given value of unknown parameters $\boldsymbol{\theta}$, becomes

$$f_{(\boldsymbol{Y}|\boldsymbol{\theta})}(\boldsymbol{y}) \propto \exp\left\{-\frac{1}{2\sigma_\epsilon^2} \left|\left| \boldsymbol{y} - \boldsymbol{g}(\boldsymbol{\theta}; \boldsymbol{x}) \right|\right|_2\right\} \tag{5.27}$$

It is interesting to note that the maximum likelihood function (5.27) is formally equivalent to the non-linear least-square optimization problem as Equation (5.16).

Once the posterior distribution of unknown parameters have been obtained, point estimates could also be defined under the Bayesian paradigm. A common Bayesian point estimate corresponds to the mode of the posterior distribution:

$$\hat{\boldsymbol{\theta}}_{\text{MAP}} = \underset{\boldsymbol{\theta} \in \Theta}{\arg\max}\ f_{(\boldsymbol{\theta}|\boldsymbol{Y}=\boldsymbol{y})}(\boldsymbol{\theta}), \tag{5.28}$$

referred to as the *maximum a posteriori* (MAP) estimate.

Markov Chain Monte Carlo algorithm

The posterior probability function for viscoelastic parameters identification is unavailable under a closed analytical form. Therefore, numerical methods are needed to perform statistical inference. The *Markov Chain Monte Carlo* simulations are frequently used to generate samples from the posterior distribution (Andrieu *et al.*, 2003).

The core of MCMC simulations is to obtain a random sample of the parameter posterior distribution. Various sampling algorithms have been developed, including the Gibbs algorithm and Metropolis-Hastings algorithm which are commonly used (Gelman *et al.*, 2013).

Gaussian variance estimation

The variance σ_ϵ^2 in Equation (5.27) is generally unknown and it could be estimated with the data by incorporating this parameter in the statistical model. Its complement conditional distribution can be estimated through the inverse Gamma distribution (Gelman *et al.*, 2013), as:

$$f_{(\sigma_\epsilon^2|\boldsymbol{Y}=\boldsymbol{y})}(\sigma_\epsilon^2) \sim \text{InvGamma}\left\{\frac{T}{2}\,,\,\frac{1}{2}\sum_{i=1}^{T}\left(y_i - g(\boldsymbol{\theta};x_i)\right)^2\right\}. \tag{5.29}$$

Updating its value within the MCMC algorithm is straightforward.

Model selection

Increasing the number of relaxation times M in the Prony series model can improve the model fit of the model prediction. However, a large number of terms may lead to overfitting, reducing the prediction accuracy and rising the required computation cost in the numerical simulation of viscoelastic structures.

To balance the model fit and the model complexity, several information criteria for model selection have been proposed in Bayesian analysis (Bishop, 2006). One of mostly used criterion is the *Bayesian Information Criterion* (BIC), which is expressed as:

$$\text{BIC}(M) = \ln f_{(\boldsymbol{Y}|\hat{\boldsymbol{\theta}}_{\text{MAP}})}(\boldsymbol{y}) - \frac{1}{2}(2M+1)\ln T, \tag{5.30}$$

where M stands for the number of parameters of the model, and T is the total number of data points. The first term of this criterion measures the model fit and the second term penalizes for complexity. Therefore, the optimal number of terms in Prony series can be obtained by maximizing the BIC.

Interval estimation

The prediction interval provides an interval for the future predictions based on the previous observations and the estimated model. The $(1-\alpha)\%$ prediction interval of the prediction $\hat{y}_h$ at the point x_h is given by

$$\hat{y}_h \pm t_{(1-\alpha/2,n-m)} \times \sqrt{\text{MSE} \times \left(1 + \frac{1}{n} + \frac{(x_h-\bar{x})^2}{\sum(x_i-\bar{x})^2}\right)}, \tag{5.31}$$

where $\{(x_i, y_i),\ i = 1,\ldots,n\}$ are observations, $t_{(1-\alpha/2,n-m)}$ is the t-multiplier which has $n-m$ degrees of freedom and m is the number of model parameters. MSE stands for the mean

square error with $n - m$ degrees of freedom, i.e.,

$$\mathrm{MSE} = \frac{\sum(y_i - \hat{y}_i)^2}{n - m}. \tag{5.32}$$

The credible interval is the interval based on the Bayesian inference that can describe the probability of an unknown parameter from the posterior probability. The $(1 - \alpha)\%$ credible interval is defined as:

$$\int f_{(\theta|Y=y)}(\theta)\mathrm{d}\theta = 1 - \alpha. \tag{5.33}$$

The computation of the credible interval is straightforward using the random sample of the posterior distribution obtained with the MCMC procedure.

5.4 Materials and methods

5.4.1 Materials

Poly(methyl methacrylate) (PMMA) and polypropylene (PP) were mechanically tested. Both materials were obtained from McMaster-Carr® (product numbers 8560K257 and 8742K233, respectively). PMMA specimens were cut by laser cutting from a rectangular sheet fabricated by casting. PP specimens were water jet cut from a rectangular sheet fabricated by extrusion. The sheet thickness was 4.23 mm.

Two different specimen geometries were investigated. `ASTM D638` standard type-I specimens were used to identify material parameters and to validate uni-dimensional model predictions, while the complex geometry specimen shown in Figure 5.2 was used to validate tri-dimensional model predictions. These two types of geometries are noted as *simple* and *complex* in the following.

5.4.2 Equipment

Tensile creep testing was performed with a MTS Insight® machine equipped with a 1 000 N load cell, at room temperature.

Axial and transverse strains were measured simultaneously with Digital Image Correlation (DIC) during each test. The investigation area in DIC analysis for simple and complex specimens and the paths used to quantitatively compare the experimental response and numerically predicted response are showed in Figure 5.3.

The DIC analysis was performed with a *VIC-3D* setup from *Correlated Solutions* (Correlated,

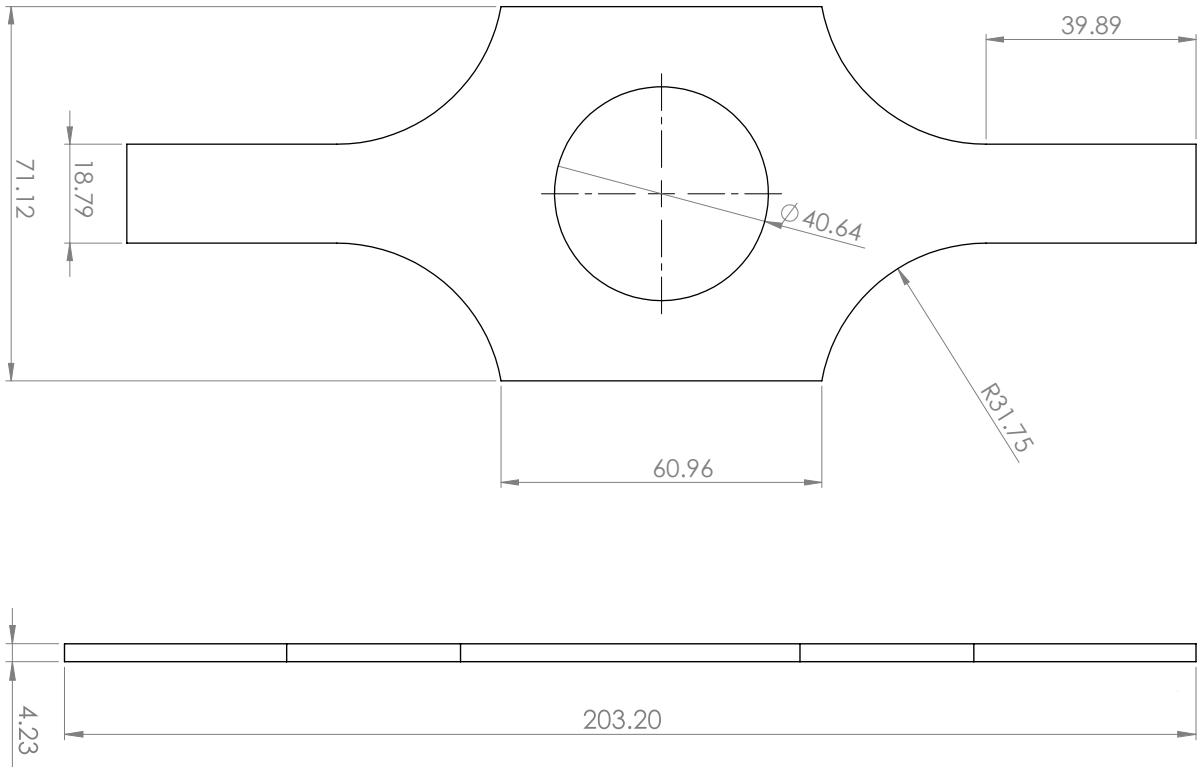

Figure 5.2 Dimensions of the complex geometry specimen (in mm).

2010). The technique relies on two parameters. The *subset* is defined as the number of pixels in the area used to track displacement between images. The *step size* is the spacing of the points that are analyzed during correlation (Tabiai *et al.*, 2019). These two parameters were set to the values automatically suggested by *VIC-3D*. The *strain filter* is also needed to smooth calculated strains. Table 5.1 lists the *VIC-3D* parameters used in this work.

5.4.3 Experiments

Determination of the linearly viscoelastic regime

The first step to identify the viscoelastic theory parameters of a polymer material is to determine its domain of linearity. Let $g(\boldsymbol{\sigma}) = \boldsymbol{\varepsilon}$ be the constitutive model, where it is

Table 5.1: Parameters used in VIC-3D analysis.

Geometry	Subset	Step	Strain filter
Simple	43	7	15
Complex	43	7	27

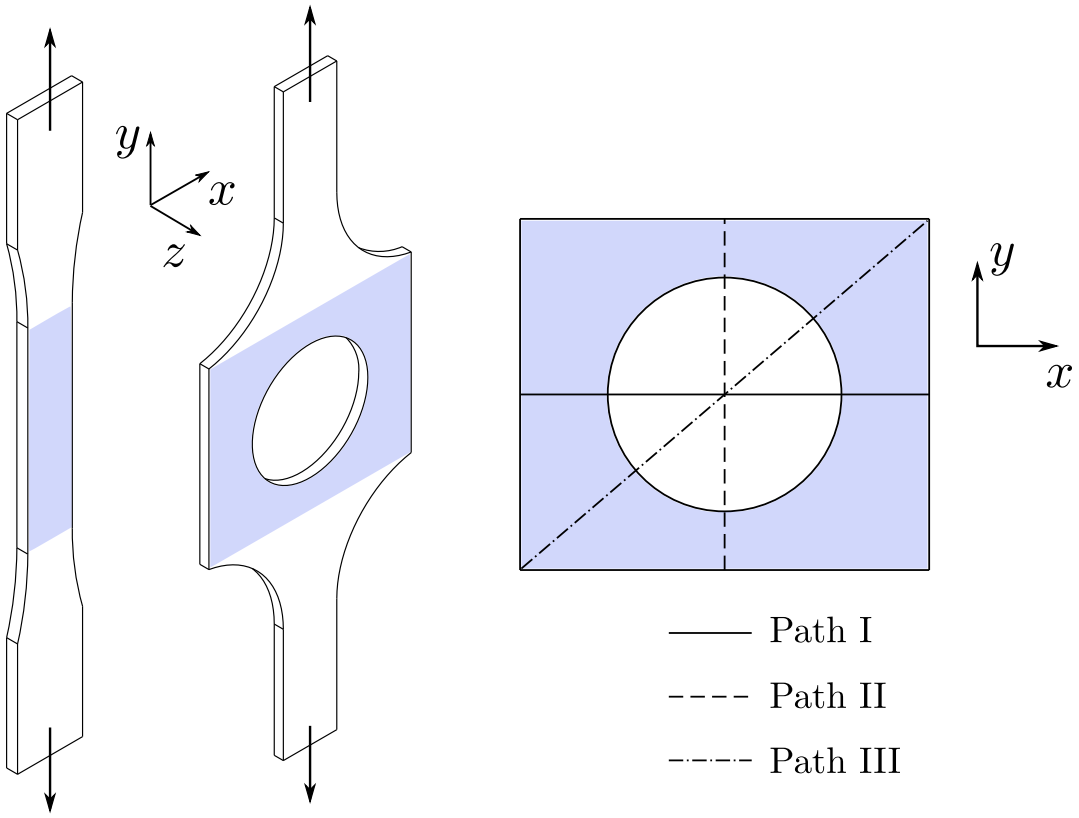

Figure 5.3 Illustration of specimens used in tensile creep tests. The arrows show the applied loading direction. The colored zones indicate the DIC investigation areas. Crossed lines on the right subfigure show the paths used to quantitatively compare between DIC measurements and FEM strain computations.

implied that $\boldsymbol{\sigma}$ and $\boldsymbol{\varepsilon}$ are functions of time. A linearly viscoelastic constitutive model should satisfy:

1. $g(\lambda\boldsymbol{\sigma}) = \lambda g(\boldsymbol{\sigma})$ where $\lambda \in \mathbb{R}$, $\forall t$,
2. $g(\boldsymbol{\sigma}^1 + \boldsymbol{\sigma}^2) = g(\boldsymbol{\sigma}^1) + g(\boldsymbol{\sigma}^2) = \boldsymbol{\varepsilon}^1 + \boldsymbol{\varepsilon}^2$, $\forall t$.

Let $\boldsymbol{\sigma}^0$ be a sufficiently small stress for which it is assumed that the material remains in its linearity range. The stress history $\boldsymbol{\sigma}^a = \lambda_a \boldsymbol{\sigma}^0$ can be assumed linear if:

$$R_{ij}\left(\boldsymbol{\sigma}^a(t)\right) \equiv \frac{\varepsilon^a_{ij}(t)/\lambda_a}{\varepsilon^0_{ij}(t)} = \frac{g(\sigma^a_{ij}(t))/\lambda_a}{g(\sigma^0_{ij}(t))} = \frac{\lambda_a g(\sigma^0_{ij}(t))/\lambda_a}{g(\sigma^0_{ij}(t))} = 1, \quad \forall t, \text{ and no sum on } ij, \tag{5.34}$$

where R_{ij} is called herein *normalized ratio* of component ij.

In this work, for both polymers, the σ_0 was set to 3 MPa. Creep tests with applied creep stresses were of 4 MPa, 5 MPa, 6 MPa, ... were sequentially performed until the ratio R was no longer constant.

It should be noted that it is impossible to perform an ideal creep experiment, during which a constant stress is applied at $t = 0^+$. There is always a ramp before the desired load is attained in practice. A constant displacement rate 2 mm/min was imposed during the ramp phase. The ramp duration varied with the applied load level, which led to loading histories that were not identical for each load level. Therefore, the ratio R was slightly larger than $\mathbf{1}$ and had a difference at the beginning caused by the ramp effect.This effect can be ignored for the latter part of experiments. Therefore, the criterion used to determine the linear regime of viscoelasticity is that the normalized ratio R remains constant in the latter phase of the creep experiment. The variance of R was used to evaluate this criterion, which is defined as:

$$\mathrm{Var}(R_{ij}(\boldsymbol{\sigma}^a)) = \frac{\sum_{i=1}^{T}\left(R_{ij}(\sigma^a(t_i)) - \bar{R}_{ij}\right)^2}{T-1} \tag{5.35}$$

where $\bar{R}_{ij}$ is the mean of $R_{ij}(\boldsymbol{\sigma}^a)$. It was assumed that the material remained in its linear regime when the variance of R_{ij} was lower than 1×10^{-6}.

Choice of loading histories

The loading histories used to identify and validate the viscoelastic constitutive theory could be selected once the linearly viscoelastic domain was determined, for each material. Figure 5.4 illustrates the typical loading history used. The applied loading initially increases to σ_1 and dwells for a period Δt_1, then the applied stress decreases to σ_2 and dwells for a period of time Δt_2. This procedure continued until the loading value reached the linearly viscoelastic limit of the material. Figure 5.5 plots the loading histories chosen for parameters identification and for the uni-dimensional validation for PMMA and PP.

Validation of identified Prony series model

The tri-dimensional viscoelastic parameters can be identified by the proposed Bayesian based method. This method is detailed in Section 5.5. The identified Prony series model was validated in two ways. The first one used the simple geometry specimens submitted to a load history which was different from that used to identify the parameters. The second method consists in mechanically testing a complex geometry specimen. The strains measured by DIC and predicted by Finite Element Method (FEM) simulation were compared to validate the identified tri-dimensional constitutive theory.

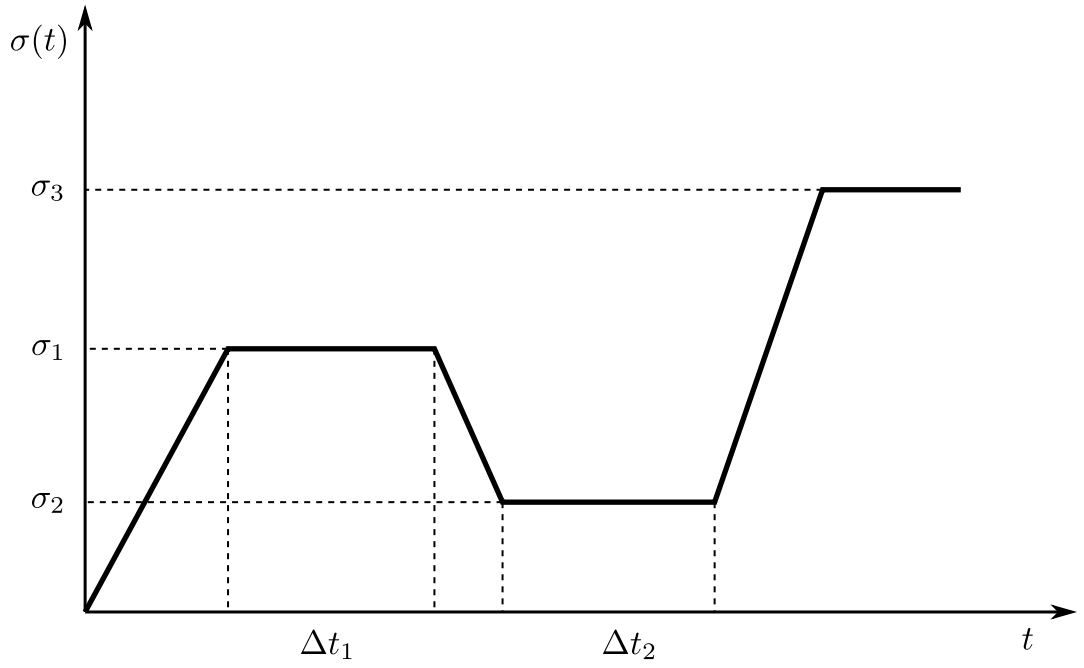

Figure 5.4 Stress histories used to identify and validate viscoelastic material constitutive theories.

Figure 5.6 illustrates the loading history used to validate the identified model on the complex specimens. The measured and predicted full strain fields were investigated at three different time steps t_a, t_b and t_c. The applied loads F_a, F_b and F_c varied from one material to the next and depended on their linearly viscoelastic regime. To ensure the specimens remained in the linearly viscoelastic regime, a preliminary FEM analysis was performed to determine if the obtained maximum von Mises stress σ'_{max} exceeded the linear viscoelasticity limit σ_{LV} for the material. If so, the applied loads were decreased to ensure that $\sigma'_{max} \leqslant \sigma_{LV}$.

5.5 Parameters identification

5.5.1 Simultaneous identification of bulk and shear creep compliances from mechanical testing

The stress tensor $\boldsymbol{\sigma}$ in the gauge section of a standardized uniaxial tensile testing specimen submitted to a uniaxial load reads

$$\sigma_{11} = \sigma_{\mathrm{I}}, \text{ others } \sigma_{ij} = 0, \tag{5.36}$$

where σ_{I} is the applied stress.

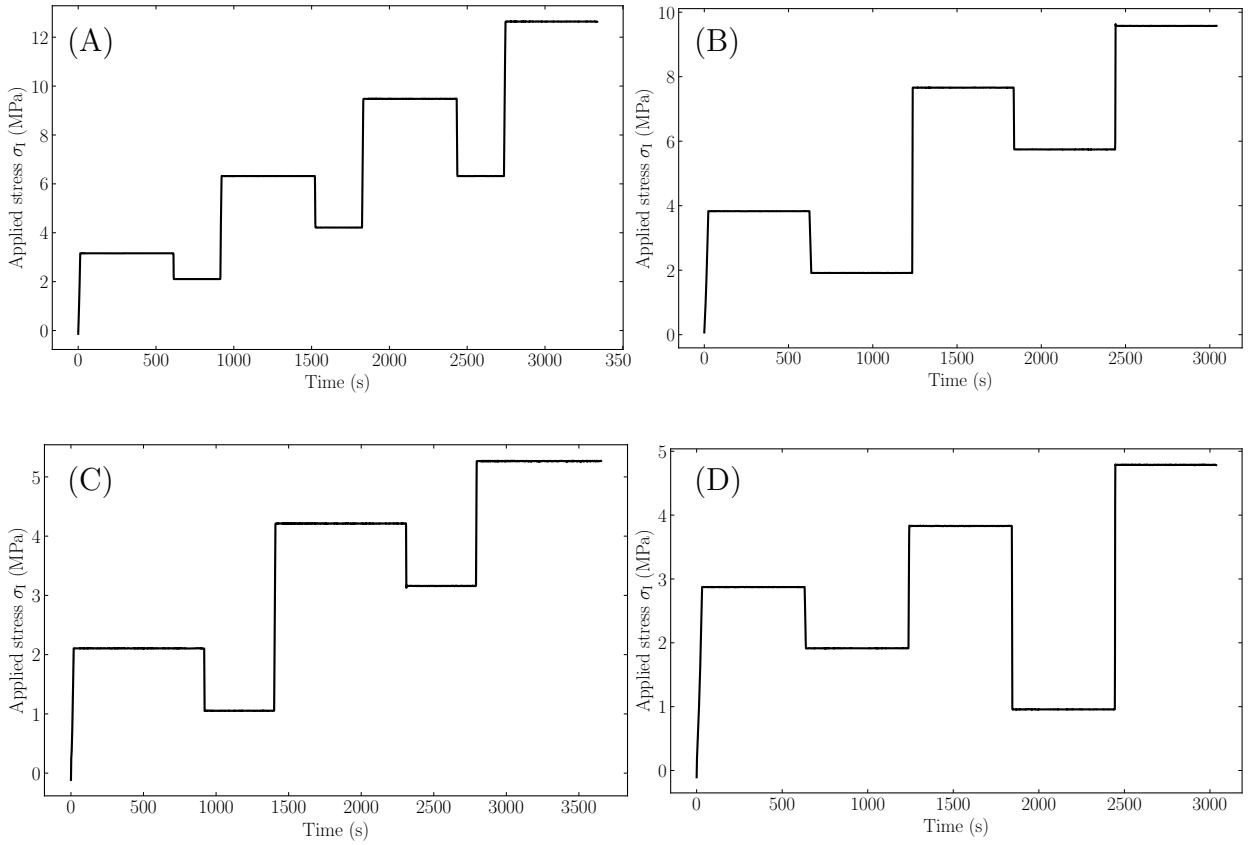

Figure 5.5 Load histories used to identify and to validate the linearly viscoelastic parameters on simple geometry specimens for PMMA and PP. (A) PMMA identification load history; (B) PMMA validation load history; (C) PP identification load history; (D) PP validation load history.

The resulting strain tensor $\boldsymbol{\varepsilon}$ reads

$$\varepsilon_{11} = \varepsilon_{\mathrm{I}},\ \varepsilon_{22} = \varepsilon_{33} = \varepsilon_{\mathrm{II}},\ \text{others } \varepsilon_{ij} = 0. \tag{5.37}$$

Let's define

$$\varepsilon^{\dagger} = \varepsilon_{\mathrm{I}} - \varepsilon_{\mathrm{II}}, \tag{5.38a}$$

$$\varepsilon^{\ddagger} = \varepsilon_{\mathrm{I}} + 2\varepsilon_{\mathrm{II}}. \tag{5.38b}$$

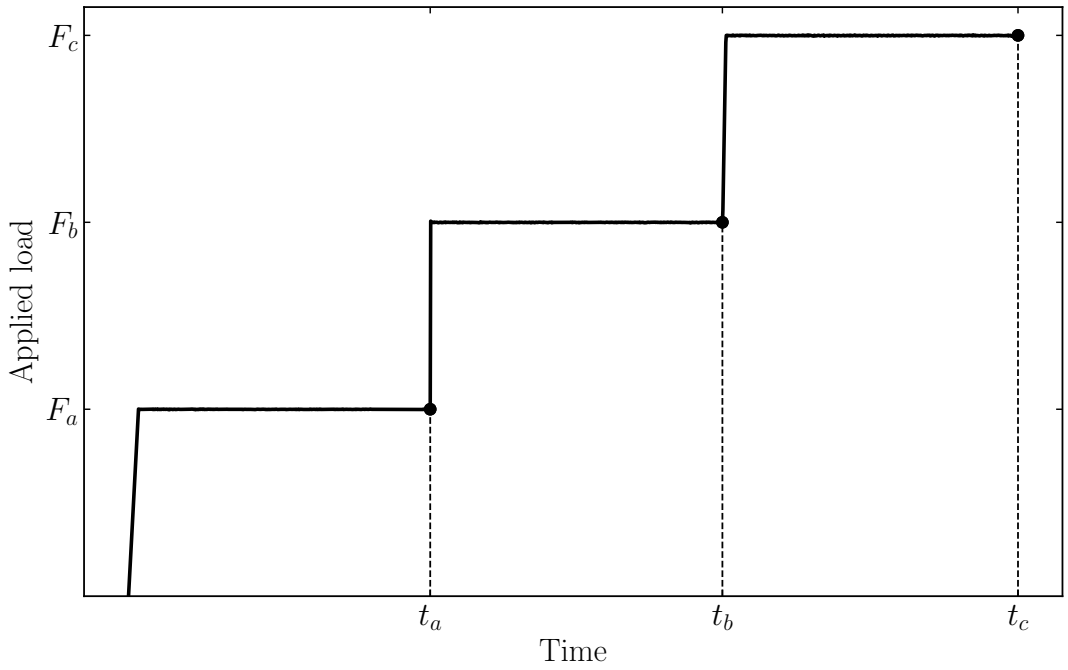

Figure 5.6 Load history used to validate the identified parameters on complex geometry specimens.

Combining Equations (5.8, 5.10, 5.12) yields,

$$2\varepsilon^{\dagger}(t) = \tilde{\mu}_0\sigma_{\mathrm{I}}(t) + \int_0^t \sum_{m=1}^{M} \tilde{\mu}_m(1 - \exp[-\lambda_m^{\mu}(t-\tau)])\frac{\mathrm{d}\sigma_{\mathrm{I}}}{\mathrm{d}\tau}\mathrm{d}\tau, \tag{5.39a}$$

$$3\varepsilon^{\ddagger}(t) = \tilde{\kappa}_0\sigma_{\mathrm{I}}(t) + \int_0^t \sum_{m=1}^{M} \tilde{\kappa}_m(1 - \exp[-\lambda_m^{\kappa}(t-\tau)])\frac{\mathrm{d}\sigma_{\mathrm{I}}}{\mathrm{d}\tau}\mathrm{d}\tau. \tag{5.39b}$$

Equation (5.39) shows that the bulk creep compliance $\tilde{\kappa}(t)$ and the shear creep compliance $\tilde{\mu}(t)$ can be identified independently of each other and that the three-dimensional optimization problem reduces to two uni-dimensional problems.

Consider an experimental creep-recovery test where the axial load $\hat{\sigma}_{\mathrm{I}}$ is applied and measured by a load cell and the resulting strains $\hat{\varepsilon}_{\mathrm{I}}$ and $\hat{\varepsilon}_{\mathrm{II}}$ are measured. $\hat{\varepsilon}^{\dagger}$ and $\hat{\varepsilon}^{\ddagger}$ can be computed from Equation (5.38) with $\hat{\sigma}_{\mathrm{I}}$. Inputting $\hat{\sigma}_{\mathrm{I}}$ into Equation (5.39) yields predicted $\check{\boldsymbol{\varepsilon}}^{\dagger}$ and $\check{\boldsymbol{\varepsilon}}^{\ddagger}$ as

$$\check{\boldsymbol{\varepsilon}}^{\dagger} = \boldsymbol{g}_{\mu}\left(\boldsymbol{\theta}^{\mu}; \hat{\boldsymbol{\sigma}}_{\mathrm{I}}\right), \tag{5.40a}$$

$$\check{\boldsymbol{\varepsilon}}^{\ddagger} = \boldsymbol{g}_{\kappa}\left(\boldsymbol{\theta}^{\kappa}; \hat{\boldsymbol{\sigma}}_{\mathrm{I}}\right), \tag{5.40b}$$

with

$$\boldsymbol{\theta}^{\mu} = \{\tilde{\mu}_0, \tilde{\mu}_1, , \ldots, \tilde{\mu}_M, \lambda_1^{\mu}, \ldots, \lambda_M^{\mu}\}\,, \tag{5.41a}$$

$$\boldsymbol{\theta}^{\kappa} = \{\tilde{\kappa}_0, \tilde{\kappa}_1, , \ldots, \tilde{\kappa}_M, \lambda_1^{\kappa}, \ldots, \lambda_M^{\kappa}\}\,, \tag{5.41b}$$

where $\boldsymbol{g}_{\mu}$ and $\boldsymbol{g}_{\kappa}$ represent the linearly viscoelastic constitutive theory of Equation (5.39). The identification problem therefore reduces to:

$$\boldsymbol{\theta}^{\mu} = \underset{\boldsymbol{\theta}^{\mu}\in\mathbb{R}^{+}}{\arg\min} \sum_{i=1}^{N} \left\| \boldsymbol{g}_{\mu}\left(\boldsymbol{\theta}^{\mu}; \hat{\boldsymbol{\sigma}}_{\mathrm{I}}^{(\mathrm{i})}\right) - \hat{\boldsymbol{\varepsilon}}^{\dagger(\mathrm{i})} \right\|_2, \tag{5.42a}$$

$$\boldsymbol{\theta}^{\kappa} = \underset{\boldsymbol{\theta}^{\kappa}\in\mathbb{R}^{+}}{\arg\min} \sum_{i=1}^{N} \left\| \boldsymbol{g}_{\kappa}\left(\boldsymbol{\theta}^{\kappa}; \hat{\boldsymbol{\sigma}}_{\mathrm{I}}^{(\mathrm{i})}\right) - \hat{\boldsymbol{\varepsilon}}^{\ddagger(\mathrm{i})} \right\|_2, \tag{5.42b}$$

where $\{\hat{\boldsymbol{\sigma}}_{\mathrm{I}}^{(\mathrm{i})}, \hat{\boldsymbol{\varepsilon}}_{\mathrm{I}}^{(\mathrm{i})}, \hat{\boldsymbol{\varepsilon}}_{\mathrm{II}}^{(\mathrm{i})}\},\ i = 1, \ldots, N$, are experimental data sets, N denoting the number of experiments.

5.5.2 Viscoelastic model prediction computation

The model predictions $\boldsymbol{g}(\boldsymbol{\theta}; \boldsymbol{x})$ need to be computed through Equation (5.8) for identifying the Prony series parameters from tensile creep test featuring arbitrary applied load histories. In this study, the numerical solution was computed using real input loading data through the recursive scheme. The time step sizes Δt corresponded to the strain measurement acquisition frequency, which was of 1 Hz.

5.5.3 Additive error assumption

In the Bayesian framework, the additive error $\boldsymbol{\epsilon}$ is assumed as a zero mean Gaussian. The applicability of this assumption in the Prony series viscoelastic parameter identification needs to be justified. In the current problem, the errors principally come from three sources.

Experimental error The experimental error consists in the measurement error, which is introduced by the DIC measurements and analysis. This measurement error is noted as $\boldsymbol{\epsilon}_e$ and can be considered as a Gaussian distribution (He *et al.*, 2018; Reu *et al.*, 2009). The variance DIC measurement error $\boldsymbol{\epsilon}_e$ depends on the subset size and its order of magnitude is 1×10^{-5} when the subset size is 43 (He *et al.*, 2018).

Model error Helmholtz's free energy Ψ is approximated by a second order Taylor expansion. This approximation introduces a model error. This error is noted as $\boldsymbol{\epsilon}_m$ and is a systematic error which is proportional to $\mathcal{O}(\varepsilon^3)+\mathcal{O}(\chi^3)$. The linearly viscoelastic strain limit for most polymer materials is approximately 0.5%, thereby the model error has the order of 1×10^{-9}.

Numerical error The numerical error refers to the truncation error which is introduced when numerically computing the integral in Equations (5.8) using a recursive scheme. This error is noted as $\boldsymbol{\epsilon}_n$ and is also a systematic error which depends on the time step size Δt and the numerical implementation scheme (Crochon *et al.*, 2010; Sorvari and Hämäläinen, 2010). The numerical error $\boldsymbol{\epsilon}_n$ has the order of magnitude of 1×10^{-8} when the time step size is of 1 s using the recursive scheme (Crochon *et al.*, 2010).

The total error in the identification problem reads

$$\boldsymbol{\epsilon} = \boldsymbol{\epsilon}_e + \boldsymbol{\epsilon}_m + \boldsymbol{\epsilon}_n. \tag{5.43}$$

Note that $\boldsymbol{\epsilon}_m$ and $\boldsymbol{\epsilon}_n$ are comparably smaller than $\boldsymbol{\epsilon}_e$. The total error can be approximated as:

$$\boldsymbol{\epsilon} \approx \boldsymbol{\epsilon}_e, \tag{5.44}$$

which is quantified as random variable with a zero mean Gaussian distribution. Therefore, the assumption of the Gaussian additive error can be used in the Bayesian framework for Prony series parameter identification.

The axial and transverse strains measurement errors, $\boldsymbol{\epsilon}_{\mathrm{I}}$ and $\boldsymbol{\epsilon}_{\mathrm{II}}$, are assumed to be two independent Gaussian distributed random variables with a zero mean. As the transformation (5.38) is performed, the errors of $\boldsymbol{\varepsilon}^{\dagger}$ and $\boldsymbol{\varepsilon}^{\ddagger}$ are the linear combinations of $\boldsymbol{\epsilon}_{\mathrm{I}}$ and $\boldsymbol{\epsilon}_{\mathrm{II}}$, which implies that they are Gaussian random variables as well, i.e.

$$\boldsymbol{\epsilon}_{\dagger} \sim \mathcal{N}(0, \sigma^2_{\epsilon^{\dagger}}), \tag{5.45a}$$

$$\boldsymbol{\epsilon}_{\ddagger} \sim \mathcal{N}(0, \sigma^2_{\epsilon^{\ddagger}}). \tag{5.45b}$$

5.5.4 Tri-dimensional viscoelastic parameters identification under the Bayesian paradigm

To identify the shear creep compliance $\tilde{\mu}(t)$ by solving Equation (5.42a) based on the Bayesian framework, the posterior function should be computed by

$$f_{(\boldsymbol{\theta}^{\mu}|\boldsymbol{Y}=\hat{\boldsymbol{\varepsilon}}^{\dagger})}(\boldsymbol{\theta}^{\mu}) \propto f_{(\boldsymbol{Y}|\boldsymbol{\theta}^{\mu})}(\hat{\boldsymbol{\varepsilon}}^{\dagger}) \times f_{\boldsymbol{\theta}^{\mu}}(\boldsymbol{\theta}^{\mu}), \tag{5.46}$$

where the likelihood function is constructed based on the assumption that $\boldsymbol{\epsilon}_{\dagger}$ is a Gaussian random variable as

$$f_{(\boldsymbol{Y}|\boldsymbol{\theta}^{\mu})}(\hat{\boldsymbol{\varepsilon}}^{\dagger}) \propto \exp\left\{-\frac{1}{2\sigma_{\epsilon\dagger}^{2}} \left|\left| \hat{\boldsymbol{\varepsilon}}^{\dagger} - \boldsymbol{g}_{\mu}(\boldsymbol{\theta}^{\mu}; \hat{\boldsymbol{\sigma}}_{\mathrm{I}}) \right|\right|_{2}\right\}, \tag{5.47}$$

and an ordered relation in the prior function is imposed to avoid identifiability issues, as

$$f_{\boldsymbol{\theta}^{\mu}}(\boldsymbol{\theta}^{\mu}) \propto \begin{cases} \frac{1}{\lambda_{1}^{\mu}} \times \ldots \times \frac{1}{\lambda_{M}^{\mu}} & \text{if } 0 < \lambda_{1}^{\mu} < \ldots < \lambda_{M}^{\mu}, \\ 0 & \text{otherwise.} \end{cases} \tag{5.48}$$

The MAP estimate can be obtained by

$$\hat{\boldsymbol{\theta}}_{\mathrm{MAP}}^{\mu} = \underset{\tilde{\mu}_{m} \in \mathbb{R}_{+},\ \lambda_{m}^{\mu} \in \mathbb{R}_{+}^{*}}{\arg\max} f_{(\boldsymbol{\theta}^{\mu}|\boldsymbol{Y}=\hat{\boldsymbol{\varepsilon}}^{\dagger})}(\boldsymbol{\theta}^{\mu}). \tag{5.49}$$

The bulk creep compliance $\tilde{\kappa}(t)$ can can be identified independently and in parallel through the same procedure.

5.5.5 Algorithm summary

The pseudo code of our proposed method to identify tri-dimensional viscoelastic parameters based on Bayesian framework is presented in Algorithm 3. The first step is to compute $\hat{\boldsymbol{\varepsilon}}^{\dagger}$ and $\hat{\boldsymbol{\varepsilon}}^{\ddagger}$ through Equation (5.38) from mechanical testing data. A parameter transform should be performed, i.e. $\boldsymbol{\varphi} = \ln \boldsymbol{\theta}$, to solve Equation (5.42) with thermodynamic constraints. The maximum number of retardation times was arbitrarily bounded to twice the number of decades of experimental data. In our study, the non-informative prior function was used and, consequently, the posterior distribution is that of Equation (5.27). This distribution was sampled using a MCMC method. The Adaptive Metropolis within Gibbs (AMWG) algorithm (Roberts and Rosenthal, 2009; Tierney, 1994) was applied in our work. Once the posterior distribution was obtained, the BIC was computed with Equation (5.30). This procedure was

repeated for $M = 1$ to $M = M_{max}$. Then, the optimal number of retardation times M_{opt} is that which maximizes the BIC. Finally, the MAP estimates of parameters can be computed from Equation (5.28).

This method has been implemented under the *Julia Programming Language* with *Mamba* package (Deonovic and J Smith, 2018) and is openly available on the Github repository *ViscoBayes* (Yue, 2020).

5.6 Results and discussion

5.6.1 Application to pseudo experiments

The first application of the proposed method was performed to identify the parameters from a numerical relaxation experiment with the loading consisting of a constant strain of 1. The pseudo experimental data was generated using a Prony series having 9 relaxation times with the known parameters which are given in Table 5.2. The resulting stress can be expressed as:

$$\sigma_{\mathrm{I}}(t) = c_0 + \sum_{m=1}^{9} c_m \exp[-\omega_m t],\ t \in \left[10^{-3}, 10^{3}\right]. \tag{5.50}$$

A Gaussian noise, which corresponds to the error in Equation (5.23), was added to the data. There numerical test cases, noted as case 1, 2, 3 and 4, with different added error variances, $\hat{\sigma}_{\epsilon}^2 = 100,\ 500,\ 1000,\ 10000$, were performed to show the robustness of the proposed method.

The proposed method was applied to this generated pseudo data set. The maximum number of relaxation times was set to $M_{\max} = 12$. The variance of the added noise is also a random variable and could be estimated by our method.

Figure 5.7 shows the BIC for the different models as a function of the number of relaxation times for four cases. The figure shows that, for all test cases, the BIC increases initially with the model complexity. Then, adding complexity to the model no longer increases the quality of the fit. The optimal number of series for representing the pseudo experimental data of each case thus can be determined. It was found that for cases 1, 2 and 3 the optimal number of series is 5 while it is 4 for test case 4. The BIC values globally decreased when a larger error variance was added, which can be explained as the precision of results was weakened

Table 5.2: Prony series model parameters used to generate pseudo experimental data.

m	0	1	2	3	4	5	6	7	8	9
ω_m	-	1×10^{-2}	$10^{-1.5}$	1×10^{-1}	$10^{-0.5}$	1	$10^{0.5}$	1×10^{1}	$10^{1.5}$	1×10^{2}
c_m	100	350	100	400	250	300	450	200	50	150

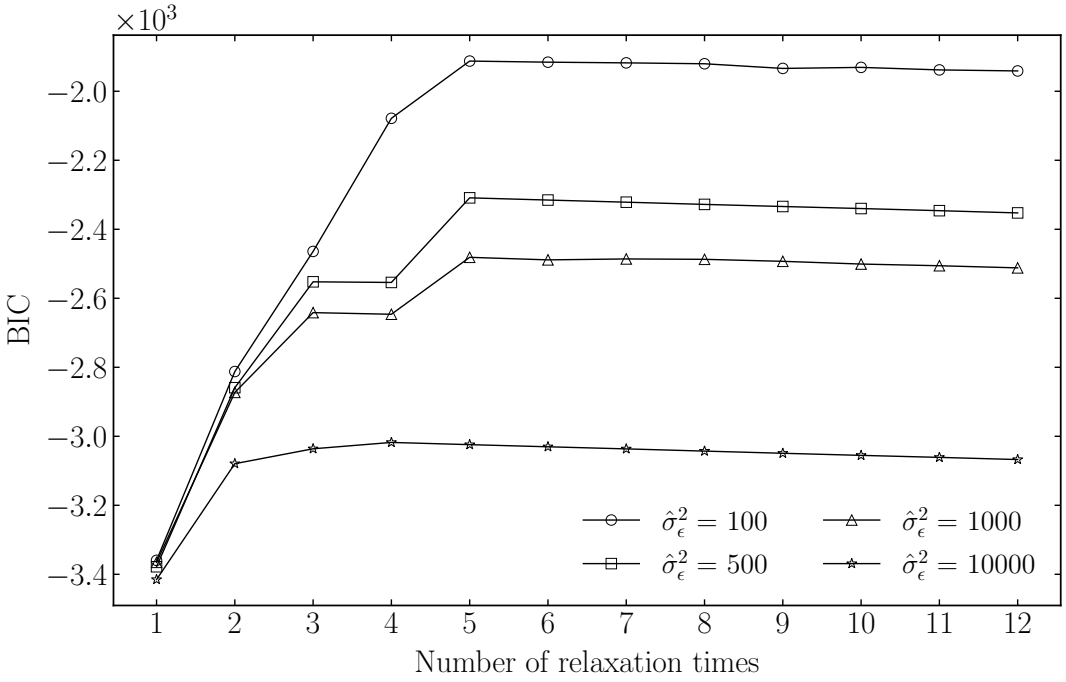

Figure 5.7 Evolution of Bayesian information criterion (BIC) with respect to number of relaxation times for pseudo experimental data of four numerical test cases.

by the experimental error.

Figure 5.8 plots the nominal stress curves generated by MAP estimates for different numbers of relaxation times M and the *true* parameters for the numerical test case 1. The figure shows that the adequacy between the true response and that predicted by models featuring 1 to 4 relaxation times increases with the number of relaxation times. However, the agreement between the true response and that predicted by models featuring more than 4 relaxation times does not improve when the number of relaxation times increases.

Using the MAP estimate of the posterior distribution as a point estimate, the $\boldsymbol{\theta}_{\text{MAP}}$ for Prony series model, the mean estimate of error variance $\check{\sigma}_\epsilon^2$ and the nominal stress curves plotted using the *true* parameters, the corresponding estimates and the generated noised data for four numerical cases are shown in Figures 5.9, 5.10, 5.11 and 5.12. The figures show that the five-relaxation times model is a very good approximation of the nine-relaxation times model for the first three cases. The salient conclusion to be drawn is that, as indicated previously, the viscoelastic kernel function can be approximated within the tolerance limits by different parameters sets, over the given experimental window. The local difference between *true* data and prediction for test case 4 was remarkable and the stress curve generated by the identified parameters yielded oscillations that were caused by the comparatively small

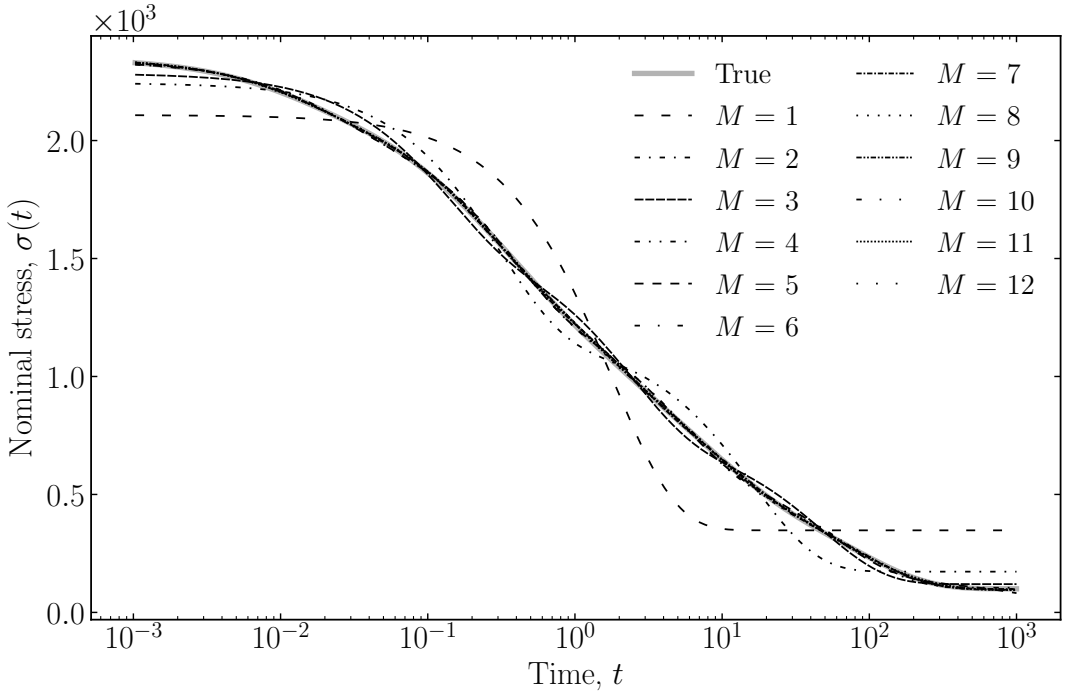

Figure 5.8 Comparison between the stress function using true parameters and MAP estimates for different number of Prony series M for the numerical test case 1 ($\hat{\sigma}_\epsilon^2 = 100$).

number of relaxation times. The method was no longer working in this test with $\hat{\sigma}_\epsilon^2 = 10000$. It should be noted that the added error in test case 4 is very large, when compared to that encountered in actual laboratory experiments.

The identified variances of each test case had an excellent agreement with its true value (within 10%), even for case 4. Therefore, the method used to estimate experimental errors can be validated by this result.

5.6.2 Application to mechanical experiments of polymer materials

Determination of the linearly viscoelastic regime

The normalized ratio $R_{ij}(\boldsymbol{\sigma})$ has three non-zero components for an isotropic viscoelastic material submitted to a uniaxial load history $\boldsymbol{\sigma}$, i.e.

$$R_{11},\ R_{22} = R_{33},\ \text{others } R_{ij} = \mathbf{0}. \tag{5.51}$$

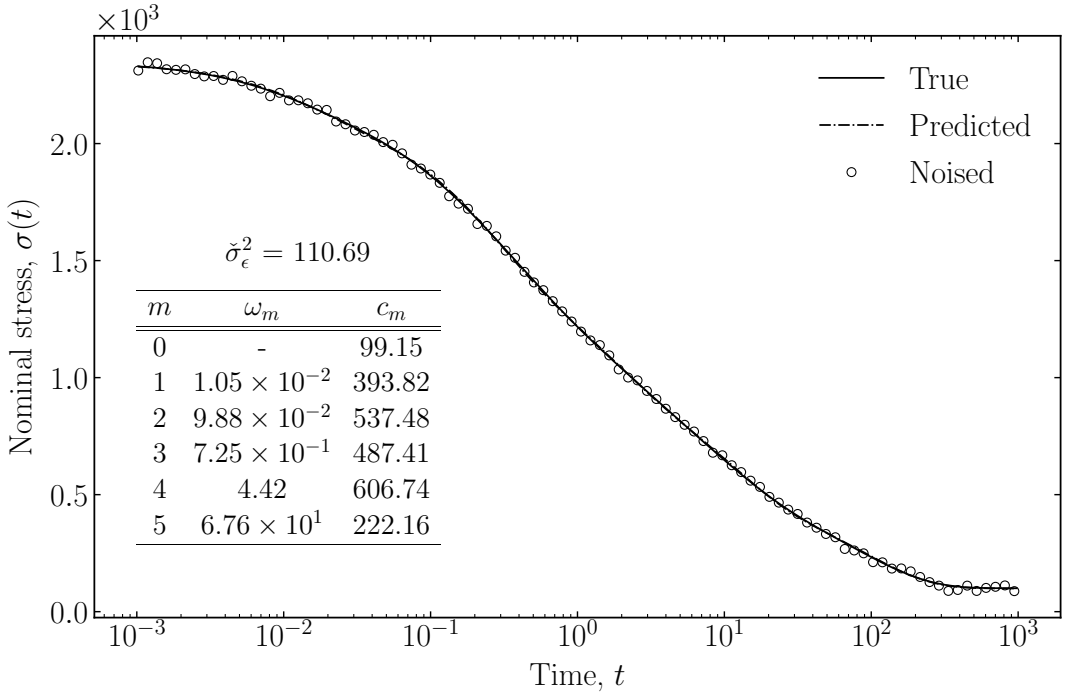

Figure 5.9 Comparison between the generated noised data and the stress function constructed using true and identified parameters for the numerical test case 1 ($\hat{\sigma}_\epsilon^2 = 100$). The table lists the mean estimate variance $\check{\sigma}_\epsilon^2$ and the MAP estimates for the identified parameters.

Their corresponding strains ε_{11} and ε_{22} can be expressed, according to Equation (5.38), as

$$\varepsilon_{11} = \frac{1}{3}\left(2\varepsilon^\dagger + \varepsilon^\ddagger\right), \tag{5.52a}$$

$$\varepsilon_{22} = \frac{1}{3}\left(\varepsilon^\ddagger - \varepsilon^\dagger\right), \tag{5.52b}$$

where $\varepsilon^\dagger$ and $\varepsilon^\ddagger$ are associated with $\tilde{\mu}(t)$ and $\tilde{\kappa}(t)$, respectively.

Note that if the viscoelastic constitutive model $\mathbf{S}(t)$ is linear, its two independent components $\tilde{\mu}(t)$ and $\tilde{\kappa}(t)$ must also be linear. Therefore, if any of ε_{11} and ε_{22} is linear, then $\tilde{\mu}(t)$ and $\tilde{\kappa}(t)$ are linear, then $\mathbf{S}(t)$ is linear. Therefore, for a given isotropic viscoelastic material, any of component ij of R can be used to determine its linear regime. In this study, R_{11}, i.e. the axial strains, was used.

The linearly viscoelastic regime of PMMA and PP have been determined by sequential creep tests. Figures 5.13 and 5.14 plot R_{11} and its variance for PMMA and PP. It was found that the ratio is no longer constant after 18 MPa for PMMA and 7 MPa for PP. Therefore, it is assumed that PMMA and PP are approximated by a linearly viscoelastic model up to 15 MPa and 6 MPa, respectively.

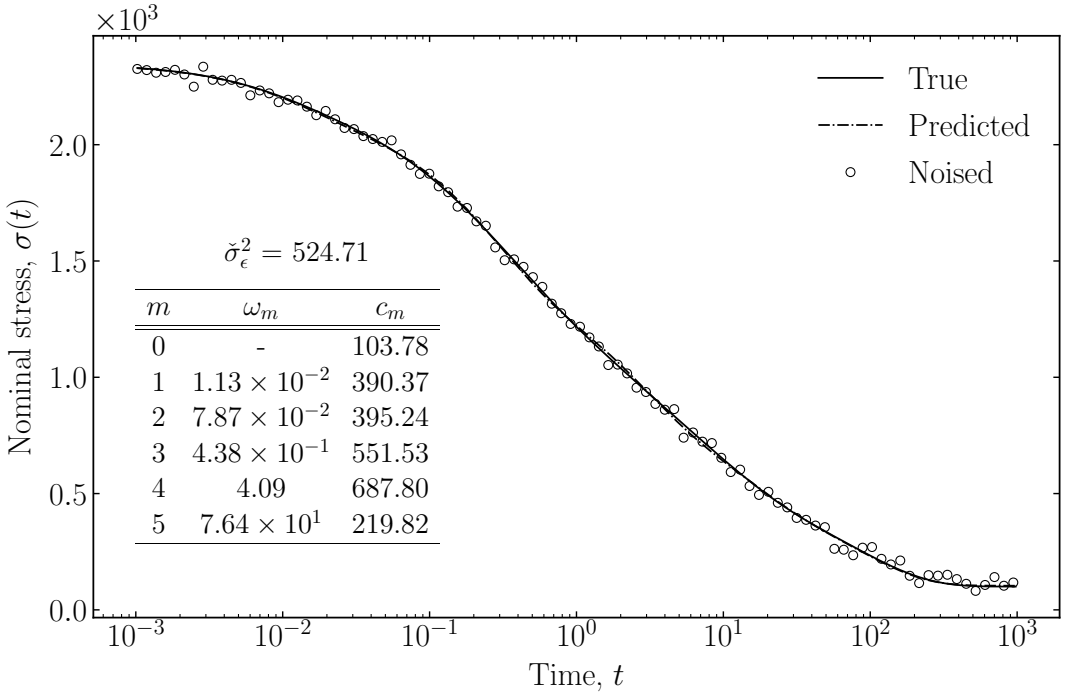

Figure 5.10 Comparison between the generated noised data and the stress function constructed using true and identified parameters for the numerical test case 2 ($\hat{\sigma}_\epsilon^2 = 500$). The table lists the mean estimate variance $\breve{\sigma}_\epsilon^2$ and the MAP estimates for the identified parameters.

Determination of the materials parameters

The proposed method was applied to the obtained experimental data to identify the three-dimensional viscoelastic constitutive model parameters. The optimal number of series of bulk and shear compliances were determined by comparing the BIC value of each model estimated by MCMC simulations. The evaluation of BIC with respect to number of series of PMMA and PP is shown in Figure 5.15. Three retardation times were required to model the shear compliance behavior of PMMA while only one retardation time was necessary to model its bulk creep compliance. Four retardation times were required to model the shear compliance behavior of PP while one retardation time was needed to model its bulk creep compliance.

Table 5.3: Maximum *a posteriori* (MAP) estimates of the Prony series parameters for PMMA.

m	λ_m^μ (s^{-1})	$\tilde{\mu}_m$ (MPa^{-1})	λ_m^κ (s^{-1})	$\tilde{\kappa}_m$ (MPa^{-1})
-	-	6.15×10^{-4}	-	2.47×10^{-4}
1	5.99×10^{-5}	2.35×10^{-5}	2.87×10^{-9}	4.01
2	7.96×10^{-3}	7.62×10^{-5}		
3	4.32×10^{-1}	2.07×10^{-4}		

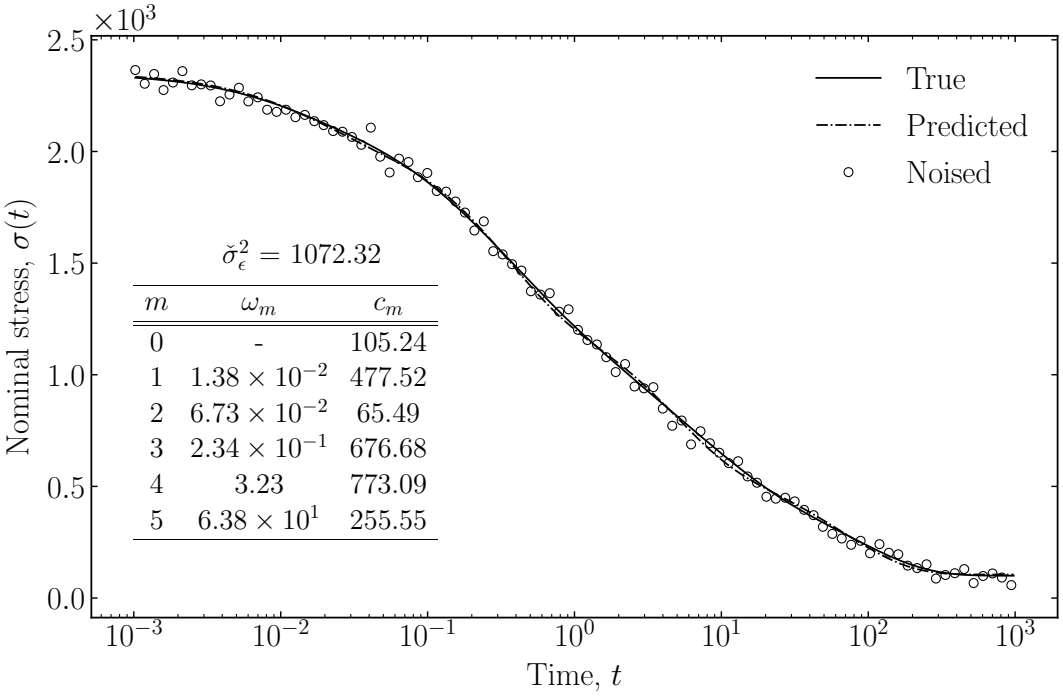

Figure 5.11 Comparison between the generated noised data and the stress function constructed using true and identified parameters for numerical test case 3 ($\hat{\sigma}^2_\epsilon = 1000$). The table lists the mean estimate variance $\check{\sigma}^2_\epsilon$ and the MAP estimates for the identified parameters.

Table 5.4: Maximum *a posteriori* (MAP) estimates of the Prony series parameters for PP.

m	λ^μ_m (s^{-1})	$\tilde{\mu}_m$ (MPa^{-1})	λ^κ_m (s^{-1})	$\tilde{\kappa}_m$ (MPa^{-1})
-	-	1.12×10^{-3}	-	1.12×10^{-3}
1	9.13×10^{-5}	9.11×10^{-4}	2.13×10^{-6}	2.68×10^{-2}
2	4.99×10^{-3}	2.15×10^{-4}		
3	5.86×10^{-2}	1.48×10^{-4}		
4	1.17	2.64×10^{-4}		

The estimated optimal viscoelastic parameters values for PMMA and PP are listed in Tables 5.3 and 5.3. Figures 5.16 and 5.17 plot the comparison between the experimental data and the predicted response of the identified constitutive theories for the identification load histories shown in Figure 5.5, as well the stochastic envelope of the mean value of the model response and the model predictions.

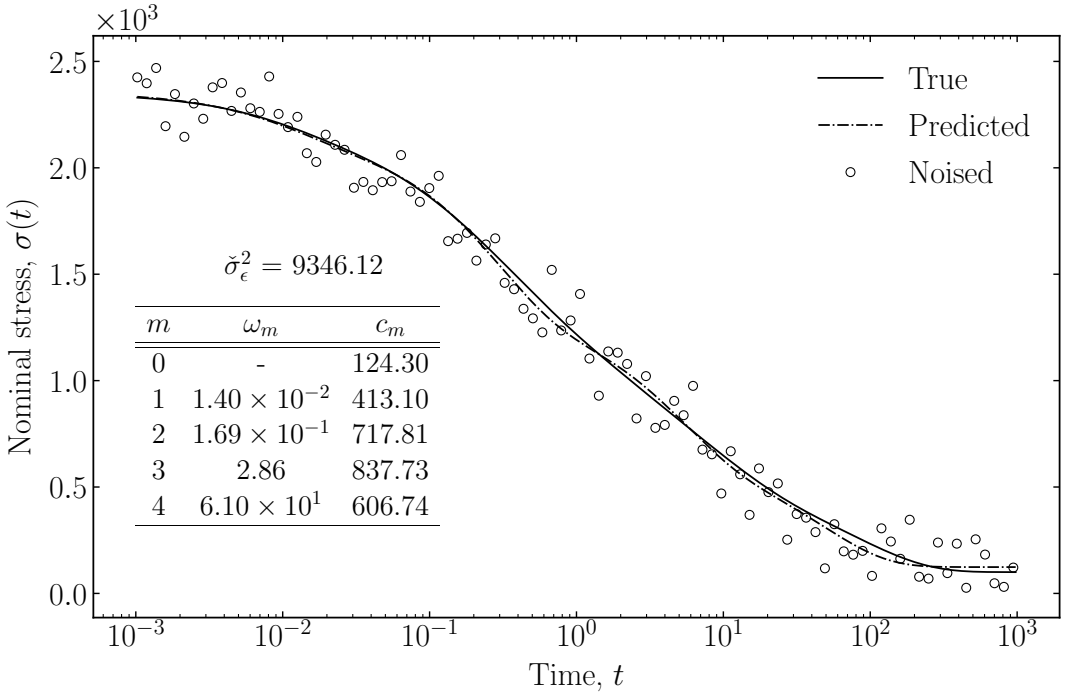

Figure 5.12 Comparison between the generated noised data and the stress function constructed using true and identified parameters for numerical test case 4 ($\hat{\sigma}_\epsilon^2 = 10000$). The table lists the mean estimate variance $\breve{\sigma}_\epsilon^2$ and the MAP estimates for the identified parameters.

Validation on simple geometry specimens

Figures 5.18 and 5.19 plot the comparison between the experimental data and the predicted response for the validation load histories shown in Figure 5.5 for PMMA and PP, as well the stochastic envelope of the mean value of the model response and the model predictions. All the figures show that the identified models reproduce the data quite well.

Note that the transverse strain values are smaller, in absolute value, than the axial strains. Consequently, the measurement errors in the transverse direction are relatively large. Therefore, the prediction intervals of the model predictions for transverse trains are generally wider than that for axial strains. The credible intervals are fairly narrow, which indicates that the identified parameters have a low level of uncertainty.

Validation on complex geometry specimens

The applied loads and investigation time steps are listed in Table 5.5. The predicted strain field in the specimen geometry depicted in Figure 5.2 was obtained by finite element simulations with ANSYS Mechanical APDL 16.1. The geometry was meshed with *SHELL 281* and

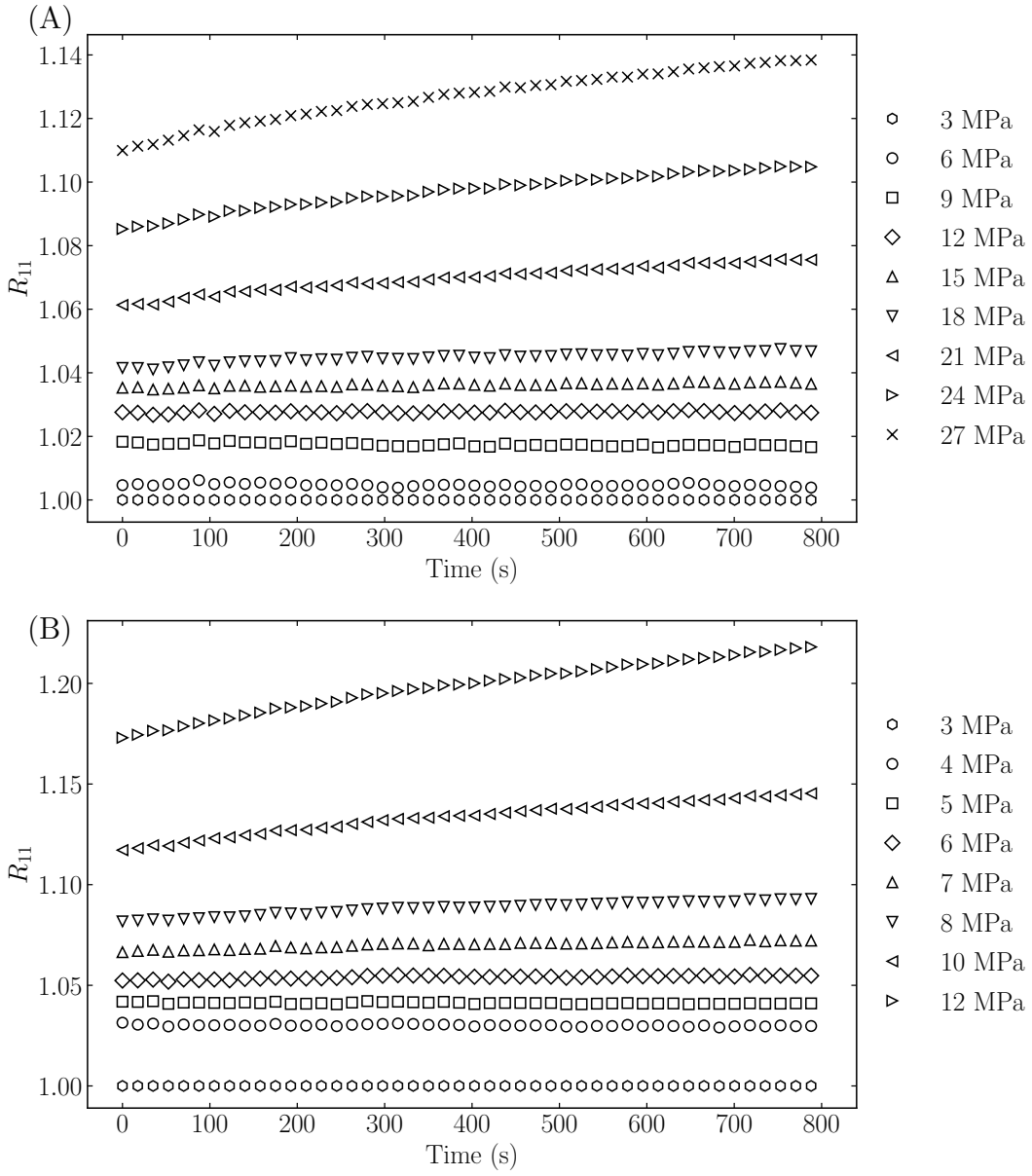

Figure 5.13 The normalized ratio R_{11} for simple specimens of (A) PMMA; (B) PP.

the linearly viscoelastic simulations were carried out with the *PRONY* options. The experimentally measured full strain field was obtained from DIC. For comparison purposes, both simulated and experimentally measured strain fields were interpolated with a triangulation-based linear method, which was realized by means of MATLAB® built-in function *griddata*.

Figures 5.20 and Figure 5.21 plot the interpolated strains in the Y-direction and the X-direction at time step t_c for PMMA and PP, respectively. Considering the noise in the DIC measurements, both X and Y direction strain results show good agreement between DIC

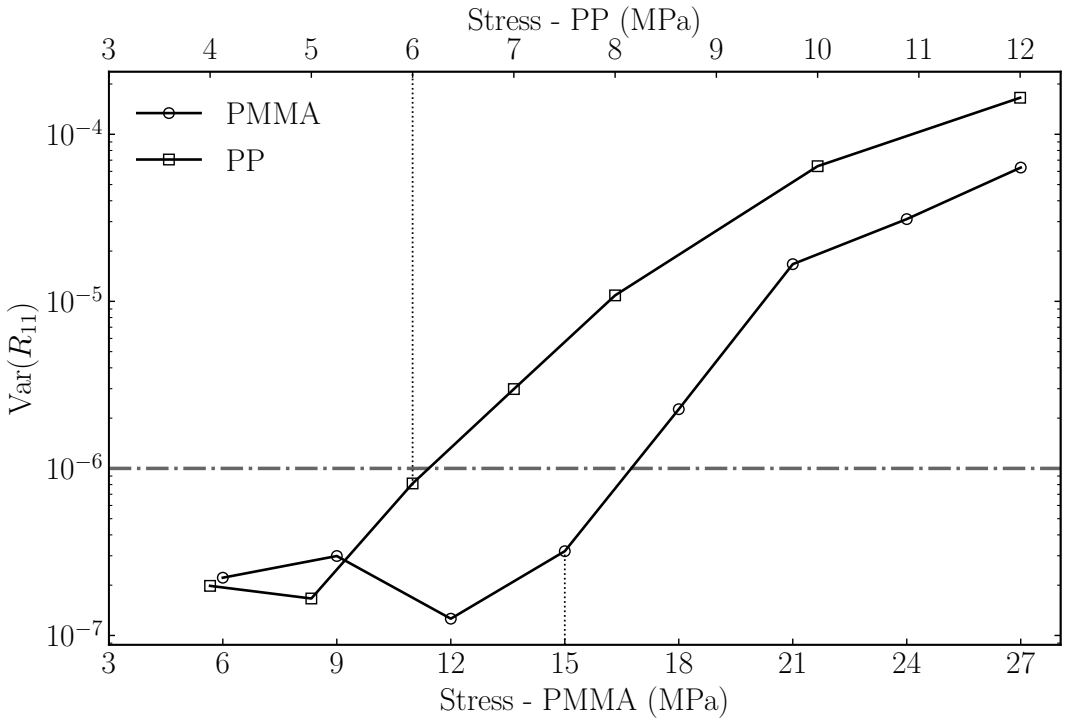

Figure 5.14 The variance of R for simple specimens of PMMA and PP. The dash-dotted lines represent the approximate limits of their linearly viscoelastic regime. The limit is between 15 MPa and 18 MPa for PMMA, while it is between 6 MPa and 7 MPa for PP.

Table 5.5: Loading parameters used in validation experiments of complex specimens.

	Force (N)			Time step(s)		
Materials	F_a	F_b	F_c	t_a	t_b	t_c
PMMA	100	200	300	619.7	1220.1	1826.5
PP	50	100	150	604.0	1208.0	1810.4

and FEM.

Several paths were chosen to quantitatively compare the predicted and experimentally measured strains, as illustrated in Figure 5.3. The comparison between the strain along these paths are represented in Figures 5.22 and 5.23 for PMMA and PP, respectively. The figures show that the predicted ε_{Y} and ε_{X} along three paths are in excellent agreement with the experimentally measured values for both materials. Except for a few strains, e.g. ε_{X} along path II for PMMA and ε_{Y} along path III for PP, all the other strain components are relatively well predicted. This discrepancy might be due to experimental error and edge effects encountered in DIC.

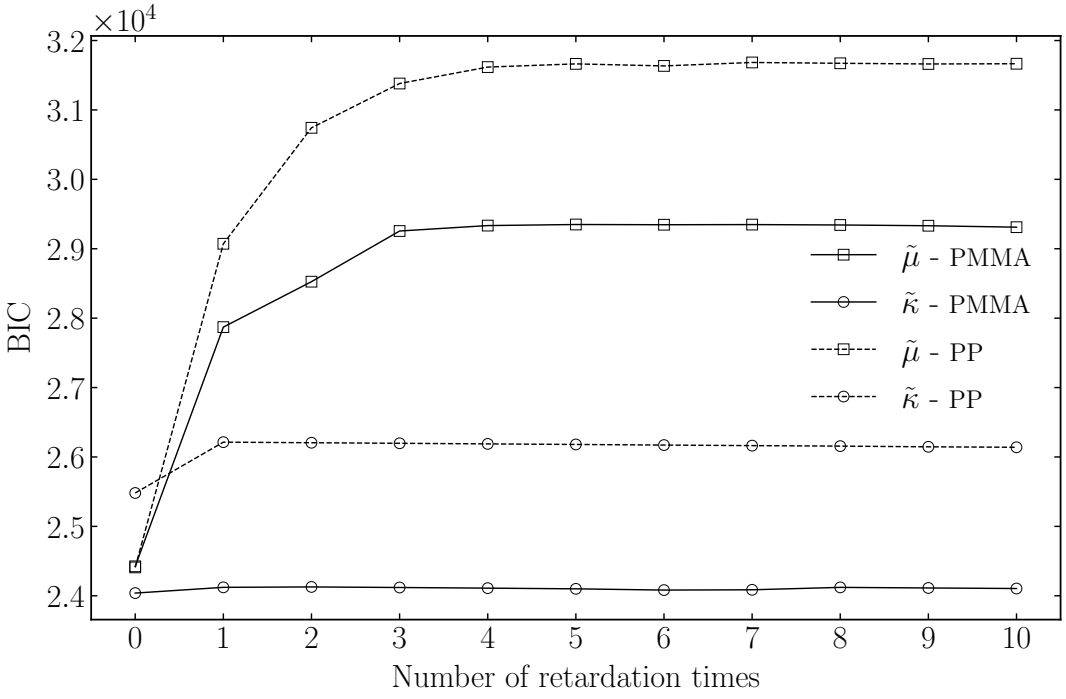

Figure 5.15 Evolution of the BIC with respect to the number of retardation times for PMMA and PP. Three retardation times were required to model the shear compliance behavior of PMMA while only one retardation time was necessary to model its bulk creep compliance. Four retardation times were required to model the shear compliance behavior of PP while one retardation time was needed to model its bulk creep compliance.

5.6.3 Discussion

Figure 5.24 plots the bulk and the shear compliance functions, $\kappa(t)$ and $\mu(t)$, generated by the identified parameters for PMMA and PP. The 99% stochastic envelope for each function were computed by 10 000 realizations from the MCMC procedure. Also shown is the relative width of the stochastic envelope for each function. The relative width is defined as the width of the interval divided by the value of the function predicted by the MAP estimate. A large relative width implies a high uncertainty of the parameters.

The shear compliance of PMMA exhibits a significant time-dependence, which increases from $7.15 \times 10^{-4}\,\mathrm{MPa}^{-1}$ to $9.41 \times 10^{-4}\,\mathrm{MPa}^{-1}$ within the experimental time window for times ranging from $1\,\mathrm{s}$ to $10^{3.5}\,\mathrm{s}$. Its relative width of the stochastic envelope has a tiny value of 0.002 in the range of $10^{0.7}\,\mathrm{s}$ to $10^{3.1}\,\mathrm{s}$. The relative width of the shear compliance has an undulation between $10^{-1.5}\,\mathrm{s}$ and $10^{0.7}\,\mathrm{s}$ with a peak value of 0.035, and is a constant of 0.011 for times ranging from $10^{-2.5}\,\mathrm{s}$ to $10^{-1.5}\,\mathrm{s}$. The bulk compliance of PMMA is nearly a constant of $2.5 \times 10^{-4}\,\mathrm{MPa}^{-1}$ from $10^{-2.5}\,\mathrm{s}$ to $1 \times 10^{2}\,\mathrm{s}$. The relative width is a constant of 0.015 in

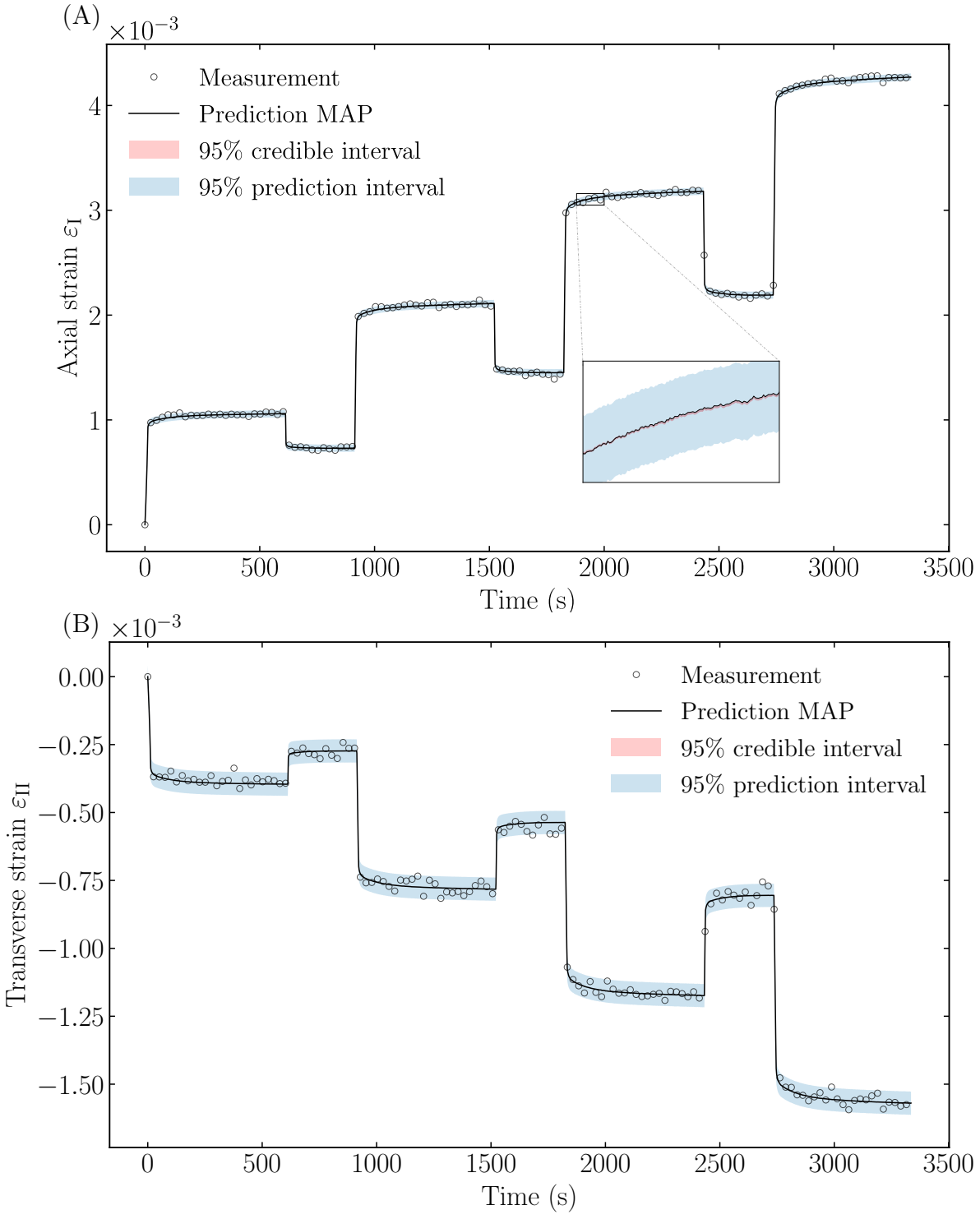

Figure 5.16 Comparison between the experimental data, the MAP estimate prediction with the identified parameters and the stochastic envelopes for identification load histories for the tensile specimens made of PMMA. (A) Axial strain; (B) Transverse strain.

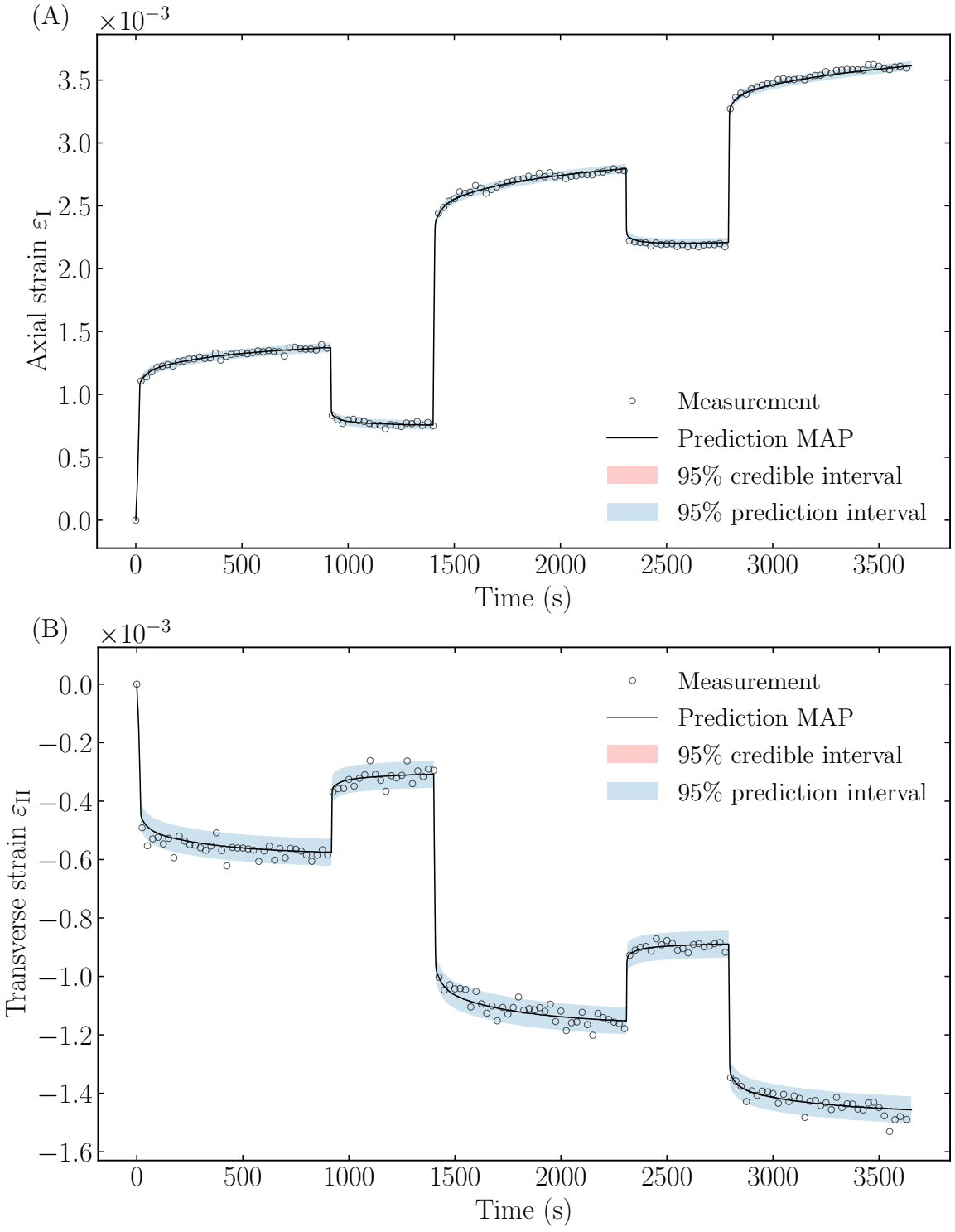

Figure 5.17 Comparison between the experimental data, the MAP estimate prediction with the identified parameters and the stochastic envelopes for identification load histories for the tensile specimens made of PP. (A) Axial strain; (B) Transverse strain.

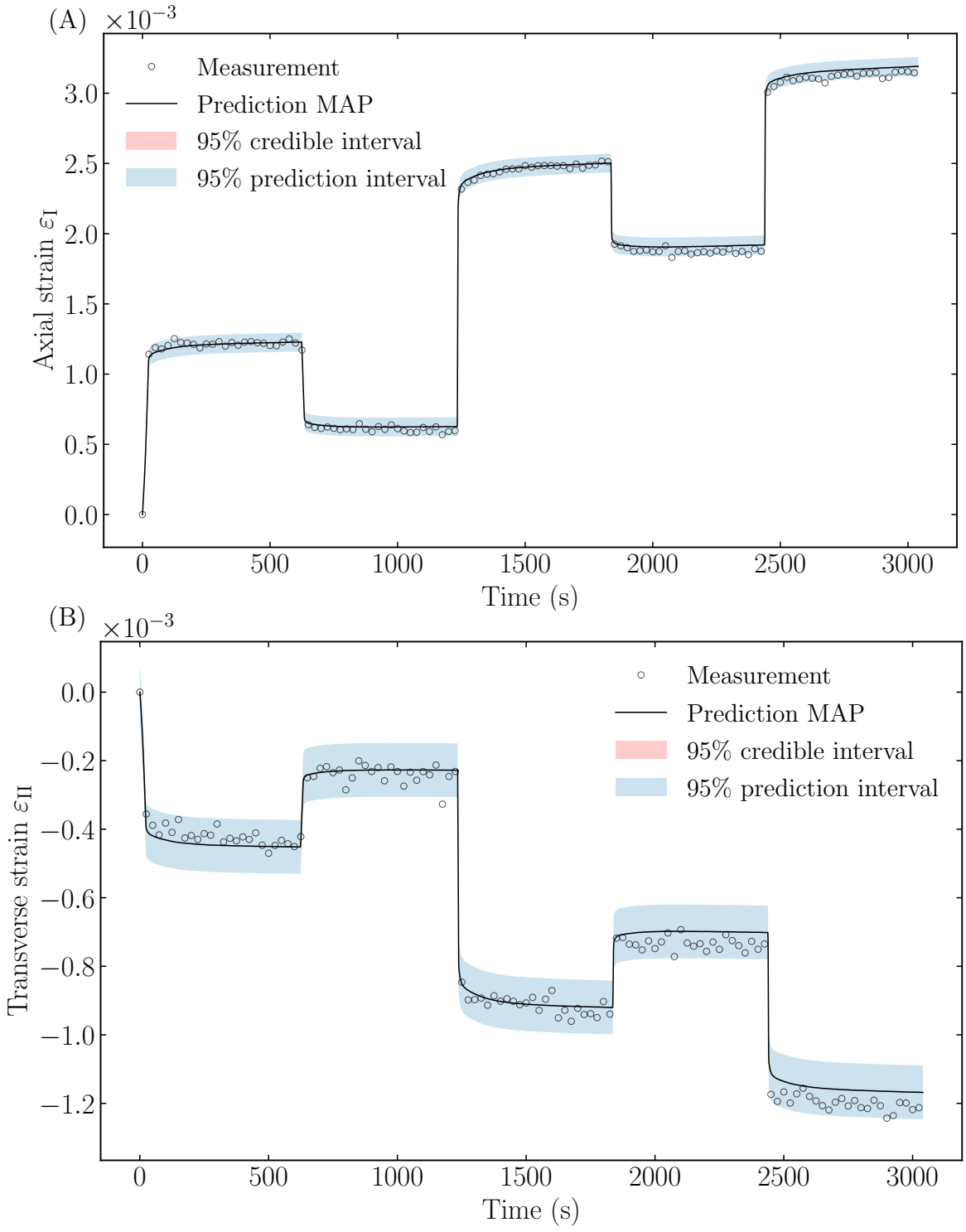

Figure 5.18 Comparison between the experimental data, the MAP estimate prediction with the identified parameters and the stochastic envelopes for validation load histories for the tensile specimens made of PMMA. (A) Axial strain; (B) Transverse strain.

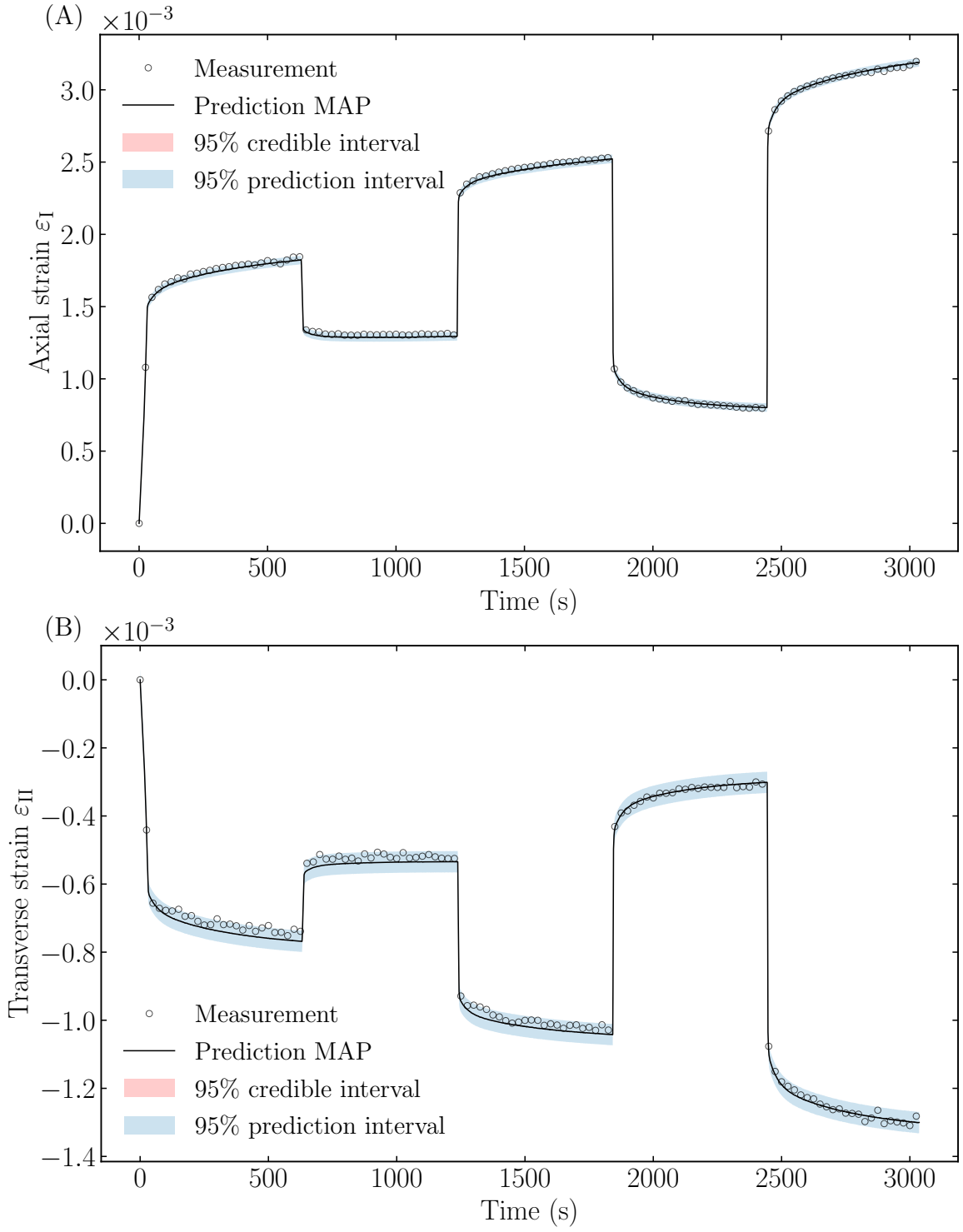

Figure 5.19 Comparison between the experimental data, the MAP estimate prediction with the identified parameters and the stochastic envelopes for validation load histories for the tensile specimens made of PP. (A) Axial strain; (B) Transverse strain.

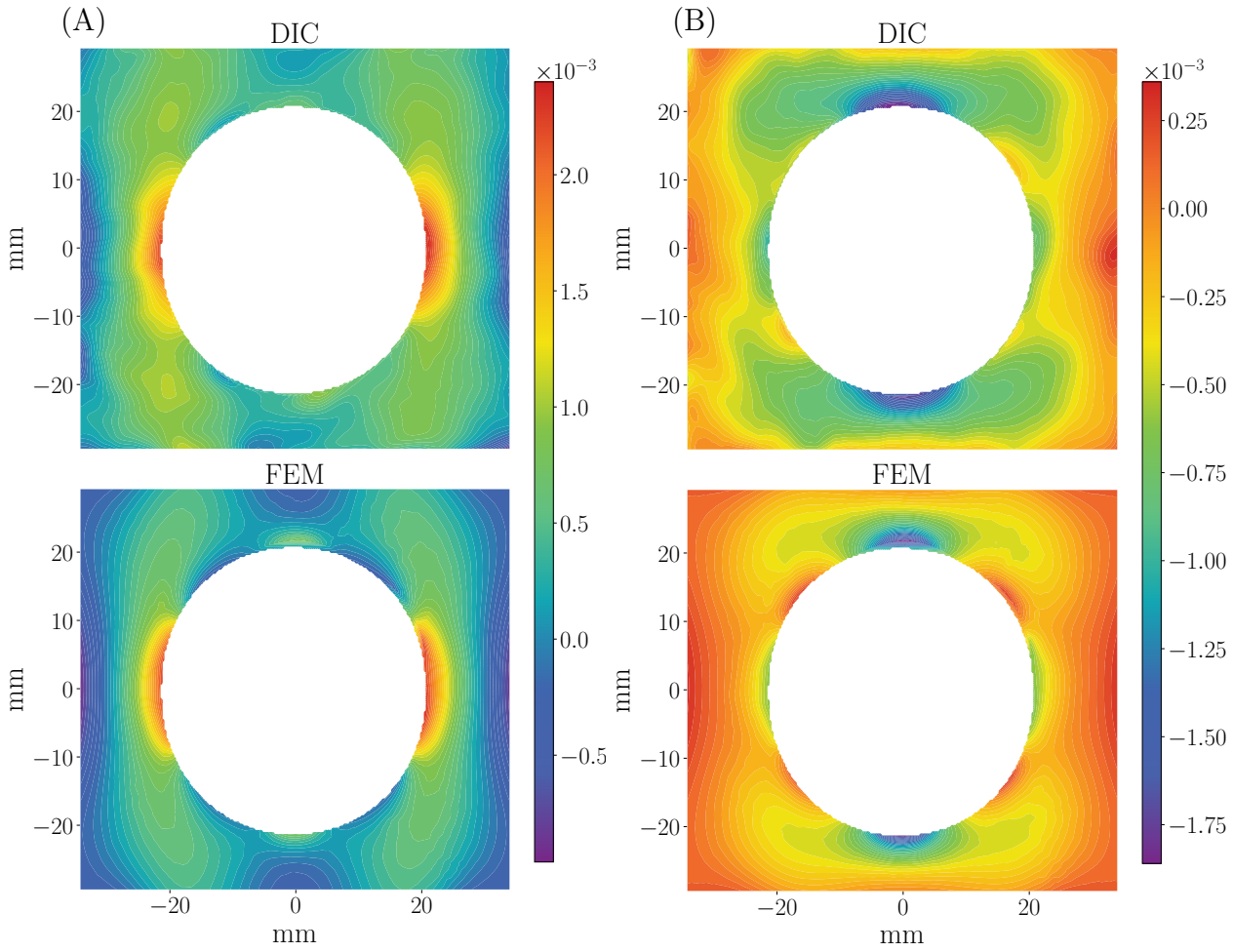

Figure 5.20 Full strain fields obtained by DIC and FEM for PMMA at time step t_c. (A) ε_{Y}; (B) ε_{X}.

the same range, and decreases to 0.007 at $10^{3.1}$ s. When time exceeds the experimental time window, both the compliance function and the relative width increase rapidly. Similar observations can be made for PP.

The low relative width range of the shear and the bulk compliance functions, from $10^{0.7}$ s to $10^{3.1}$ s for both polymers, implies that the mechanical behavior of the materials during the experimental time window is determined by the kernel functions within this range. Note that the lower limit of this range corresponds to the sampling localization range, while the upper limit lies between the limit of the experiment time window and the sampling localization range. The relative width of the shear and the bulk compliance functions increases outside this range, since it relies on fewer information. However, the instantaneous properties for the shear and the bulk properties for both polymers can be well captured from the mechanical

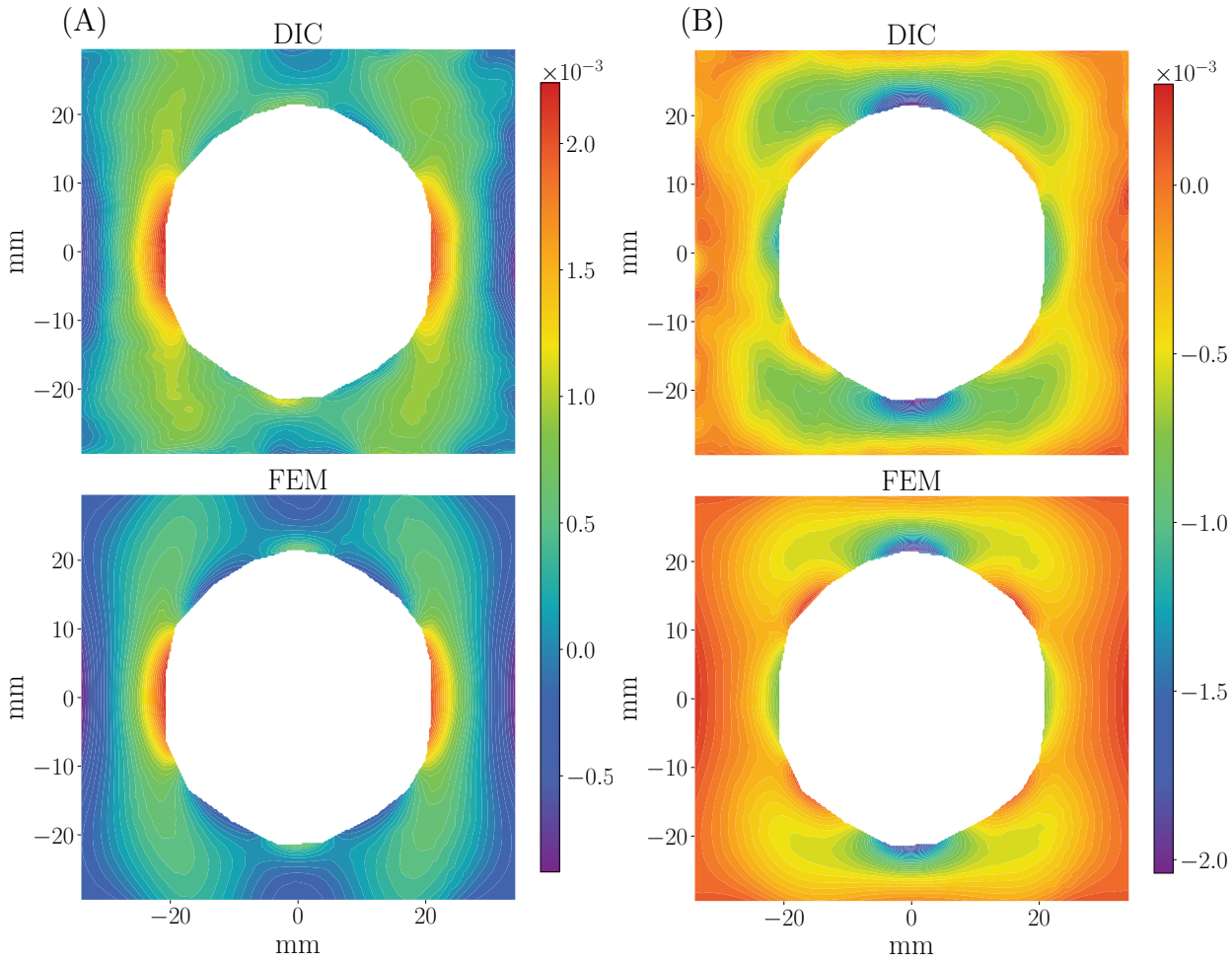

Figure 5.21 Full strain fields obtained by DIC and FEM for PP at time step t_c. (A) ε_{Y}; (B) ε_{X}.

tests. This observation is supported by the fact that the relative width of compliance functions decreases to a constant in the range of $10^{-2.5}$ s to $10^{-1.5}$ s. Consequently, there is an undulation in the shear compliance function for times ranging from $10^{-1.5}$ s to $10^{0.5}$ s, indicating that the information during this period affects lightly the shear properties of the material. No undulation was observed in the bulk function since the bulk compliance is nearly a constant in the range of $10^{-2.5}$ s to 1×10^{2} s. This observation agrees with a generally accepted behavior for polymers that the time-dependence of the bulk property is noticeably small, when compared to the shear property (Qvale and Ravi-Chandar, 2004; Sane and Knauss, 2001). However, few experimental data on the three-dimensional viscoelasticity of PMMA and PP at room temperature are reported in the literature, limiting the comparison between the measured results in this work and the literature data.

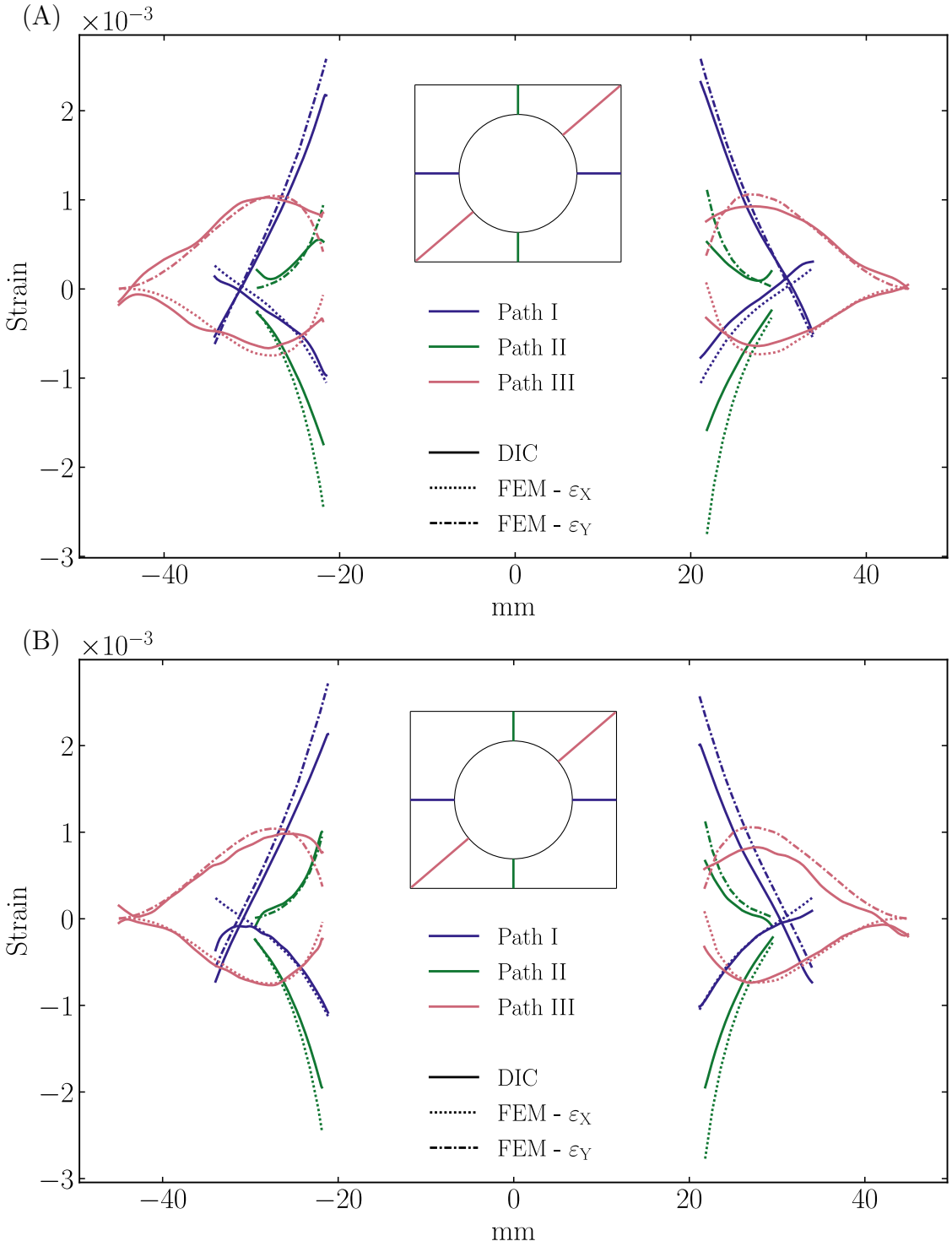

Figure 5.22 Strains obtained by DIC and FEM along three paths for complex specimens of (A) PMMA ; (B) PP. Solid lines represent FEM results. Dashed lines represent DIC results.

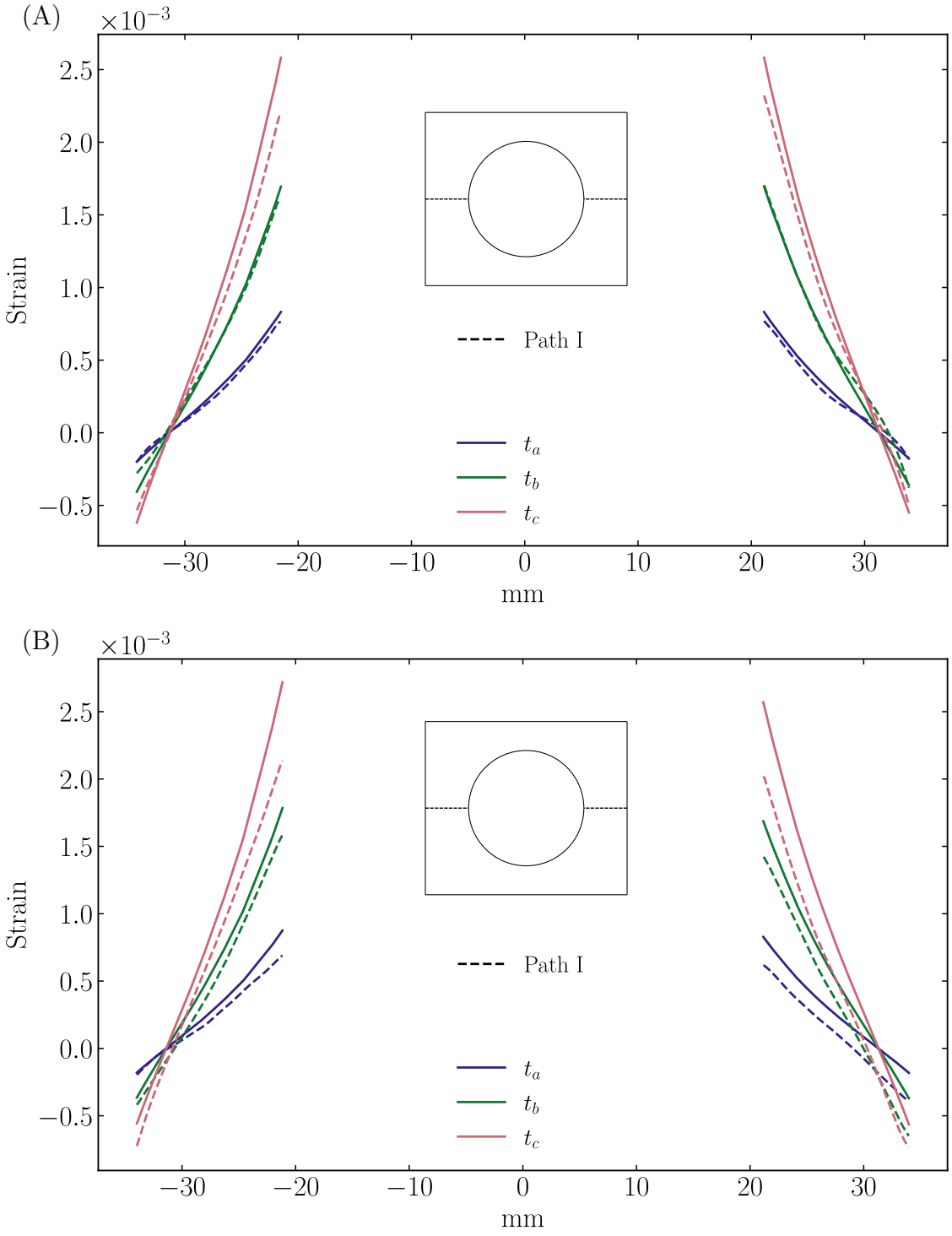

Figure 5.23 Strain ε_{Y} obtained by DIC and FEM along path I at different time steps for complex specimens of (A) PMMA; (B) PP. Dashed lines represent DIC results.

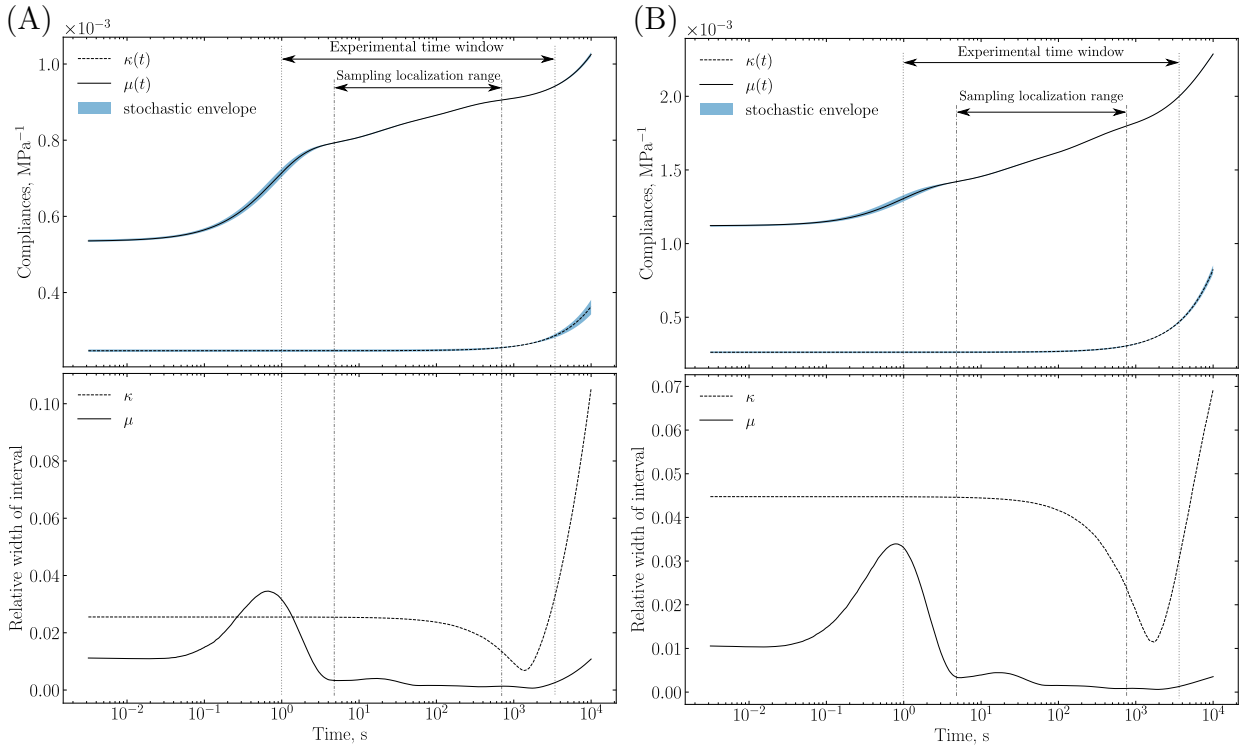

Figure 5.24 The bulk and the shear compliance functions generated with the identified parameters and their 99% stochastic envelopes for (A) PMMA; (B) PP, as well the relative width of the stochastic envelope for each function. The solid line represent the shear compliance and the dash line stands for the bulk compliance.

When compared to other existing methods, the main advantage of our proposed method is that it delivers the smallest number of retardation times for the maximum accuracy. We compared our identification procedure results to the improved collocation methods proposed by Lévesque *et al.* (2008). The shear compliances $\tilde{\mu}(t)$ identification (corresponding $\boldsymbol{\varepsilon}^{\dagger}$) was compared.

The sum of squared estimate of errors (SSE) is considered as the variable valuating the precision of each method, which is defined as follow:

$$\mathrm{SSE} = \sum_{t=1}^{T} \left(\hat{\varepsilon}_t^{\dagger} - \check{\varepsilon}_t^{\dagger} \right)^2, \tag{5.53}$$

where T denotes the number of experimental data points, $\hat{\varepsilon}^{\dagger}$ and $\check{\varepsilon}^{\dagger}$ represents the experimental measurements and the predictions from the used identified parameters, respectively.

Figure 5.25 plots the evolution of the SSE with respect to the number of series identified by our proposed method and the conventional method. The Prony series model can be cut down

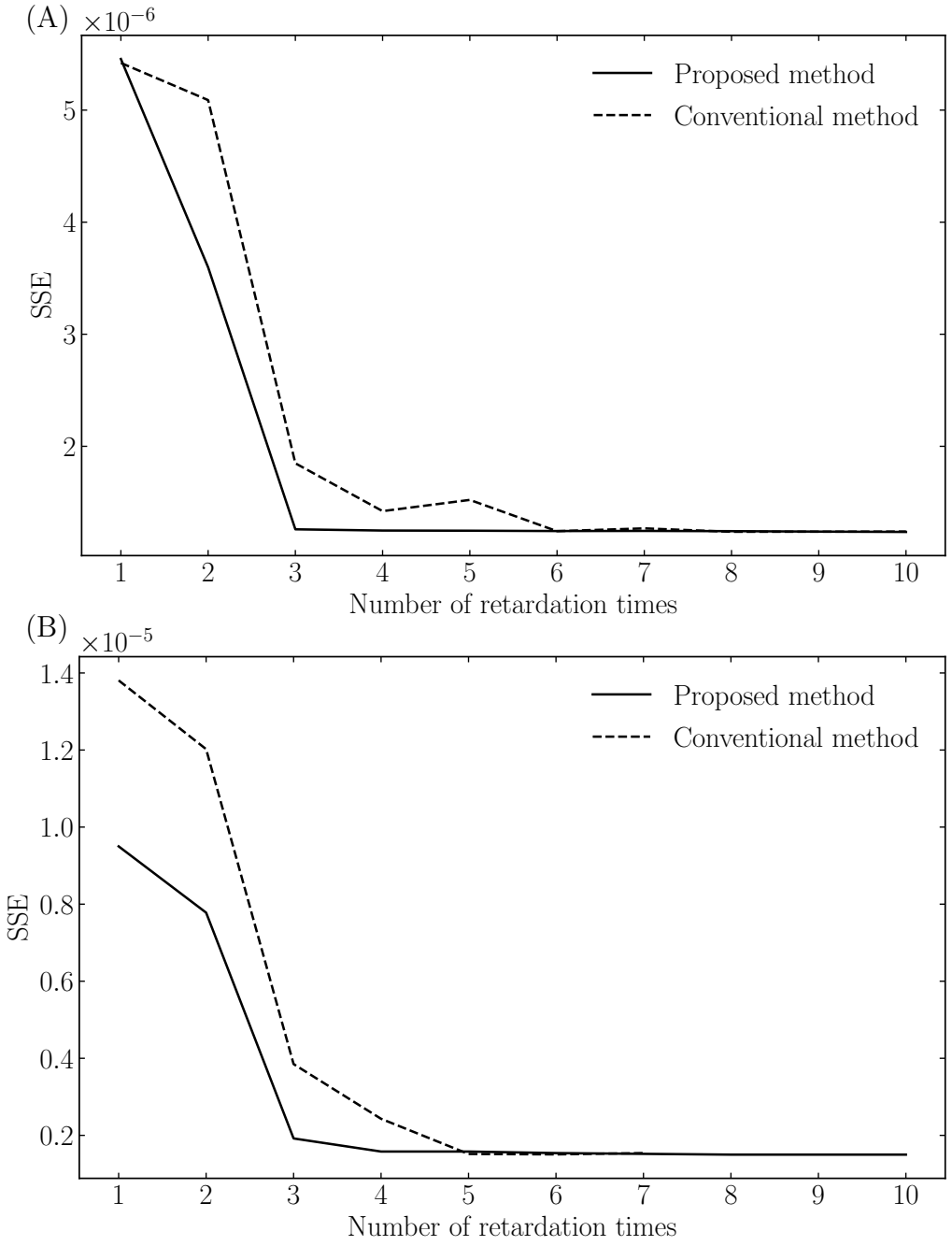

Figure 5.25 Evolution of the residual of experimental data and predictions with respect to number of retardation times identified by the proposed method and the conventional method for (A) PMMA; (B) PP. Using the proposed method, the SEE stays stable after $M = 3$, which means that using only three retardation times can predict viscoelastic behavior for PMMA. However, for the conventional method, the SSE converged after $M = 6$ and led to same value of the proposed method. While the number of retardation times was reduced from 5 to 4 for PP.

to 3 series using our proposed method to replace the conventional method with 6 series to reach the same accuracy for PMMA, while the number of series can be reduced from 5 to 4 for PP. It should be noted that the experimental time windows in this study was from 1×10^{-1} s to 1×10^{3} s which is quite short. For a longer experimental time window, e.g. the problem of time-temperature superposition problem of viscoelastic materials, large number of series are generally required by using conventional method. In this application, our method is reduced the number of retardation times, which is a desirable feature to reduce the computational cost in finite element simulation involving viscoelastic materials.

Using our proposed method, all viscoelastic parameters are free to explore the whole parameters space. Therefore, the optimal number of series identified by our method is the minimum for representing the given experimental data. However, there may exist different parameters values with same number of series according to the nature of Prony series.

Our proposed method requires a significant computational cost, when compared to the conventional method. For example, for the comparison example, our method required 30 minutes of computation while it required 5 minutes for the conventional method. However, if the constitutive theory is subsequently used in lengthy finite element simulations, the initial time invested should remain marginal.

5.7 Conclusion

The main contribution of this work lies in the proposed Bayesian inference based method to identify three-dimensional Prony series viscoelastic constitutive theory. The results obtained using the Bayesian framework show an excellent agreement with the experimental data for either standard specimen and complex geometry specimen under different loads. Moreover, it can reduce the number of relaxation times in the constitutive model.

The proposed Bayesian based identification method was applied only to the linearly viscoelastic behavior in this study. However, this method could be extended to identify other behaviors of polymer solid, such as non-linearities with respect to stress or temperature effects.

Appendix: Numerical implementation

Algorithm 3 Tri-dimensional viscoelastic parameters identification.

1: Read N groups experimental data $\{\hat{\boldsymbol{\sigma}}_{\mathrm{I}}^{(\mathrm{n})}, \hat{\boldsymbol{\varepsilon}}_{\mathrm{I}}^{(\mathrm{n})}, \hat{\boldsymbol{\varepsilon}}_{\mathrm{II}}^{(\mathrm{n})}\},\ n = 1, \ldots, N$.
2: Compute $\{\hat{\boldsymbol{\varepsilon}}^{\dagger(\mathrm{n})}, \hat{\boldsymbol{\varepsilon}}^{\ddagger(\mathrm{n})}\},\ n = 1, \ldots, N$ using Equation (5.38)
3: Input maximal number of characteristic times $M_{\max}$
4: Let $\boldsymbol{x} = \bigcup\limits_{1 \le n \le N} \{\hat{\boldsymbol{\sigma}}_{\mathrm{I}}^{(\mathrm{n})}\}$, $\boldsymbol{y}^{\kappa} = \bigcup\limits_{1 \le n \le N} \{\hat{\boldsymbol{\varepsilon}}^{\ddagger(\mathrm{n})}\}$, $\boldsymbol{y}^{\mu} = \bigcup\limits_{1 \le n \le N} \{\hat{\boldsymbol{\varepsilon}}^{\dagger(\mathrm{n})}\}$
5: **for** $M = 1, 2, \ldots, M_{\max}$ **do**
6: Compute posterior distribution $f_{(\boldsymbol{\theta}^{\mu} | \boldsymbol{Y} = \boldsymbol{y}^{\mu})}(\boldsymbol{\theta}^{\mu})$ and $f_{(\boldsymbol{\theta}^{\kappa} | \boldsymbol{Y} = \boldsymbol{y}^{\kappa})}(\boldsymbol{\theta}^{\kappa})$ by MCMC algorithm
7: Compute MAP estimates $\hat{\boldsymbol{\theta}}^{\kappa}_{\mathrm{MAP}}$ and $\hat{\boldsymbol{\theta}}^{\mu}_{\mathrm{MAP}}$ by Equation (5.28)
8: Compute $BIC(M^{\kappa})$ and $BIC(M^{\mu})$ using Equation (5.30)
9: **end for**
10: Obtain $M^{\kappa}_{\mathrm{opt}}$ and M^{μ}_{opt}

CHAPTER 6 ARTICLE 2: ON THE STRAIN MEASUREMENT FOR THERMOPLASTICS WITH BI-AXIAL EXTENSOMETER IN THERMO-MECHANICAL TESTING: A CASE OF CHARACTERIZING TEMPERATURE AND PHYSICAL AGING EFFECTS ON POLYCARBONATE

L. Yue, J. Jalbert, M. C. Heuzey and M. Lévesque . Submitted to *Experimental Mechanics* on February 14, 2022. *Minor changes were made following the jury's comments when compared to the submitted version.*

6.1 Abstract

Characterizing the mechanical behavior of materials at elevated temperatures is critical for the design and development of polymer systems for use in complex operating conditions. The commonly used Dynamic Mechanical Analysis (DMA) does not apply to the investigation of the three-dimensional properties of materials. A combination of a mechanical testing system and an environmental chamber with extensometer measurements is more suitable for this purpose. However, the bi-axial extensometer suffers errors in measuring strains in thermoplastic specimens at elevated temperatures due to its characteristics. This brief technical note analyzes the sources of measurement errors with an extensometer and proposes a robust, straightforward and easy-to-follow experimental procedure for three-dimensional mechanical testing at high temperatures, using temperature and physical aging effects characterization experiments of polycarbonate as a case study. The experimental results show reproducibility and reliability. The methodology described in this work can serve as a protocol to guide other types of three-dimensional thermo-mechanical testing with a bi-axial extensometer.

6.2 Introduction

Characterizing the mechanical behavior of polymers at elevated temperatures is required in industries like aerospace where composites parts made of thermoplastics are used. Most existing investigations into the mechanical properties of polymers involving temperature and physical aging effects rely mainly on Dynamic Mechanical Analysis (DMA) measurements (Courtois, Hirsekorn, *et al.*, 2019; Guo and Bradshaw, 2009; Kovacs *et al.*, 1963; Meyer *et al.*, 1965; O'connell and McKenna, 1997; O'Connell and McKenna, 2002). The technique, however, features limitations of that only uni-dimensional properties can be investigated dur-

ing these tests. Besides that, several specialized experimental setups have been developed to determine the three-dimensional properties of polymers Emri and Prodan (2006); Qvale and Ravi-Chandar (2004); Sane and Knauss (2001). However, these devices are not widely used in engineering due to their accessibility. Tensile testing frames allow various experimental set-ups and, thus, can be easily used to characterize the three-dimensional properties of materials at elevated temperatures, when equipped with an environmental chamber and strain measurement equipment.

To measure three-dimensional strains at elevated temperatures, the bi-axial extensometer is the most convenient and cost-efficient method (Knauss *et al.*, 2008), when compared to other techniques such as strain gauges and Digital Image Correlation (DIC). However, due to the nature of the extensometer, particularly when measuring strains in a thermoplastic specimen, the knife edges of the extensometer penetrate into the specimen, resulting in measurement errors. A common solution is to wait long enough for this penetration to cease, as manufacturers recommend. This approach, however, is not feasible at elevated temperatures because physical aging continues to affect the specimen's mechanical properties. Therefore, measuring strains in thermoplastic specimens at elevated temperatures with a bi-axial extensometer is delicate and challenging. To the best of our knowledge, there is no standard procedure to account for the drifts of the extensometer at elevated temperature, and researchers have rarely detailed their approach to addressing this issue.

This brief technical note aims to analyze errors in measuring three-dimensional strains in a thermoplastic specimen with a bi-axial extensometer in thermo-mechanical testing and propose a relatively easy-to-follow and straightforward procedure for eliminating these errors. The methodology is applied to the characterization of the temperature and physical aging effects on the mechanical properties of polycarbonate as a case study. This paper is organized as follows: Section 6.3 analyzes the sources of measurement errors with an extensometer; Section 6.4 details the methodology for characterizing the temperature and physical aging effects for polycarbonate; Experimental results are presented in Section 6.5; Section 6.6 concludes this work.

6.3 Sources of measurement errors with an extensometer

A bi-axial extensometer can simultaneously measure the axial and transverse strains of a specimen during mechanical testing. This type of extensometer can yield an accuracy of at least 0.5% of the readings, meeting ASTM E83 or ISO 9513 standards (Knauss *et al.*, 2008). However, strain measurements are subject to environmental influences that result in drift, which arises from two primary sources.

Temperature sensitivity Alike most electronic sensors, the transducer in the extensometer is susceptible to temperature, which causes the extensometer's measurement results to drift when the temperature changes. When the extensometer is powered, heat is generated by the current flow, causing a temperature change, and the resulting drift is known as the *warm-up drift* (Womack, 2020c). This drift generally stabilizes after the device has been plugged in for a few minutes. When the ambient temperature changes, the extensometer experiences a *thermal drift* (Womack, 2020b). This drift includes not only the response of the sensor to the temperature change but also records the deformation of the load cell, test machine, or other device subjected to the temperature change. Distinguishing the different factors that cause thermal drift remains a challenge (Womack, 2020b).

Knife edges To hold the extensometer on the specimen, the knife edges are usually rather sharp. Therefore, the knife edge penetrates into the specimen when the extensometer is mounted and cause the *penetration drift* (Knauss *et al.*, 2008). This drift is particularly noticeable when testing thermoplastic polymers. Since the extensometer is manually mounted on the specimen, the knife-edge position and the contact force (Knauss *et al.*, 2008), i.e., the force applied to attach the knife-edge, may differ between tests, introducing measurement error.

6.4 Experimental methodology

6.4.1 Materials and equipment

A polycarbonate (PC) (#PE-1220R-MP from *Lavergne, Inc*) was investigated in this work. ASTM D638 standard type-I specimens were manufactured by injection molding. The mechanical testing was conducted on a MTS® Insight electromechanical machine equipped with a 1 000 N load cell. A LBO-series environmental chamber from *Thermcraft Inc* was installed on the Insight machine. The axial and transverse strains were measured simultaneously using a bi-axial extensometer (Model 3560) from *Epsilon Technology, Corp.* An external type `T` thermocouple was used to measure the specimen temperature during tests. *National Instruments* (NI) devices were used for data acquisition (see below).

The MTS Insight machine was controlled by the software `TestSuite TW`. The resulting force and displacement signals were transmitted to the software `LabVIEW` through the module NI-9239. Thermocouple and extensometer measurements were acquired by the modules NI-9211 and NI-9237, respectively, and transmitted to `LabVIEW`. The temperature of the environmental chamber was controlled by a temperature controller that also communicated with

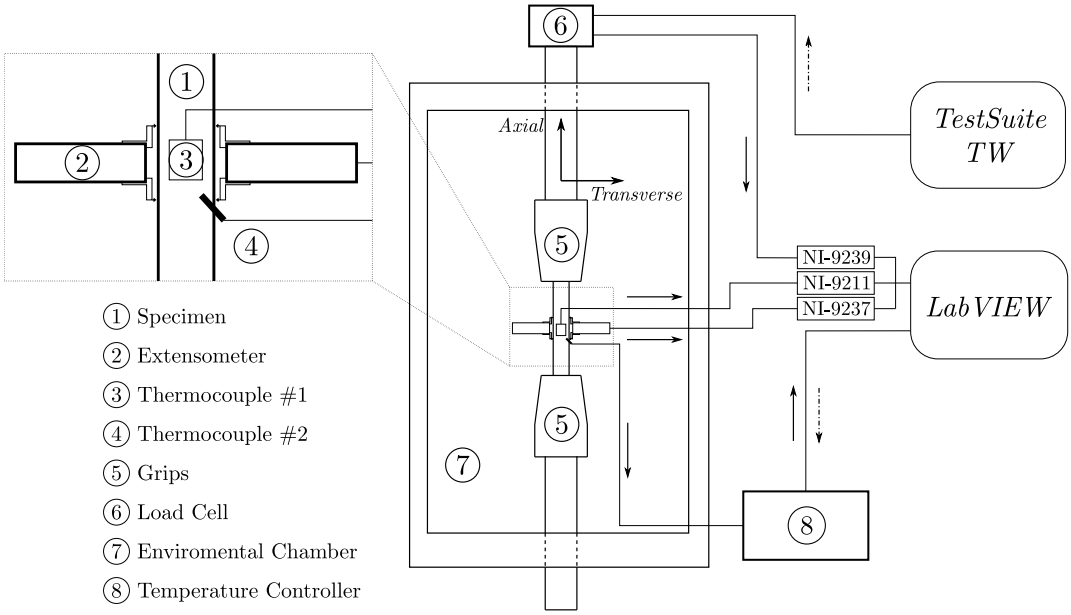

Figure 6.1 Illustration of the experimental set-up used to characterize the temperature and physical aging effect on PC. The solid and dashed-dot arrows indicate the data acquisition and the control signals, respectively. Thermocouple #1 represents the external thermocouple that was attached to the specimen, while thermocouple #2 stands for the built-in thermocouple of the environmental chamber which was placed close to the specimen.

`LabVIEW`. Figure 6.1 illustrates the experimental set-up and indicates the communication between equipment.

6.4.2 Temperature sensitivity test of the extensometer

The temperature sensitivity test was performed to investigate the response of the extensometer to a change in temperature. The pined extensometer was placed in the environmental chamber to record the axial and transverse readings subjected to a temperature history. In this test, the specimen was not installed and the extensometer was placed directly on the bottom grip. The built-in pin of the extensometer is used to lock the position of its knife edges; therefore, with the pin fixed, the readings represent only the response of the extensometer to changes in the surrounding temperature.

The temperature sensitivity of the extensometer is nearly constant with respect to temperature (Womack, 2020a). Furthermore, the accumulation of drift introduced by temperature will be subtracted in the results (see Section 6.4.4 for details). Thus, we are more concerned with how the extensometer readings change qualitatively with temperature than a quantitative sensitivity analysis in this temperature sensitivity test. Therefore, any temperature

above room temperature can be chosen in the temperature sensitivity tests. In this work, three temperature sensitivity tests were performed, two at 40 °C and one at 80 °C. The temperature was set to increase from room temperature to test temperature in 10 minutes for all three tests. A thermocouple was placed near the center of the extensometer to record the temperature.

6.4.3 Mechanical testing

The specimen was first mounted on the grips using a level to ensure it was parallel to the machine's axial direction (see Figure 6.1 for a representation of the axial axis). The environmental chamber's built-in thermocouple was placed very close to the external thermocouple that was attached to the gauge section of the specimen. Then, the bi-axial extensometer was installed on the specimen, and the axial and transverse readings were zeroed after removing the pins of the extensometer. The door of the environmental chamber was then closed to start heating up. Synchronously, the Insight machine began executing the program with the specified load history. The ventilation, air conditioning, and electrical systems of the laboratory were kept operational during each mechanical test to maintain stable ambient conditions throughout the experiment.

Sequential creep-recovery tests were performed at elevated temperature based on Struik's methodology (Struik, 1977). The time for heating the furnace from room temperature to the characterization temperature was fixed at 20 minutes. It was then maintained at the characterization temperature for 1 hour to ensure that the specimen reached its thermal equilibrium, considering heat transfer. A creep test (#0) of 10 minutes was first conducted to align the grips of the tensile test machine 2 hours after the specimen achieved thermal equilibrium. Then, three creep-recovery tests (#1, #2 and #3) were successively performed 4, 8, and 16 hours after achieving thermal equilibrium to characterize temperature and physical aging effects on the mechanical properties of PC. Each creep test lasted 20 minutes, ensuring that, during each creep-recovery test, the duration of the recovery phase was at least ten times longer than the creep to allow the material to recover fully. Meanwhile, the duration of each creep test was less than 10% of the aging time to ignore aging effects during the current load step, as required in Struik (1977). The applied stress σ_0 was set to 10 MPa in all creep tests to ensure that the specimens were in their linear range.

The mechanical test, which includes four creep-recovery tests, is noted as *characterization test* in this work. In comparison, a *correction test* was performed following each characterization test, in which the temperature history was identical to the characterization test, but only the creep test #0 was conducted, and the load was then held at zero until the test was

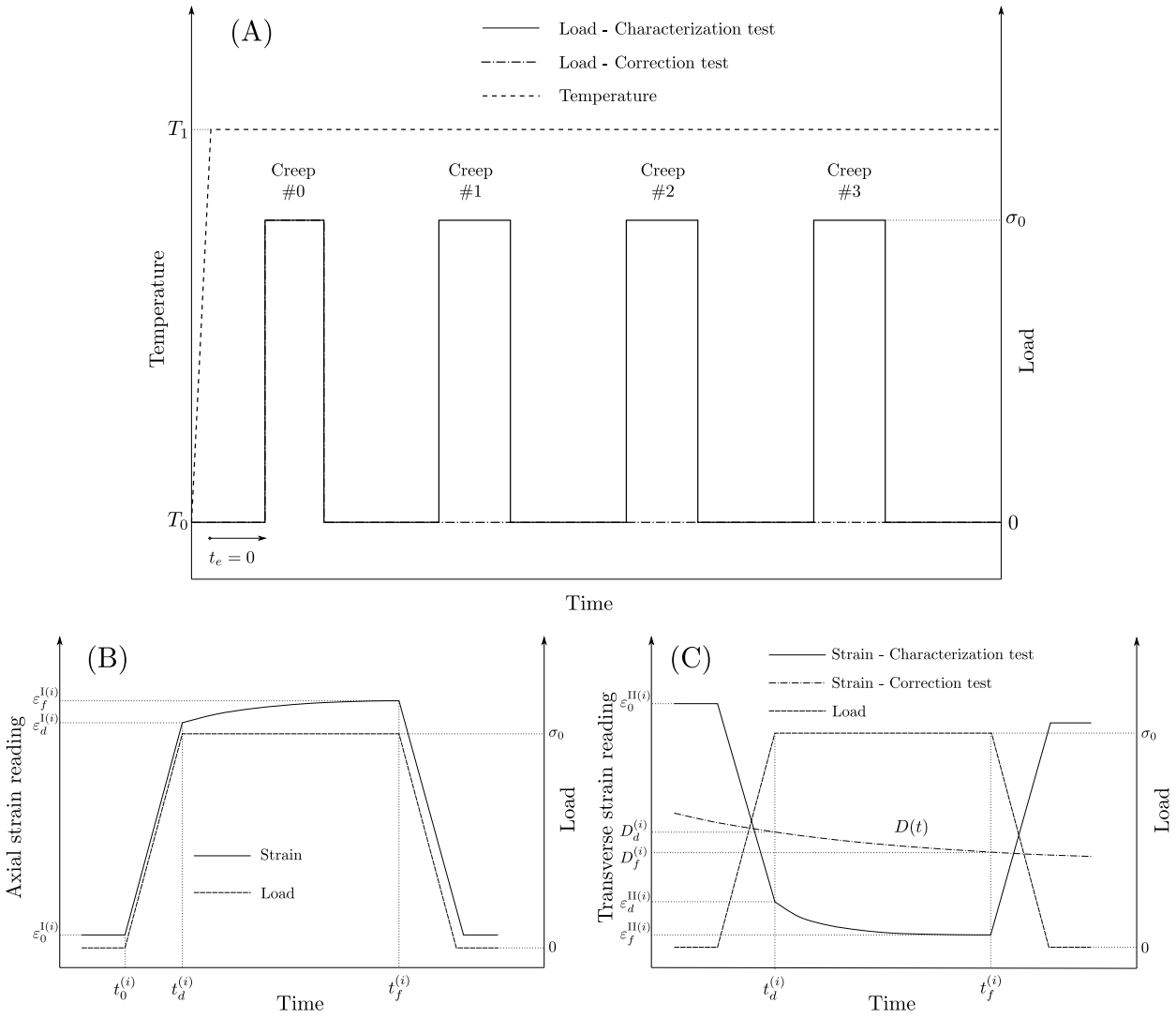

Figure 6.2 Illustration of the loading and temperature histories of the thermo-mechanical test and the resulting axial and transverse strains during a creep test. (A) Loading and temperature history used to characterize the temperature and physical aging effect of polymers based on Struik's methodology. σ_0 stands for the applied load. T_0 and T_1 are the room and investigation temperature, respectively. Creep test #0 indicates the first creep test used to align grips. Creep tests #1, #2 and #3 are creep tests performed at t_e = 4 h, 8 h and 16 h, respectively. t_e represents the aging time. Schematic illustration for the correction of extensometer measurements during creep test #i, from $t_d^{(i)}$ to $t_f^{(i)}$, for (B) axial strains ε^{I}; (C) transverse strains $\varepsilon^{\mathrm{II}}$. The warm-up and thermal drifts of axial and transverse strain measurements can be removed by subtracting the strain reading $\varepsilon_0^{(i)}$ before the load is applied. The penetration drift for transverse strains during the creep test in a characterization test can be eliminated by subtracting the change in transverse reading during the corresponding correction test, i.e., $D^{(i)}(t)$.

completed. The temperature and loading histories for the characterization and correction tests are illustrated in Figure 6.2(A).

In this work, thermo-mechanical tests were carried out on two specimens at 120 °C. The two characterization tests were performed 14 and 42 days after the specimens were manufactured, respectively. Each corresponding correction test was performed immediately after the characterization test was completed. The coefficient of thermal expansion (CTE) of PC specimens is assumed to be constant when there is no temperature gradient (Van Krevelen and Te Nijenhuis, 2009).

6.4.4 Strain measurement correction

Axial and transverse strains are required to characterize the three-dimensional effects of temperature and physical aging on the mechanical response. The axial strain is computed by dividing the axial measurement by the gauge length of 50 mm, while the transverse strain is computed by dividing the transverse measurement by the width of the specimen.

For axial measurements ε^{I}, the effect of penetration drift is negligible; therefore, only the warm-up and thermal drifts need to be addressed. These temperature-induced drifts occur instantaneously, thus they are constant with respect to time when the temperature is stable. Therefore, if the temperature of the extensometer remains constant, the warm-up and thermal drift in axial readings during each creep test can be corrected directly by subtracting the reading before the load is applied from the reading during the creep test. For the sake of illustration, consider creep test $\#i$ in a characterization test, i.e., the time during which the load is applied is from $t_d^{(i)}$ to $t_f^{(i)}$. Then, the axial strain measurement during the creep test $\#i$ can be corrected by:

$$\varepsilon^{\mathrm{I}}_{\mathrm{corrected}}(t) = \varepsilon^{\mathrm{I}}(t) - \varepsilon_0^{\mathrm{I}(i)}, \text{ for } t \in \left[t_d^{(i)}, t_f^{(i)}\right], \tag{6.1}$$

where $\varepsilon_0^{\mathrm{I}(i)}$ represents the axial strain reading before the load is applied. Figure 6.2(B) illustrates the correction for the axial strain measurement of the extensometer. Since a load of 0 N is applied before each creep test, the strain due to thermal expansion of the material and the shrinkage of the specimen due to the previous physical aging are also removed, resulting in a measurement curve representing the material's mechanical axial strain at the specified temperature and physical aging conditions.

The warm-up and thermal drifts of transverse measurements $\varepsilon^{\mathrm{II}}$ can be eliminated by the same procedure as that used for the axial measurements. Furthermore, since penetration drift significantly affects transverse strain measurements, it must also be compensated for. Note

that the associated correction test has the same temperature history as the characterization test, except that the axial load is zero from $t_d^{(i)}$ to $t_f^{(i)}$. The transverse reading $D(t)$ change during this period is due to the extensometer's penetration drift and the effect of physical aging on the transverse strain. Assuming that the effect of physical aging occurred during the creep test is ignored (Guo and Bradshaw, 2007), the negative increment in $D(t)$ represents the penetration drift. Unlike temperature-induced drift, which occurs instantaneously, penetration drift increases over time as the knife edges continuously pierce into the specimen. Therefore, the penetration drift during the creep test $\#i$ can be corrected by subtracting the change of transverse reading in the correction test, i.e., $D(t) - D_d^{(i)}$, from the characterization test results from $t_d^{(i)}$ to $t_f^{(i)}$. The full correction of transverse measurement can be obtained by:

$$\varepsilon^{\mathrm{II}}_{\mathrm{corrected}}(t) = \varepsilon^{\mathrm{II}}(t) - \varepsilon_0^{\mathrm{II}(i)} - \left(D(t) - D_d^{(i)}\right), \text{ for } t \in \left[t_d^{(i)}, t_f^{(i)}\right], \tag{6.2}$$

where $\varepsilon_0^{\mathrm{II}(i)}$ represents the transverse strain reading before the load is applied. $D_d^{(i)}$ is the transverse reading in the correction test at $t_d^{(i)}$. Figure 6.2(C) illustrates the correction for the transverse strain measurement of the extensometer. Note that the correction test was performed immediately after the associated characterization test, so the physical aging effect that occurred at room temperature between the correction and characterization test is considered negligible.

6.5 Results and discussion

The response of the extensometer itself to changes in temperature was first investigated, which allows a qualitative look at the features of the temperature-introduced drifts of the extensometer. Figure 6.3(A) presents the axial and transverse readings of the pined extensometer during temperature sensitivity tests. As the temperature in the environmental chamber increased, the axial readings initially increased and then decreased until they stabilized after one hour. The figure shows that the thermal drift is more significant at 80 °C than at 40 °C. Moreover, two 40 °C tests have different values for the final stable readings, even though their temperature histories are identical, which shows that the warm-up and thermal drifts of the extensometer are somewhat random. The axial reading and the temperature at the beginning of the test at 80 °C are detailed in Figure 6.3(B). The temperature raised with a constant gradient to 65 °C until 280 s, and the axial reading of the extensometer also increased continuously. Thereafter, the temperature continued to increase, but the gradient gradually decreased due to the automatic temperature control, resulting in a decrease in the axial reading. This indicates that the thermal drift in the axial reading is related to both the temperature and the temperature change gradient. In comparison, the transverse readings

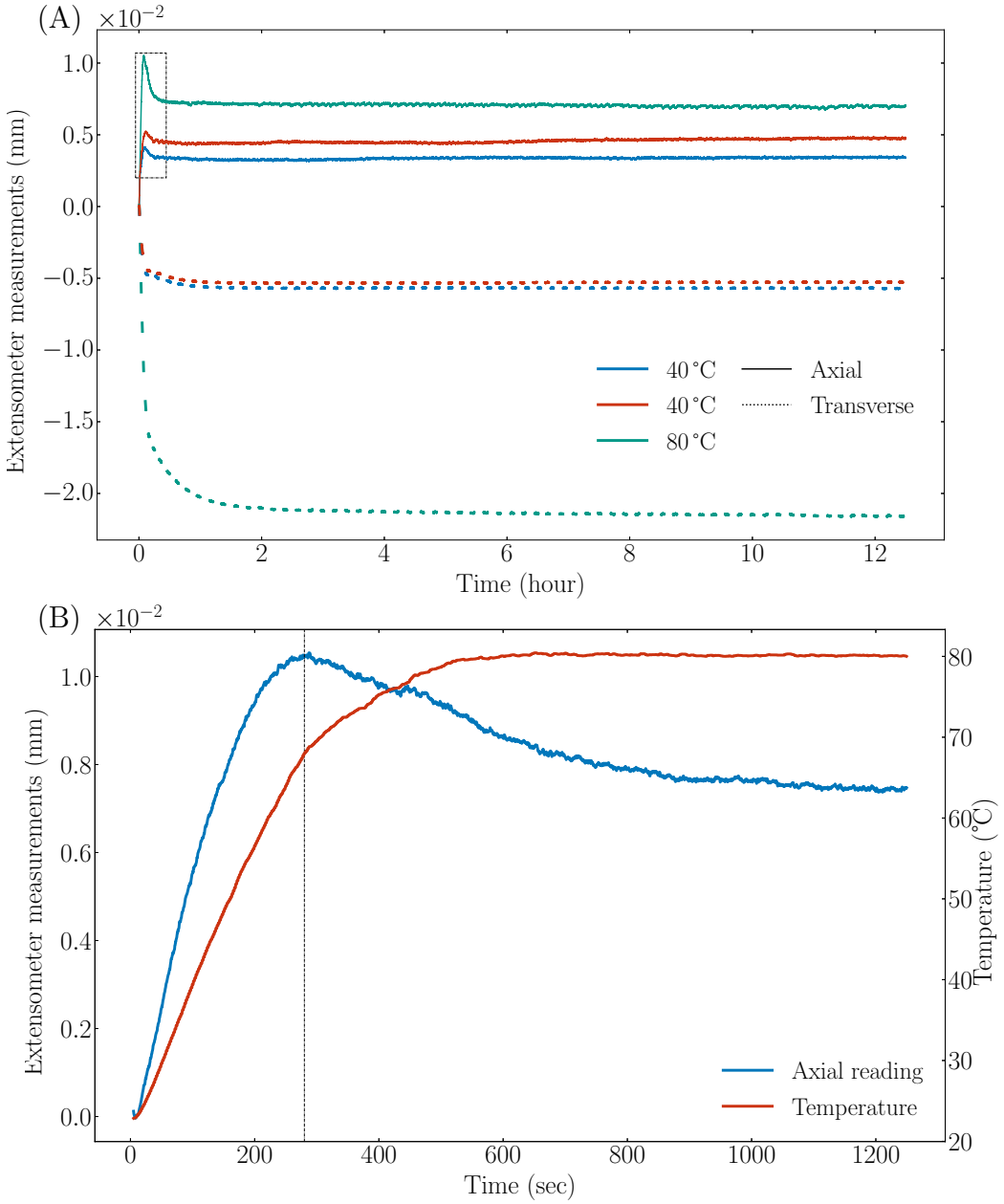

Figure 6.3 Extensometer's readings and temperature during three temperature sensitivity tests of the pined extensometer. (A) Axial and transverse readings during three tests; (B) Axial reading and temperature at the beginning of the test at 80 °C (the framed zone in (A)). The thermal drift of the axial measurement of the extensometer is related to both temperature and temperature gradient, and it takes an hour for the axial reading to stabilize. Transverse readings are affected by temperature changes and are not sensitive to temperature gradients, and it takes longer to stabilize when compared to axial readings.

were unaffected by the temperature gradient and continued to decrease as the temperature

increased. However, the time required to achieve stability is slightly longer than for the axial direction, taking approximately two hours. Therefore, the temperature-introduced drifts in both axial and transverse readings were stabilized before creep test #1 was run and can be corrected through the procedure detailed in Section 6.4.4. Note that these drifts were all subtracted and the creep tests were conducted under isothermal conditions. Thus the quantitative investigation of the response of the extensometer to the temperature is not required in the current work.

Figure 6.4 depicts the axial measurements with the extensometer and the axial strains for each creep test during two thermo-mechanical tests conducted at 120 °C. At the beginning of each thermo-mechanical test, axial measurements significantly increased due to the thermal expansion of the specimen and the warm-up and thermal drifts of the extensometer, followed immediately by a decrease caused by thermal drift. This decrease continued until the load of creep test #0 was applied, caused by the effect of physical aging at high temperatures. This continuous physical aging made the specimen stiffer, resulting in the strain readings decreasing while the load dwelled at 0 N. Likewise, the strain decrease during each recovery phase can also be explained by the effect of continuous physical aging, which is consistent with previous research findings (Grassia and D'Amore, 2009; Grassia and D'Amore, 2006). Once the warm-up and thermal drifts are corrected, the axial strains during each creep test are essentially identical, except for a minimal vertical offset with the order of magnitude of 1×10^{-6} mm/mm.

The transverse measurements, as well as the corrected transverse strains in two thermo-mechanical tests conducted at 120 °C, are shown in Figure 6.5. As for the axial measurements, there is a difference between the transverse measurements for the two tests, which is due to the random warm-up drift of the extensometer and the clamping force that is not the same from test to test. It can be found that the extensometer's transverse readings began to decrease immediately after the test began, and this trend continued for the next 20 hours. This process involves the material's thermal expansion, the effect of physical aging, the warm-up and thermal drifts, and the penetration drift caused by the extensometer knife edge piercing into the specimen, which consistently increased over time until the end of the test. Once temperature-introduced drifts are compensated for, the corrected transverse strains during each creep test are nearly identical for two tests, with a slight offset of 3×10^{-5} mm/mm. It can also be found that the continuously increasing penetration drift slightly affects the transverse readings, especially for the latter part of the creep test. After correcting the penetration drift, the transverse strain readings at the end of two tests changed from -2.61×10^{-3} to -2.56×10^{-3} ($\uparrow$ 1.92%) and from -2.56×10^{-3} to -2.51×10^{-3} ($\uparrow$ 1.95%), respectively.

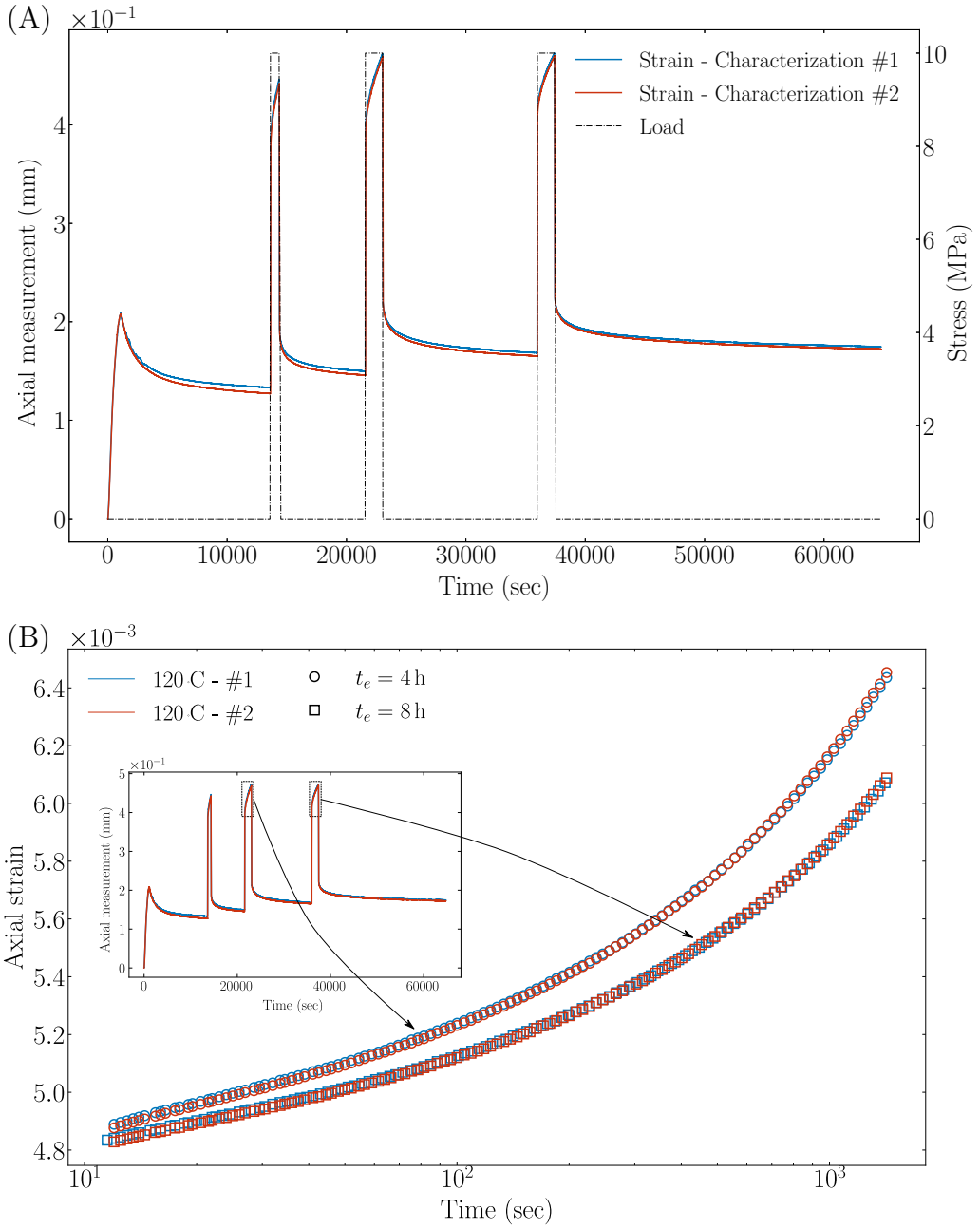

Figure 6.4 Measured and corrected axial strains during two thermo-mechanical tests conducted at 120 °C. (A) The full axial strain measurements with the bi-axial extensometer ; (B) The corrected axial strain during creep tests #1 and #2. For each thermo-mechanical test, the time is set to zero at the moment the load is applied. Although slight differences can be found in the axial measurements through the extensometer between the two tests due to the drift of the extensometer, the corrected axial strain is almost the same, except for an offset of the order of 1×10^{-6} mm/mm. The axial results show reproducibility.

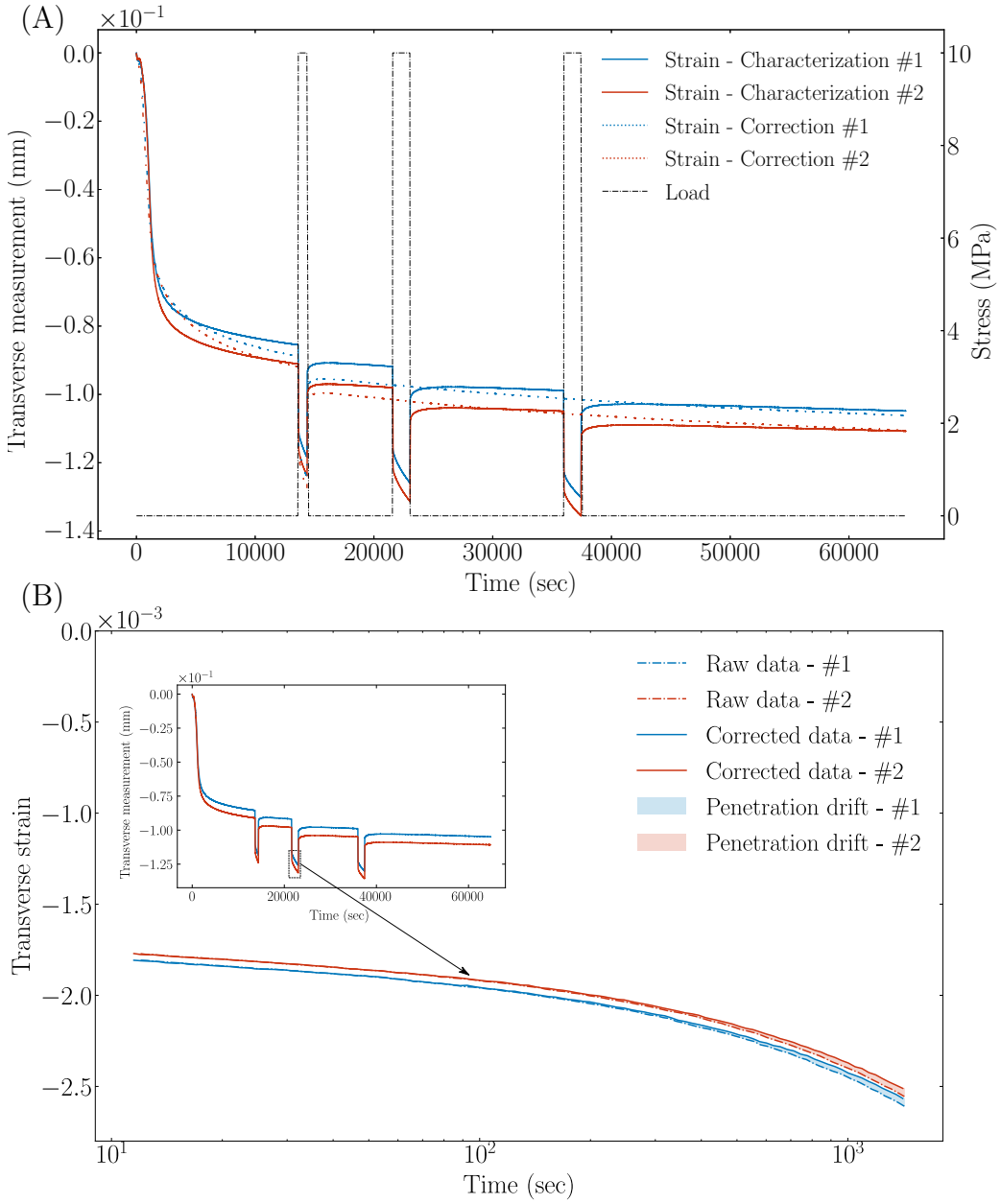

Figure 6.5 Measured and corrected transverse strain results during two thermo-mechanical tests at 120 °C. (A) The full transverse strain measurements with the bi-axial extensometer; (B) The corrected transverse strain during creep tests #1 for each thermal-mechanical test. The *raw data* represents the transverse strains corrected for the warm-up and thermal drifts, while the *corrected data* stands for those subtracting all drifts. The difference between these two data represents the continuously increasing penetration drift during each test, which slightly affects the transverse results, resulting an error of 1.9% at the end of creep test #1 for both two tests. The corrected transverse strains for two tests have a relatively slight offset of 3×10^{-5} mm/mm, which demonstrate reproducibility of results.

The volumetric strain $\varepsilon^{\ddagger}$ can be computed from the axial and transverse strains to identify the bulk behavior of materials (Yue *et al.*, 2021), which is expressed as:

$$\varepsilon^{\ddagger} = \varepsilon^{\mathrm{I}} + 2\varepsilon^{\mathrm{II}}. \tag{6.3}$$

To yield thermodynamic consistency, the time-dependent bulk compliance of the viscoelastic material must be monotonic (Bouleau, 1991). Therefore, the monotonicity of the strain $\varepsilon^{\ddagger}$ can demonstrate the reliability of the experimental results.

Figure 6.6 presents corrected strains $\varepsilon^{\ddagger}$ for two tests (creep #1) at 120 °C. It can be found that there was a pronounced drop in the strain $\varepsilon^{\ddagger}$ at the end of both tests, which lacks physical meaning. This indicates that although the penetration drifts slightly influenced the transverse measurements (approximately 1.9%), it significantly affected the results for the characterization of polymers, especially for the bulk property. After correction, the strain increased monotonically, implying that the corrected results were thermodynamically

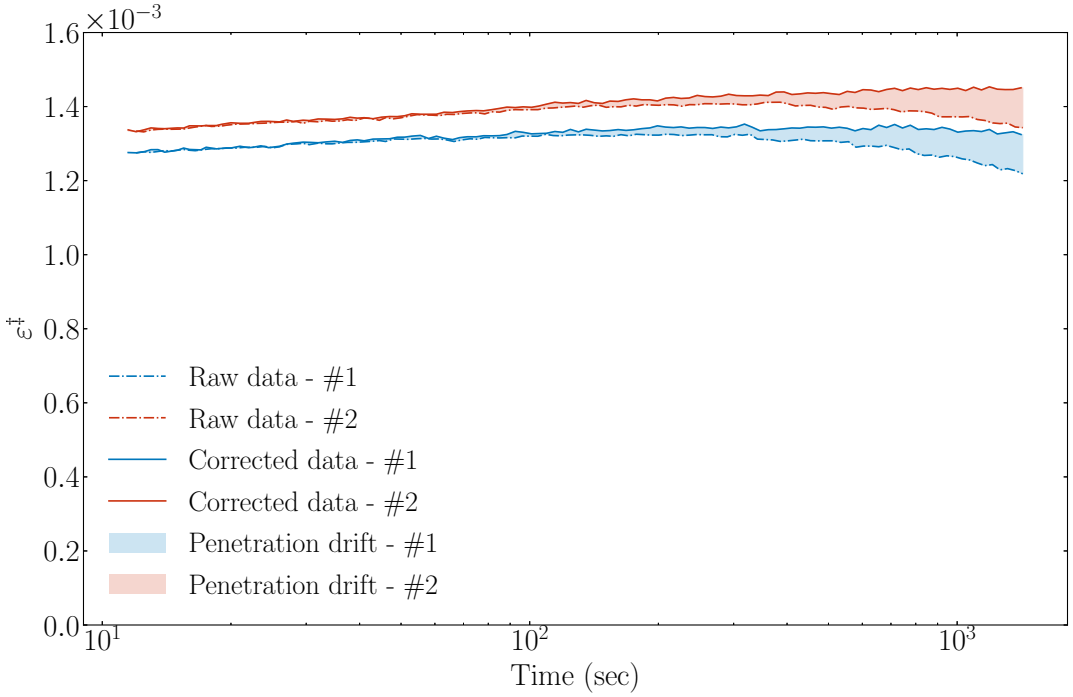

Figure 6.6 Comparison of strains $\varepsilon^{\ddagger}$ with and without the removal of the penetration drift during creep test #1 in two thermal-mechanical tests at 120 °C. The *raw data* were computed by subtracting only the warm-up and thermal drifts from the axial and transverse strains, whereas the *corrected data* were obtained from raw data by subtracting the penetration drift. After removing the penetration drift in the transverse strain, strains $\varepsilon^{\ddagger}$ increased monotonically over time, which were thermodynamically consistent.

consistent. Moreover, strains $\varepsilon^{\ddagger}$ are nearly identical for both experiments, except for a few minimal offsets of the order of 1×10^{-5} mm/mm.

The reproducibility of experimental results in this work can be proved by the slight vertical offsets between the corrected results for two characterization tests. Consider that the physical aging effect of PC at room temperature for 28 days is much smaller than that of aging for 4 hours at 120 °C, these offsets may be caused by the error introduced by the manual installation of the extensometer. While these offsets are small, they can still affect the results in some tests. For example, when characterizing the bulk properties of the polymer at different temperatures, these offsets of measurement are likely to override the amount of change in bulk modulus at different temperatures because the bulk modulus itself does not change much with temperature (Qvale and Ravi-Chandar, 2004). Therefore, if more prominent precision is required, it is necessary to use a non-contact technique, such as DIC, to measure strains during thermo-mechanical testing.

6.6 Conclusion

The main contribution of this work was to analyze the errors of strain measurements with a bi-axial extensometer in thermo-mechanical testing and propose solutions for eliminating these errors. Two experiments at 120 °C demonstrated the reproducibility of the experimental results, thereby attesting the reliability of the proposed experimental procedure.

The methodology presented in this work can be used to characterize the temperature and physical aging effects on viscoelasticity of polymer materials and provide guidance for other mechanical testing, such as the characterization of elastic modulus and Poisson's ratio, involving polymer materials at high temperatures. Moreover, this experimental procedure can serve as a protocol for future research involving the characterization of the three-dimensional properties of polymers or polymer composites within a bi-axial extensometer in thermo-mechanical testing.

Declaration of competing interest

The authors declare that they have no known competing financial interests or personal relationships that could have appeared to influence the work reported in this paper.

Acknowledgments

This research was partially funded by the Natural Sciences and Engineering Research Council (NSERC) of Canada, Discovery Grant RGPIN-06412-2016 and GRPIN-2019-05048, and Fonds de Recherche du Québec Nature et technologies (FRQNT), Team Research Project 146219. The authors greatly acknowledge Dr. Qingkai Meng from *Lavergne, Inc* for providing PC pellets, Anic Desforges from Department of Chemical Engineering Polytechnique Montréal for assisting the injection molding of PC specimens and Tanja Pelzman from Department of Mechanical Engineering Polytechnique Montréal for her assistance in troubleshooting the thermocouple.

CHAPTER 7 ARTICLE 3: ON THE PARAMETERS IDENTIFICATION OF THREE-DIMENSIONAL AGING-TEMPERATURE DEPENDENT VISCOELASTIC SOLIDS THROUGH A BAYESIAN APPROACH

L. Yue, M. C. Heuzey, J. Jalbert and M. Lévesque. Submitted to *Mechanics of Time-Dependent Materials* on March 1, 2022. *Minor changes were made following the jury's comments when compared to the submitted version.*

7.1 Abstract

Temperature and physical aging effects are present in the long-term mechanical properties of solid polymers under complex working conditions. In addition, these effects on the three-dimensional behavior of polymer solids, such as shear and bulk properties, are critical for developing polymer composite systems but are rarely addressed. We extend the previously proposed Bayesian framework method in this work to simultaneously identify the viscoelastic, temperature, and physical aging related model parameters. We apply this methodology to three-dimensional experimental data from non-isothermal physical aging tests on polycarbonate. The experimental results are in excellent agreement with the predictions with the identified parameters.

7.2 Introduction

With the increasing use of polymer composites in engineering, it has become critical to investigate the performance of materials under a variety of complex working conditions. The mechanical property changes of polymers due to temperature and physical aging have garnered considerable attention to improve prediction accuracy (Bradshaw and Brinson, 1997a; Courtois, Marcin, *et al.*, 2019; Crochon *et al.*, 2015; McKenna *et al.*, 1995; Struik, 1977). The majority of research has, however, been concentrated on uni-dimensional mechanical properties of polymer solids, which limits the predictions capabilities in demanding applications, like aerospace, for components submitted to real service conditions.

A Bayesian framework based method for automatically and robustly identifying three-dimensional viscoelastic parameters from experimental data has been proposed in our previous work (Yue *et al.*, 2021). This method is capable of not only accurately identifying viscoelastic parameters but also of determining the optimal number of required parameters. However, it is limited to viscoelastic solids at room temperature. The purpose of this work

consists in extending the previously proposed method for three-dimensional viscoelasticity by incorporating temperature and physical aging effects. The viscoelastic parameters with the optimal number of Prony series, along with the temperature and physical aging model parameters, can be derived simultaneously.

This paper is organized as follows. Section 7.3 recalls notions of physical aging and the time-temperature superposition (TTS) principle for viscoelasticity. The experimental details and methodologies are listed in Section 7.4. Section 7.5 describes the identification method for viscoelastic, temperature and physical aging model parameters. Section 7.6 applies the identification method to polycarbonate specimens and compares the experimental data and the predictions with the identified parameters. Section 7.7 concludes this work.

7.3 Background

7.3.1 Physical aging of polymers

Physical aging manifests itself through a variation of viscoelastic properties as a function of time, for temperatures below the glass transition temperature (T_g) and under no influence from any other external stimuli (Hutchinson, 1995; White, 2006). A polymer remains in its thermodynamic equilibrium state above its T_g. However, when it is quenched from a temperature above its T_g to a temperature below its T_g, the molecular rearrangements that occur rapidly at the equilibrium state are significantly slowed down to a range that the material cannot maintain an equilibrium with the cooling rate. As a result, the polymer remains in the non-equilibrium state and towards equilibrium through a process called physical aging. Physical aging typically increases the brittleness and the stiffness of the polymer (Struik, 1977).

Physical aging effects on the mechanical properties of polymers can be measured by the classical methodology proposed by Struik (1977). The aging test usually starts with an annealing period, named "rejuvenation" (McKenna, 2003), during which the polymer is submitted to a temperature above its T_g for a while to erase its previous thermal or aging histories. Next, the specimen is quenched to the specified temperature below its glass transition temperature and kept at this temperature. Then, a sequence of creep and recovery tests is performed on the material. The aging test can be classified as *isothermal* or *non-isothermal* depending on whether the temperature reaches the target temperature directly or undergoes a complex temperature history before arriving to the test temperature.

The effects of temperature and aging on mechanical properties have received a great deal of attention (Bradshaw and Brinson, 1997a; Courtois, Marcin, *et al.*, 2019; Crochon *et al.*,

2015; Guo and Bradshaw, 2007; Hernández *et al.*, 2017; McKenna *et al.*, 1995; Struik, 1977). Especially, Brinson, Bradshaw, and Guo have done a remarkable series of studies on non-isothermal physical aging (Bradshaw and Brinson, 1997a, 1997b; Guo and Bradshaw, 2009; Guo *et al.*, 2009). They have proposed several models for characterizing the effects of physical aging and accurately predicting the long-term mechanical properties of polymers to within a 10% error.

However, most works found in the literature have focused on studying the changes for uni-dimensional mechanical properties of polymers or polymer composites in the long term. The related three-dimensional issues have rarely been addressed. Therefore, this work focuses on the changes of three-dimensional mechanical properties of polymers submitted to different temperatures and aging conditions.

7.3.2 Linear viscoelasticity and temperature-time effect

The three-dimensional linearly viscoelastic constitutive theory can be represented using a hereditary integral form (Biot, 1954; Lévesque *et al.*, 2008) as:

$$\boldsymbol{\varepsilon}(t) = \int_0^t \mathbf{S}(t-\tau) : \frac{\mathrm{d}\boldsymbol{\sigma}}{\mathrm{d}\tau}\mathrm{d}\tau, \tag{7.1}$$

where $\boldsymbol{\sigma}$ stands for the applied stress tensor and $\boldsymbol{\varepsilon}$ represents the resulting strain tensor. $\mathbf{S}(t)$ refers to the so-called retardation kernel function, which must be positive and monotonic to yield the thermodynamic consistency (Bouleau, 1991). Different viscoelastic constitutive theories can be adopted by altering the expression of $\mathbf{S}(t)$. The Prony series model is widely used in engineering to simulate linear viscoelasticity by describing the retardation kernel as:

$$\mathbf{S}(t) = \mathbf{S}^{(0)} + \sum_{m=1}^{M} \mathbf{S}^{(m)}(1 - \exp[-\lambda_m t]), \tag{7.2}$$

where $\mathbf{S}^{(0)}$ is the instantaneous creep compliance, $\mathbf{S}^{(m)}$ denote creep compliances which are positive semidefinite tensors and λ_m are reciprocal retardation times associated with the compliances $\mathbf{S}^{(m)}$. M stands for the total number of retardation times.

To evaluate the viscoelastic properties of polymers at different temperatures, the time-temperature superposition (TTS) principle is generally utilized, which relates the material properties under a service condition to its properties in a reference state by a so-called *shift factor* (Christensen, 2012). The creep compliance $\mathbf{S}(t)$ of a material aged for a time t_e at temperature T can be obtained by shifting the creep compliance $\mathbf{S}^{\mathrm{ref}}(t)$ when aged for a

reference time t_e^{ref} at reference temperature T^{ref} by:

$$\mathbf{S}(t;T,t_e) = a_v(T,t_e)\ \mathbf{S}^{\text{ref}}\left(\frac{t}{a(T,t_e)};T^{\text{ref}},t_e^{\text{ref}}\right), \tag{7.3}$$

where $a(T,t_e)$ and $a_v(T,t_e)$ respectively denote horizontal and vertical shift factors that depend on temperature and physical aging. The shift factor $a_v(T,t_e)$ is generally found to have little effect, when compared to the horizontal shift factor, and can be considered to be close to unity in most cases (Bradshaw and Brinson, 1999; Crochon *et al.*, 2015; Sullivan *et al.*, 1993). The horizontal shift factor $a(T,t_e)$ can be decomposed into the product of the temperature shift factor a_T and the aging shift factor a_{t_e} (Bradshaw and Brinson, 1997b; Struik, 1977), leading to:

$$a(T,t_e) = a_T a_{t_e}. \tag{7.4}$$

The temperature shift factor a_T is commonly mathematically described by the Arrhenius equation (Christensen, 2012) and the Williams-Landel-Ferry (WLF) model (Williams *et al.*, 1955) which is expressed as:

$$\log a_T = -\frac{C_0(T-T^{\text{ref}})}{C_1+(T-T^{\text{ref}})}, \tag{7.5}$$

where C_0 and C_1 denote universal constants. The aging shift factor a_{te} for an isothermal aging test can be evaluated by Struik (1977)

$$a_{t_e}(t_e,T) = \left(\frac{t_e}{t_e^{\text{ref}}}\right)^{\mu(T)}, \tag{7.6}$$

where μ stands for the shift rate depending on the temperature and is assumed constant during aging. The aging time t_e is defined as the time elapsed since the specimen was quenched to the aging test temperature T. However, Equation (7.6) is no longer valid for non-isothermal aging tests undergoing complex thermal histories due to the memory effects (Bradshaw and Brinson, 1997a).

Bradshaw and Brinson proposed the continuous shift factor (CSF) method to compute the mechanical properties of polymers during a non-isothermal aging test (Bradshaw and Brinson, 1997a, 1997b). Based on the effective time theory (Brinson and Gates, 1995; Knauss and Emri, 1981), Equation (7.1) becomes

$$\boldsymbol{\varepsilon}(t) = \int_0^t \mathbf{S}(\phi(t)-\phi(\tau)) : \frac{\mathrm{d}\boldsymbol{\sigma}}{\mathrm{d}\tau}\mathrm{d}\tau, \tag{7.7}$$

where the effective time ϕ is utilized in this method to record the accumulative effects of temperature and physical aging throughout the complex thermal history, i.e. $\mathrm{d}\phi = a_T a_{t_e}(\xi)\mathrm{d}\xi$. Due to the absence of an analytical form for ϕ, a reasonable function must be chosen to fit Equation (7.7) to experimental data; shift factors can then be evaluated. This method is able to accurately simulate and predict the long-term mechanical behavior of polymers. However, the choice of fitting function for the effective time is arbitrary and artificial.

Guo and Bradshaw developed the KAHR-a_{t_e} method to predict the mechanical response of polymers during long-term non-isothermal physical aging (Guo and Bradshaw, 2009; Guo *et al.*, 2009). In this method, based on experimental observations (McKenna *et al.*, 1995; Struik, 1977, 1988), the relationship between the aging shift factor a_{t_e} and the structural shift factor a_δ has been assumed as:

$$a_{t_e}(a_\delta)\Big|_T = \left(\frac{c_0}{a_\delta}\right)^{c_1};\ c_0, c_1 > 0, \tag{7.8}$$

where T is the temperature at which the mechanical load is applied, c_0 and c_1 are temperature dependent constants. According to the KAHR model (Kovacs *et al.*, 1979), a_δ can be expressed as:

$$a_\delta = \exp[-\zeta\delta], \tag{7.9}$$

where ζ is a material parameter. δ denotes the specific volume recovery response, defined as the normalized departure from the equilibrium state of the polymers during physical aging, and can be determined by:

$$\delta(z) = -\Delta\alpha \int_0^z R(z-\varsigma)\frac{\mathrm{d}T}{\mathrm{d}\varsigma}\mathrm{d}\varsigma, \tag{7.10}$$

with

$$R(z) = \exp\left[-\left(\frac{z}{\tau_\alpha}\right)^{\beta_\alpha}\right], \tag{7.11}$$

and

$$z(t) = \int_0^t \frac{\mathrm{d}\xi}{a_T a_\delta}, \tag{7.12}$$

where $\Delta\alpha = \alpha_l - \alpha_g$ represents the difference in the coefficient thermal expansion (CTE) between the liquid and glassy states of the polymer. R is the normalized retardation function of the reduced time z with the material parameters τ_α and β_α. The temperature shift factor is given by (Kovacs *et al.*, 1979):

$$a_T = \exp[-\Delta\alpha\zeta e^b(T - T_r)], \tag{7.13}$$

where T_r is a reference temperature and b is a material constant. Thus, six parameters (ζ,

b, c_0, c_1 τ_α, β_α) are required in this model that must be determined through non-isothermal aging tests.

The KAHR-a_{t_e} model can be also extended to incorporate the temperature effect on the material response (Guo and Bradshaw, 2009). To do this, a shift factor $a_{T,\delta}$ is defined to scale a_δ of the reference aging time t_e^{ref} from the test temperature T to the reference temperature T^{ref} as:

$$a_{T,\delta} = a_{\delta,\text{iso}}\left(T^{\text{ref}}, t_e^{\text{ref}}\right) \Big/ a_{\delta,\text{iso}}\left(T, t_e^{\text{ref}}\right), \tag{7.14}$$

where $a_{\delta,\text{iso}}$ is the isothermal structural shift factor that can be evaluated by Equation (7.9) at different temperatures and aging times. Finally, the shift factor that combines the non-isothermal physical aging and the temperature effect becomes:

$$a_{t_e}(a_\delta)\Big|_T = \left(\frac{c_0}{a_\delta a_{T,\delta}}\right)^{c_1}. \tag{7.15}$$

When compared to the CSF method, the KAHR-a_{t_e} model combines the physical aging specific volume model (KAHR model) and experimental observations. Therefore, the KAHR-a_{t_e} model is used in this work to model mechanical properties evolution during a non-isothermal physical aging test.

Note that there is no closed-form analytical expression for $a_{t_e}(a_\delta)|_T$ in the KAHR-a_{t_e} model. Therefore a_{t_e} must be numerically evaluated for the given experimental condition (Guo *et al.*, 2009). The temperature history during a non-isothermal aging test can be expressed by:

$$T(t) = T_g + \sum_{m=0}^{M} H(t-\tau_m)\Delta T_m, \tag{7.16}$$

where τ_m and ΔT_m denote the time and the temperature change at the mth temperature jump, respectively. $H(t)$ is the Heaviside function. Differentiating Equation (7.12) and substituting Equations (7.9, 7.10, 7.11, 7.13) leads to

$$\frac{\mathrm{d}z}{\mathrm{d}t}(z) = \exp\left[\Delta\alpha\zeta\left\{e^b\left(T(z)-T_r\right) - \int_0^z R(z-\varsigma)\frac{\mathrm{d}T}{\mathrm{d}\varsigma}\mathrm{d}\varsigma\right\}\right]. \tag{7.17}$$

When substituting Equation (7.16) into the integral term in Equation (7.17), the derivative of z becomes

$$\frac{\mathrm{d}z}{\mathrm{d}t}(z) = \exp\left[\Delta\alpha\zeta\left\{e^b\left(T_p-T_r\right) - \sum_{m=0}^{p}\Delta T_m R\left(z-\tilde{\tau}_m\right)\right\}\right], \text{ for } t\in[\tau_p,\tau_{p+1}], \tag{7.18}$$

where $\tilde{\tau}_m = z(\tau_m)$. Equation (7.18) is an ordinary differential equation (ODE) of z with the

initial condition $z(0) = 0$. Once this ODE is solved, it is straightforward to compute all required variables in the KAHR-a_{t_e} model.

7.3.3 Three-dimensional viscoelastic properties of polymers

When modeling or characterizing the three-dimensional viscoelastic properties of polymers, it is often assumed that the bulk modulus or Poisson's ratio of the material is constant. Thus, the three-dimensional problem can be reduced to a uni-dimensional problem in most cases (Courtois, Marcin, *et al.*, 2019; Crochon *et al.*, 2015). However, this assumption may be violated, especially if the test duration is sufficiently long, or when investigating the effect of temperature on mechanical properties of polymers (Lu *et al.*, 1997; Qvale and Ravi-Chandar, 2004).

In the context of linear viscoelasticity, the use of any two of the four material functions (the Young's modulus, the shear modulus, the bulk modulus, and Poisson's ratio) is sufficient to model the three-dimensional properties of isotropic materials (Lu *et al.*, 1997). These two material functions must be determined simultaneously (Tschoegl *et al.*, 2002). Several methods have been proposed to determine the bulk modulus and other material functions simultaneously.

To determine the bulk behavior of polymethylmethrylate (PMMA), Lu *et al.* (1997) measured the Young's modulus and Poisson's ratio of planar specimens, and the Young's and shear functions of cylindrical specimens. The bulk function of PMMA was then computed using the material functions measured from the two tests, respectively. It was found that the bulk function requires a high level of measurement accuracy; consequently, the bulk function cannot be robustly derived from the other material functions and must be determined directly from the experiments.

Several special experimental configurations have been developed to measure the bulk properties of polymers. For example, an atmospheric pressure chamber was used to measure the dynamic bulk compliance of PMMA and polyvinyl acetate (PVAc) (Sane and Knauss, 2001), and a confined compression set-up was used to determine the bulk and shear relaxation response of PMMA and polycarbonate (PC) (Qvale and Ravi-Chandar, 2004). However, the measurement accuracy of the bulk behavior of polymers is susceptible to errors caused by experimental set-up. For example, it was found that a gap of 1.27×10^{-2} mm between the specimen and the equipment could introduce errors up to 30% in the bulk properties measurement (Qvale and Ravi-Chandar, 2004). In addition, the accessibility of these devices limits their widespread use in engineering.

In our previous work (Yue *et al.*, 2021), a relatively simple method was used to simultaneously determine the bulk and shear functions of polymers by measuring the axial and transverse strains of a tensile specimen. In a tensile test with an applied uni-axial load, a strain transformation can be defined as:

$$\varepsilon^{\dagger} = \varepsilon_{\mathrm{I}} - \varepsilon_{\mathrm{II}}, \tag{7.19a}$$

$$\varepsilon^{\ddagger} = \varepsilon_{\mathrm{I}} + 2\varepsilon_{\mathrm{II}}, \tag{7.19b}$$

where ε_{I} and $\varepsilon_{\mathrm{II}}$ denote the axial and transverse strain measurements, respectively. Then, $2\varepsilon^{\dagger}$ and $3\varepsilon^{\ddagger}$ are the deviatoric and the volumetric strain and can therefore be used to directly determine the shear and bulk properties of the material, respectively. It should be noted that the accuracy of this method depends on the accuracy of the transverse strain measurements, particularly for characterizing the bulk behavior.

7.3.4 Viscoelastic parameters identification

Identifying viscoelastic parameters from experimental data is an ill-posed problem, which means that the parameters identified might not be unique, and small perturbations in experiments can have a relatively significant effect on the identification process. To overcome this ill-posedness and obtain the optimal number of Prony series, a Bayesian framework based identification method has previously been proposed (Yue *et al.*, 2021).

In a mechanical experiment, the relationship between experimental measurements $\boldsymbol{y}$, e.g. the measured strains in creep tests, and model predictions $\boldsymbol{g}(\boldsymbol{\theta}; \boldsymbol{x})$ with the submitted excitation $\boldsymbol{x}$, e.g. the applied stress in creep tests, can be drawn using an observation model with an additive error $\boldsymbol{\epsilon}$ as

$$y_i = g(\boldsymbol{\theta}; x_i) + \epsilon_i, \ i = 1, \ldots, T, \tag{7.20a}$$

$$\epsilon_i \sim \mathcal{N}(0, \sigma_{\epsilon}^2), \tag{7.20b}$$

where $\boldsymbol{\epsilon}$ is assumed as a zero mean Gaussian variable with variance σ_{ϵ}^2. $\boldsymbol{\theta}$ stands for the vector of constitutive model parameters, e.g. $\boldsymbol{\theta} = \{\tilde{\mu}_0, \tilde{\mu}_1, \ldots, \tilde{\mu}_M, \lambda_1^{\mu}, \ldots, \lambda_M^{\mu}\}$ for a viscoelastic shear compliance constitutive model.

The parameter identification problem can be turned equivalently into the problem of determining the posterior distribution of unknown parameters with known experimental data (Kaipio and Somersalo, 2006). According to the Bayesian paradigm, the posterior function

can be calculated by:

$$f_{(\boldsymbol{\theta}|\boldsymbol{Y}=\boldsymbol{y})}(\boldsymbol{\theta}) \propto f_{(\boldsymbol{Y}|\boldsymbol{\theta})}(\boldsymbol{y}) \times f_{\boldsymbol{\theta}}(\boldsymbol{\theta}), \tag{7.21}$$

where the likelihood function $f_{(\boldsymbol{Y}|\boldsymbol{\theta})}$ is computed based on the assumption that the additive error is a Gaussian random variable as:

$$f_{(\boldsymbol{Y}|\boldsymbol{\theta},\sigma_\epsilon^2)}(\boldsymbol{y}) \propto \exp\left\{-\frac{1}{2\sigma_\epsilon^2}\left|\left|\, \boldsymbol{y} - \boldsymbol{g}(\boldsymbol{\theta};\boldsymbol{x}) \,\right|\right|_2\right\}, \tag{7.22}$$

where σ_ϵ can be evaluated by

$$f_{(\sigma_\epsilon^2|\boldsymbol{Y}=\boldsymbol{y},\boldsymbol{\theta})}(\sigma_\epsilon^2) \sim \text{InvGamma}\left\{\frac{T}{2}\,,\ \frac{1}{2}\sum_{i=1}^{T}\left(y_i - g(\boldsymbol{\theta};x_i)\right)^2\right\}. \tag{7.23}$$

An ordered relation in the prior function is imposed to avoid identifiability issues as

$$f_{\boldsymbol{\theta}}(\boldsymbol{\theta}) \propto \begin{cases} \frac{1}{\lambda_1} \times \ldots \times \frac{1}{\lambda_M} & \text{if } 0 < \lambda_1 < \ldots < \lambda_M, \\ 0 & \text{otherwise.} \end{cases} \tag{7.24}$$

The numerical evaluation of Equation (7.21) can be conducted by the *Markov Chain Monte Carlo* (MCMC) simulation (Gelman *et al.*, 2013). Then, the point estimates for parameters is obtained from the *maximum a posteriori* (MAP) estimate as

$$\hat{\boldsymbol{\theta}}_{\text{MAP}} = \underset{\boldsymbol{\theta}\in\mathbb{R}^+}{\arg\max}\ f_{(\boldsymbol{\theta}|\boldsymbol{Y}=\boldsymbol{y})}(\boldsymbol{\theta}). \tag{7.25}$$

Finally, the optimal number of Prony series M can be obtained by maximizing the *Bayesian Information Criterion* (BIC) (Schwarz, 1978), which is expressed as

$$\text{BIC}(M) = \ln f_{(\boldsymbol{Y}|\hat{\boldsymbol{\theta}}_{\text{MAP}})}(\boldsymbol{y}) - \frac{1}{2}(2M+1)\ln T. \tag{7.26}$$

7.4 Material and methods

7.4.1 Materials

The material investigated in this work was polycarbonate (PC) with a glass transition temperature of 150 °C. The virgin PC pellet (Product number PE-1220R-MP) was provided by *Lavergne, Inc.* The pellets were dried at 120 °C for 24 h, afterward, ASTM D638 standard type-I specimens were manufactured at 300 °C by injection molding with a *Sumitomo* SE-50S machine. The specimens were conserved in a desiccator to avoid moisture degradation effects

after the manufacture until mechanical testing.

7.4.2 Equipment

Tensile creep testing was conducted with a MTS® Insight electromechanical machine equipped with a 1 000 N load cell, whose precision is ±0.1 N. The Insight machine was controlled by the software *TestSuite TW Elite*. A LBO-series environmental chamber from *Thermcraft, Inc* was installed on the Insight machine. The temperature was controlled in the air surrounding the specimen with the thermal controller while monitoring the temperature of the specimen was achieved with a thermocouple set in its gauge section.

Axial and transverse strains were measured by a bi-axial extensometer (Model 3560) from *Epsilon Technology, Corp.* Axial strains were measured by averaging two gauges in axial direction with a gauge length of 50 mm. Transverse strains were obtained by only one gauge in the lateral direction.

7.4.3 Experiments

In this work, sequential creep-recovery tests were performed at various temperatures based on the classical methodology proposed by Struik for evaluating non-isothermal physical aging effect (Struik, 1977). However, several modifications were made in the mechanical testing.

The physical aging was considered to begin directly from the time the specimen had been manufactured. Therefore, no further rejuvenation was required to remove the previous temperature history at the beginning of the test. The specimens then underwent two stages of physical aging. One was the period during which the specimens were conserved in the desiccator at room temperature (around 20 °C). The other stage was the sequential creep-recovery tests performed on the specimens at elevated temperatures. For the sake of clarity and convenience, the time elapsed at the room temperature is referred to as *aged time* and at elevated temperature as *aging time*.

In the second physical aging stage, four creep-recovery tests were performed for each specimen. The first creep test was used to adjust the position of grips of the Insight machine and was ignored for the aging properties investigation. Then, three creep tests were performed after the temperature up-jump, i.e., aging times of 4 h, 8 h, and 16 h, respectively. The duration of each creep test was set to 20 minutes. Thus, the aging time was at least ten times greater than the creep phase to ignore aging effects during creep testing, as required in Struik's methodology (Struik, 1977).

Figure 7.1 illustrates the loading and temperature histories used to identify the linearly

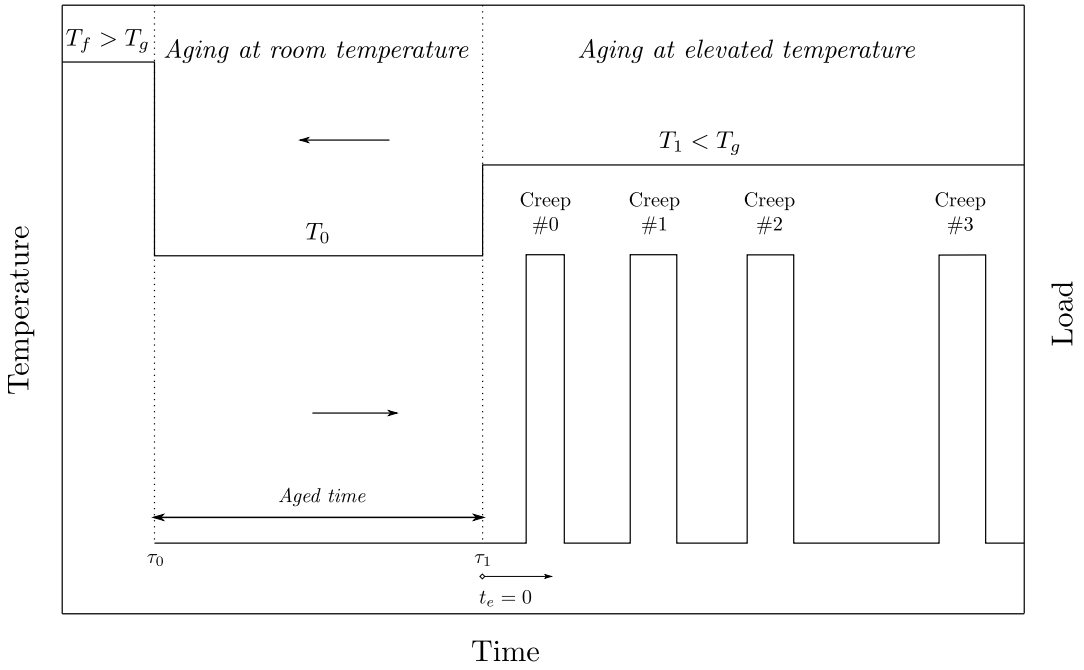

Figure 7.1 Illustration of the loading and temperature histories during the non-isothermal aging tests. T_f is the manufacture temperature, T_0 represents the room temperature and T_1 denotes the investigation temperature. τ_0 and τ_1 stand for the time of the temperature jumps. Aging time t_e starts from the specimen heated to T_1. Creep test #0 indicates the first creep test was used to adjust the position of grips. Creep tests #1, #2 and #3 are the creep tests at $t_e = 4\,\text{h}$, $8\,\text{h}$ and $16\,\text{h}$, respectively.

viscoelastic properties combined with the temperature and the physical aging effects. In all creep tests, the applied stress was set to 10 MPa, resulting in a strain of approximately 0.5% to ensure that the specimens were in their linear range since the PC exhibits linear viscoelasticity when the stress does not exceed 24 MPa or the strain is less than 1.0% (Qaiser and Price, 2011). The non-isothermal aging test with the four creep tests is noted as *characterization test* in the following.

It should be noted that the experimental measurement of transverse strain has a comparatively large error when compared to axial strain. This error is primarily caused by the penetration drift of the bi-axial extensometer. Because the knife edge of the extensometer is significantly stiffer than the specimen, the knife edge penetrates the specimen continuously throughout the experiment, which is especially important for long-term or elevated temperature tests. Therefore, a correction test was performed immediately after each mechanical test to eliminate this drift. Only the creep test #0 was conducted during the correction test, then the load was maintained at zero until the end of the test. Thus, the variation of transverse measurements during the correction test is due to the penetration drift. The transverse

measurement can be corrected by subtracting this variation value from the characterization test. Details of the mechanical testing are presented in our technical note (Yue *et al.*, 2022).

The temperatures investigated in this work were 40 °C, 60 °C, 80 °C, 100 °C, and 120 °C. Two tests were performed at each temperature with an interval of approximately one month between tests to evaluate the physical aging effect at room temperature. Two additional tests were performed at room temperature (20 °C) to set as the reference data. The detailed experimental conditions of characterization tests, including temperature, aged time, and aging time, are shown in Table 7.1.

7.5 Parameters identification

7.5.1 Shear and bulk properties estimation

The three-dimensional parameters identification problem can be reduced to two independent uni-dimensional problems, i.e., bulk and shear properties, by performing the strain transformation of Equation (7.19). The experimentally measured momentary shear compliance $\underset{\sim}{\tilde{\boldsymbol{\mu}}} = (\tilde{\mu}_i : i = 1, \ldots, T)$ and bulk compliance $\underset{\sim}{\tilde{\boldsymbol{\kappa}}} = (\tilde{\kappa}_i : i = 1, \ldots, T)$ for each creep load step

Table 7.1: The detailed experimental conditions for characterization tests. Investigation temperature indicates the temperature at which the specimens were tested during four sequential creep-recovery tests. Aged time denotes the duration the specimen was aged at room temperature. Aging time represents the time elapsed at the investigated temperature. 4 h, 8 h and 16 h correspond to creep tests #1, #2 and #3, respectively. ⋆The specimen was broken before the creep test #3 was conducted; thus, only two creep tests were performed.

Test index	Investigation temperature (°C)	Aged time (h)	Aging time (h)
1	20	569	4, 8, 16
2	20	665	4, 8, 16
3	40	89	4, 8, 16
4	40	787	4, 8, 16
5	60	114	4, 8, 16
6	60	810	4, 8, 16
7	80	139	4, 8, 16
8	80	738	4, 8, 16
9	100	307	4, 8, 16
10	100	952	4, 8, 16
11	120	356	4, 8⋆
12	120	1024	4, 8, 16

can be computed as:

$$\underset{\sim}{\tilde{\boldsymbol{\mu}}} \equiv \underset{\sim}{\tilde{\mu}}(t) = \frac{\varepsilon^{\dagger}(t) - \varepsilon^{\dagger}(0)}{2\sigma_{\mathrm{I}}}, \tag{7.27a}$$

$$\underset{\sim}{\tilde{\boldsymbol{\kappa}}} \equiv \underset{\sim}{\tilde{\kappa}}(t) = \frac{\varepsilon^{\ddagger}(t) - \varepsilon^{\ddagger}(0)}{3\sigma_{\mathrm{I}}}, \tag{7.27b}$$

where t is defined as the time elapsed since the load is applied in each creep test. σ_{I} represents the submitted uni-axial load during creep tests.

The shear creep compliance $\tilde{\mu}(t)$ at the reference state was modeled by a Prony series type linearly viscoelastic constitutive model as

$$\tilde{\mu}^{\mathrm{ref}}(t) = \tilde{\mu}_0 + \sum_{m=1}^{M} \tilde{\mu}_m (1 - \exp[-\lambda_m^{\mu} t]). \tag{7.28}$$

The shear creep compliance at the state (T, t_e) can be computed by the TTS principle as

$$\tilde{\mu}(t; T, t_e) = \tilde{\mu}^{\mathrm{ref}}(t/a_{t_e|T}; T^{\mathrm{ref}}, t_e^{\mathrm{ref}}), \tag{7.29}$$

where $a_{t_e|T}$ is the shift factor related to the state (T, t_e) and can be evaluated by the KAHR-a_{t_e} model as per Equation (7.15).

In summary, to model the shear properties of the material for a given temperature and aging history, the viscoelastic parameters ($\tilde{\mu}_0$, $\tilde{\mu}_m$, λ_m^{μ}) and the KAHR-a_{t_e} model parameters (ζ, b, τ_α, β_α, c_0, c_1) of the material need to be identified. It should be noted that the parameters c_0 and c_1 are temperature-dependent. Therefore, the relationship between these two parameters and the test temperature should also be determined. The parameter identification can be achieved in two steps. First, the viscoelastic parameters of the material in the reference state and the corresponding shift factors for the data under different test conditions are estimated. Then, the parameters of the KAHR-a_{t_e} model are identified from the obtained shift factors. The bulk properties of the material can be identified independently and in parallel through the same procedure.

7.5.2 Viscoelastic parameters identification

The reference state in this work was chosen as the first creep data in the first test, i.e. $T^{\mathrm{ref}} = 20\,^{\circ}\mathrm{C}$ and $t_e^{\mathrm{ref}} = 569\,\mathrm{h} + 4\,\mathrm{h}$. The parameters identification problem of the shear behavior

can be expressed as:

$$\boldsymbol{\theta}^{\mu} = \underset{\boldsymbol{\theta}^{\mu}\in\mathbb{R}^{+}}{\arg\min} \sum_{\mathrm{k}=1}^{\mathrm{K}} \left\| \tilde{\boldsymbol{\mu}}^{(\mathrm{k})}\left(\tilde{\mu}_0, \tilde{\mu}_m, \lambda_m^{\mu}/a_{t_e|T}^{\mu,\mathrm{k}}\right) - \underset{\frown}{\tilde{\boldsymbol{\mu}}}^{(\mathrm{k})} \right\|_2 \tag{7.30}$$

with

$$\boldsymbol{\theta}^{\mu} = \left\{\tilde{\mu}_0, \tilde{\mu}_1, , \ldots, \tilde{\mu}_M, \lambda_1^{\mu}, \ldots, \lambda_M^{\mu}, a_{t_e|T}^{\mu,1}, \ldots, a_{t_e|T}^{\mu,\mathrm{K}}\right\}, \tag{7.31}$$

where $\tilde{\boldsymbol{\mu}}^{(\mathrm{k})}$ and $\underset{\frown}{\tilde{\boldsymbol{\mu}}}^{(\mathrm{k})}$ denote the predicted and experimentally measured shear creep compliance during creep test #k, respectively. $(\tilde{\mu}_0, \tilde{\mu}_m, \lambda_m^{\mu})$ are the viscoelastic parameters of the shear behavior at the reference state, $a_{t_e|T}^{\mu,\mathrm{k}}$ is the shift factor that shifts the viscoelastic mechanical property in the #k creep test to the reference state. Equation (7.30) can be solved based on the Bayesian method proposed in our previous work (Yue *et al.*, 2021).

To construct the posterior function to solve Equation (7.30), the likelihood function is computed by

$$f_{(\boldsymbol{Y}|\boldsymbol{\theta}^{\mu})}(\underset{\frown}{\tilde{\boldsymbol{\mu}}}) \propto \prod_{\mathrm{k}=1}^{\mathrm{K}} \exp\left\{-\frac{1}{2\sigma_{\tilde{\mu}}^2} \left\| \underset{\frown}{\tilde{\boldsymbol{\mu}}}^{(\mathrm{k})} - \tilde{\boldsymbol{\mu}}^{(\mathrm{k})}\left(\tilde{\mu}_0, \tilde{\mu}_m, \lambda_m^{\mu}/a_{t_e|T}^{\mu,\mathrm{k}}\right) \right\|_2\right\}, \tag{7.32}$$

and the prior function is imposed using Equation (7.24). The MAP estimates of viscoelastic parameters and shift factors can be obtained with the MCMC simulation by

$$\hat{\boldsymbol{\theta}}_{\mathrm{MAP}}^{\mu} = \underset{\boldsymbol{\theta}^{\mu}\in\mathbb{R}^{+}}{\arg\max}\ f_{(\boldsymbol{\theta}^{\mu}|\boldsymbol{Y}=\underset{\frown}{\tilde{\boldsymbol{\mu}}})}(\boldsymbol{\theta}^{\mu}). \tag{7.33}$$

7.5.3 KAHR-a_{t_e} model parameters identification

Once the shift factors are obtained through Equation (7.33), the KAHR-a_{t_e} model parameters $\boldsymbol{\theta}^{t_e}$ can be identified through:

$$\boldsymbol{\theta}^{t_e} = \underset{\boldsymbol{\theta}^{t_e}\in\mathbb{R}^{+}}{\arg\min} \left\| \boldsymbol{a}_{t_e|T}\left(\boldsymbol{\theta}^{t_e}; T(t), t_e\right) - \hat{\boldsymbol{a}}_{t_e|T} \right\|_2, \tag{7.34}$$

where $\hat{\boldsymbol{a}}_{t_e|T} = \left(a_{t_e|T}^{\mu,1}, \ldots, a_{t_e|T}^{\mu,\mathrm{K}}\right)$ denotes the shift factors estimated from Equation (7.33). The shift factor $\boldsymbol{a}_{t_e|T}$ is computed using Equation (7.15) with the parameters $\boldsymbol{\theta}^{t_e}$ and the specified experimental circumstances $(T(t), t_e)$.

The numerical evaluation of $\boldsymbol{a}_{t_e|T}$ can be accomplished following the procedure proposed by Guo *et al.* (2009) and is detailed in Algorithm 4. The difference of the thermal expansion coefficients in the liquid and glassy state $\Delta\alpha$ can be experimentally measured. Lomellini (1992) obtained $\Delta\alpha = 4.2 \times 10^{-4}\,\mathrm{K}^{-1}$ for PC by dilatometric measurements, which is consis-

tent with other reported data that range from $2.3\times10^{-4}\,\mathrm{K}^{-1}$ to $4.2\times10^{-4}\,\mathrm{K}^{-1}$ (Van Krevelen and Te Nijenhuis, 2009). Therefore, the value of $4.2\times10^{-4}\,\mathrm{K}^{-1}$ is used in this work. The other parameters in the KAHR-a_{t_e} model parameters (ζ, b, τ_α, β_α, c_0, c_1) were identified by solving Equation (7.34) using the Levenberg-Marquardt algorithm by a *Matlab* build-in function `lsqnonlin`. Equation (7.18) needs to be solved in each optimization iteration, which was performed by the function `ode113` in *Matlab*.

7.6 Results and discussion

Figure 7.2 plots the full axial and transverse measurements during a non-isothermal aging test at 100 °C, i.e., characterization test #9, and the subsequent correction test. At the beginning of the characterization and correction tests, the axial measurements were nearly identical, as they were subjected to the same loading history. Likewise, the transverse measurements in both tests were also basically comparable, except for a 5×10^{-3} mm offset due to measurement errors. These results demonstrate the repeatability of experimental data. The experimental measurements and error analysis is not the objective of this work and is therefore detailed in our technical note (Yue *et al.*, 2022).

Figure 7.3 depicts the strains $\varepsilon^\dagger$ and $\varepsilon^\ddagger$ for different temperatures and physical aging conditions, which were computed using Equation (7.19) from the measured axial and transverse strains. For clarity, only one test result at each temperature is presented here. The results chosen being the second test at each temperature, i.e., tests #2, #4 ... #12. Different col-

Algorithm 4 Numerical evaluation of a_{t_e} in the KAHR-a_{t_e} model

1: Determine τ_m and ΔT_m from temperature history of the non-isothermal physical aging test at characterization temperature T
2: Set the initial value of $z(0) = 0$ and $\tilde{\tau}_0 = 0$
3: **for** $p = 0, 1$ **do**
4: Set $t \in [\tau_p, \tau_{p+1}]$
5: **for** $m = 0, p$ **do**
6: Solve Equation (7.18) using `ode113`
7: Compute $\tilde{\tau}_m = z(\tau_m)$
8: **end for**
9: **end for**
10: Compute $R(z)$ using Equation (7.11)
11: Obtain $\delta(z)$ using Equation (7.10)
12: Calculate a_δ using Equation (7.9)
13: Compute $a_{T,\delta}$ using Equation (7.14) with temperatures T and T^{ref}
14: Evaluate $a_{t_e}(a_\delta)\Big|_T$ using Equation (7.15)

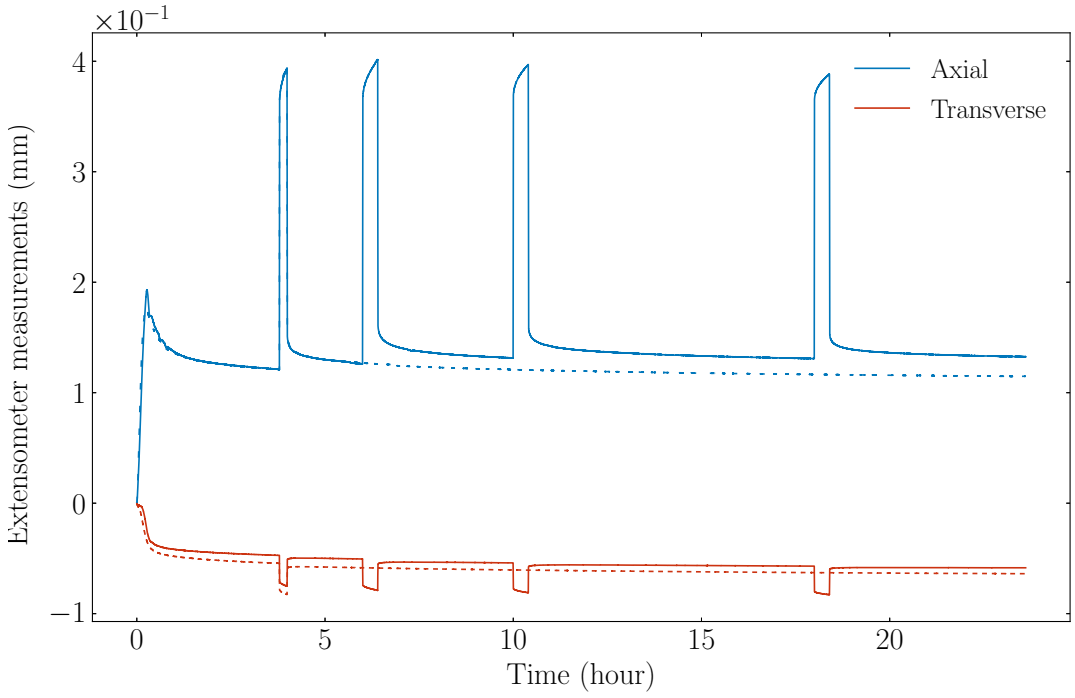

Figure 7.2 Full axial and transverse strains measured by the biaxial extensometer during test #9 and the subsequent correction test. The solid and dashed lines indicate the measurements during the characteristic and correction tests, respectively. The axial measurements were almost identical in both tests, while only slight offset differences were found in the transverse measurements. These results show the reproducibility of the experimental data.

ors are used to differentiate the temperatures and various markers are used to indicate the different aging times respectively.

The shear behavior of PC varies significantly at different temperatures and physical aging conditions. The strain $\varepsilon^{\dagger}$ at 20 °C with an aging time of 4 hours changed from 5.58×10^{-3} to 5.85×10^{-3} ($\uparrow$ 5.4%) in 20 minutes, from 6.23×10^{-3} to 6.92×10^{-3} ($\uparrow$ 11.3%) at 80 °C under the same aging conditions, and from 6.70×10^{-3} to 8.96×10^{-3} ($\uparrow$ 34.3%) at 120 °C. Meanwhile, as the aging time increased, $\varepsilon^{\dagger}$ varied from 6.62×10^{-3} to 8.44×10^{-3} ($\uparrow$ 27.5%) after 8 hours of aging and from 6.49×10^{-3} to 7.91×10^{-3} ($\uparrow$ 21.9%) over 16 hours at 120 °C. At 20 °C, the results for the three aging time conditions were nearly comparable. The strain changed from 5.58×10^{-3} to 5.87×10^{-3} ($\uparrow$ 5.1%) with an aging time of 4 hours, from 5.58×10^{-3} to 5.86×10^{-3} ($\uparrow$ 5.0%) over 8 hours and from 5.58×10^{-3} to 5.85×10^{-3} ($\uparrow$ 4.8%) after 16 hours of aging. The aging effect was not substantial at room temperature. The magnitude of strain during the creep test is directly proportional to the material's compliance. The greater the strain produced under the same loading conditions, the more compliant the material is. The change in strain during the creep test represents the viscoelasticity of the material.

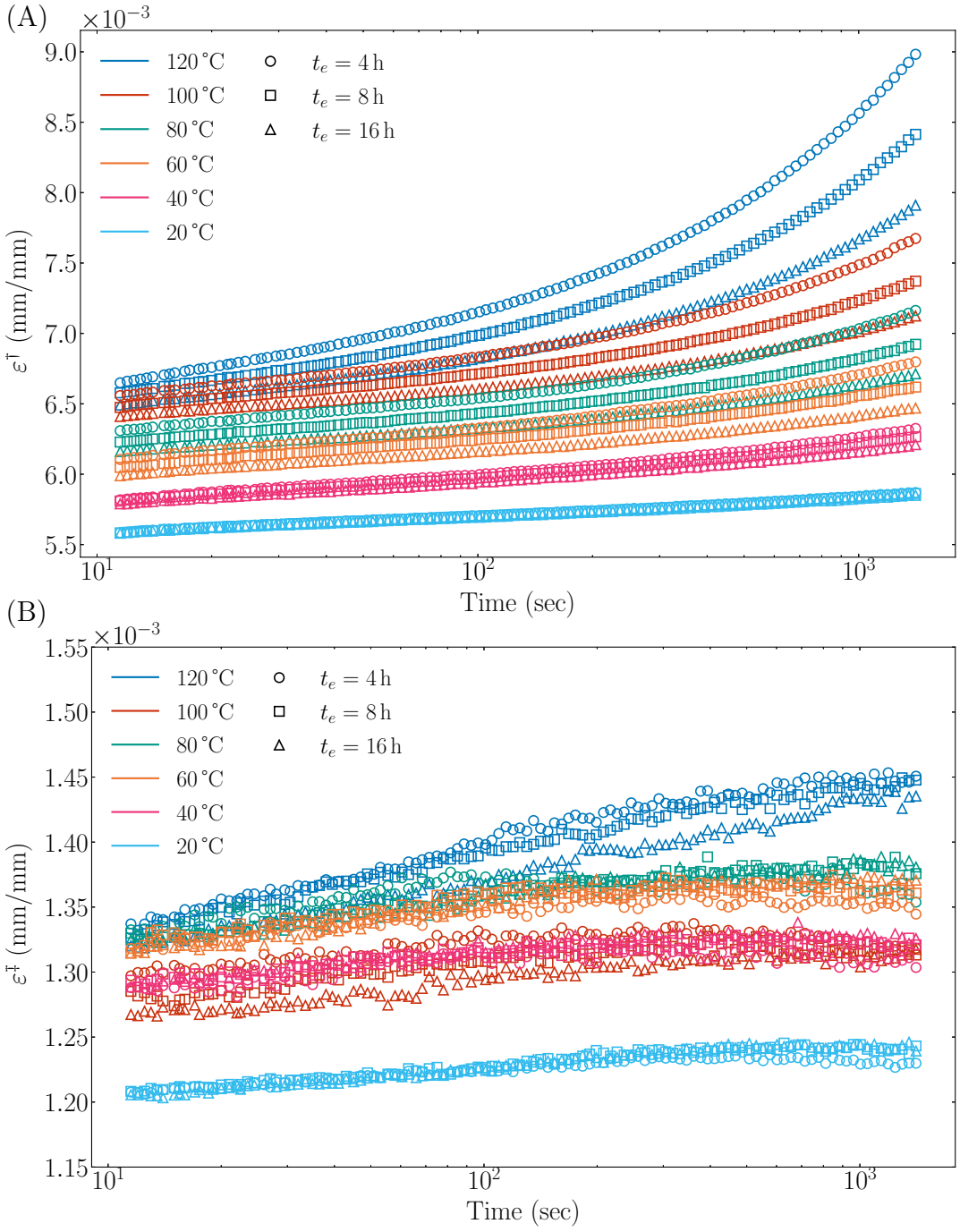

Figure 7.3 Experimentally measured strains $\varepsilon^{\dagger}$ and $\varepsilon^{\ddagger}$ during the creep tests with aging times of 4, 8 and 16 hours in characterization tests at 20 °C, 40 °C, 60 °C, 80 °C, 100 °C and 120 °C for PC; (A) Strain $\varepsilon^{\dagger}$, (B) Strain $\varepsilon^{\ddagger}$. The shear behavior of PC is remarkably temperature- and aging-dependent in terms of mechanical properties. In contrast, the bulk behavior shows only temperature dependence, and aging dependence is not apparent.

Similarly, the more significant the strain changes, the more viscoelastic the material is. The experimental observations demonstrate that both compliance and viscoelasticity of the shear behavior of PC specimens increase significantly with increasing temperature, but decrease as the aging time increases. The changes become more apparent as the temperature increases. Therefore, the effect of temperature and physical aging on the shear properties should be addressed simultaneously.

The bulk properties of PC are not as significantly affected by physical aging. The test results for three different aging times at each temperature are nearly identical, so the aging effect on the bulk property of PC can be ignored. And the effect of temperature on bulk behavior is small, when compared to that of shear. The strain $\varepsilon^{\ddagger}$ at 20 °C increased from 1.19×10^{-3} to 1.23×10^{-3} ($\uparrow$ 3.4%) in 20 minutes, from 1.26×10^{-3} to 1.31×10^{-3} ($\uparrow$ 3.9%) at 80 °C, and from 1.35×10^{-3} to 1.45×10^{-3} ($\uparrow$ 7.4%) at 120 °C. It shows that compliance and viscoelasticity of the bulk behavior of PC specimens increase with increasing temperature; therefore, the temperature effect on the bulk behavior of PC needs to be evaluated. In addition, the magnitude of $\varepsilon^{\ddagger}$ did not appear to be directly related to the test temperature in tests from 40 °C to 100 °C. However, considering the order of magnitude of the strains $\varepsilon^{\ddagger}$ is of 10^{-3} mm/mm, which is relatively small, and the difference in the magnitude of the strains at different temperatures are around 5%. These offsets are most likely due to the errors in installing the extensometer during the test.

7.6.1 Viscoelastic parameters

The three-dimensional viscoelastic constitutive model parameters and the shift factors of PC specimens were identified from the data by the Bayesian framework method. The optimal number of series of shear and bulk compliances were obtained by comparing the BIC value of each model estimated by MCMC simulations. The evaluation of BIC with respect to the number of Prony series of the shear and bulk properties of PC is shown in Figure 7.4. Nine Prony series were required to model the shear compliance of PC while only two retardation times were necessary to evaluate its bulk compliance.

The coefficient of determination R^2 was used to evaluate the precision of prediction of shear and bulk results, which is computed as follow:

$$R^2 = 1 - \frac{\sum_i (s_i - \underset{\sim}{s}_i)^2}{\sum_i \left(\underset{\sim}{s}_i - \frac{1}{n} \sum_i \underset{\sim}{s}_i \right)^2}, \text{ for } s = \tilde{\mu} \text{ or } \tilde{\kappa}, \tag{7.35}$$

where n denotes the total number of experimental data points, $\underset{\sim}{s}$ and s represent the experi-

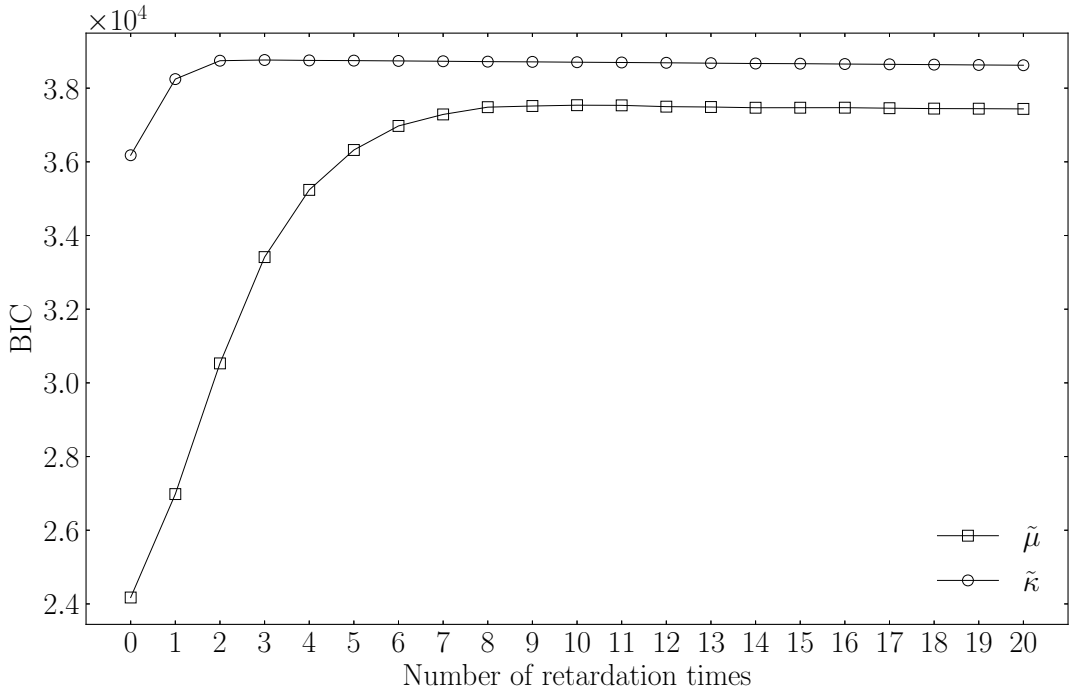

Figure 7.4 Evolution of the BIC with respect to the number of retardation times for shear and bulk properties of PC. Nine retardation times were required to model the shear compliance behavior of PC while only two Prony series were necessary to model its bulk creep compliance.

Table 7.2: Maximum a posteriori (MAP) estimates of the Prony series shear and bulk parameters for PC at the reference state, i.e., $T^{\text{ref}} = 20\,^{\circ}\text{C}$ and $t_e^{\text{ref}} = 573\,\text{h}$.

m	λ_m^{μ} (s^{-1})	$\tilde{\mu}_m$ (MPa^{-1})	λ_m^{κ} (s^{-1})	$\tilde{\kappa}_m$ (MPa^{-1})
-	-	2.60×10^{-4}	-	3.85×10^{-5}
1	1.31×10^{-9}	1.86×10^{-4}	1.08×10^{-4}	2.71×10^{-6}
2	2.21×10^{-8}	2.26×10^{-5}	7.74×10^{-3}	1.30×10^{-6}
3	2.12×10^{-7}	1.41×10^{-5}		
4	2.29×10^{-6}	1.33×10^{-5}		
5	3.11×10^{-5}	1.10×10^{-5}		
6	3.07×10^{-4}	9.07×10^{-6}		
7	4.20×10^{-3}	6.99×10^{-6}		
8	5.79×10^{-2}	6.01×10^{-6}		
9	7.61×10^{-1}	1.61×10^{-5}		

mental measurements and the predictions with identified parameters, respectively.

The estimated optimal viscoelastic parameters values for PC are listed in Table 7.2. Figure 7.5 plots the comparison between the experimental data and predicted response of shear and bulk compliances. The master curves were constructed from the identified parameters and the corresponding shift factors. The shear compliance result shows a remarkable agreement

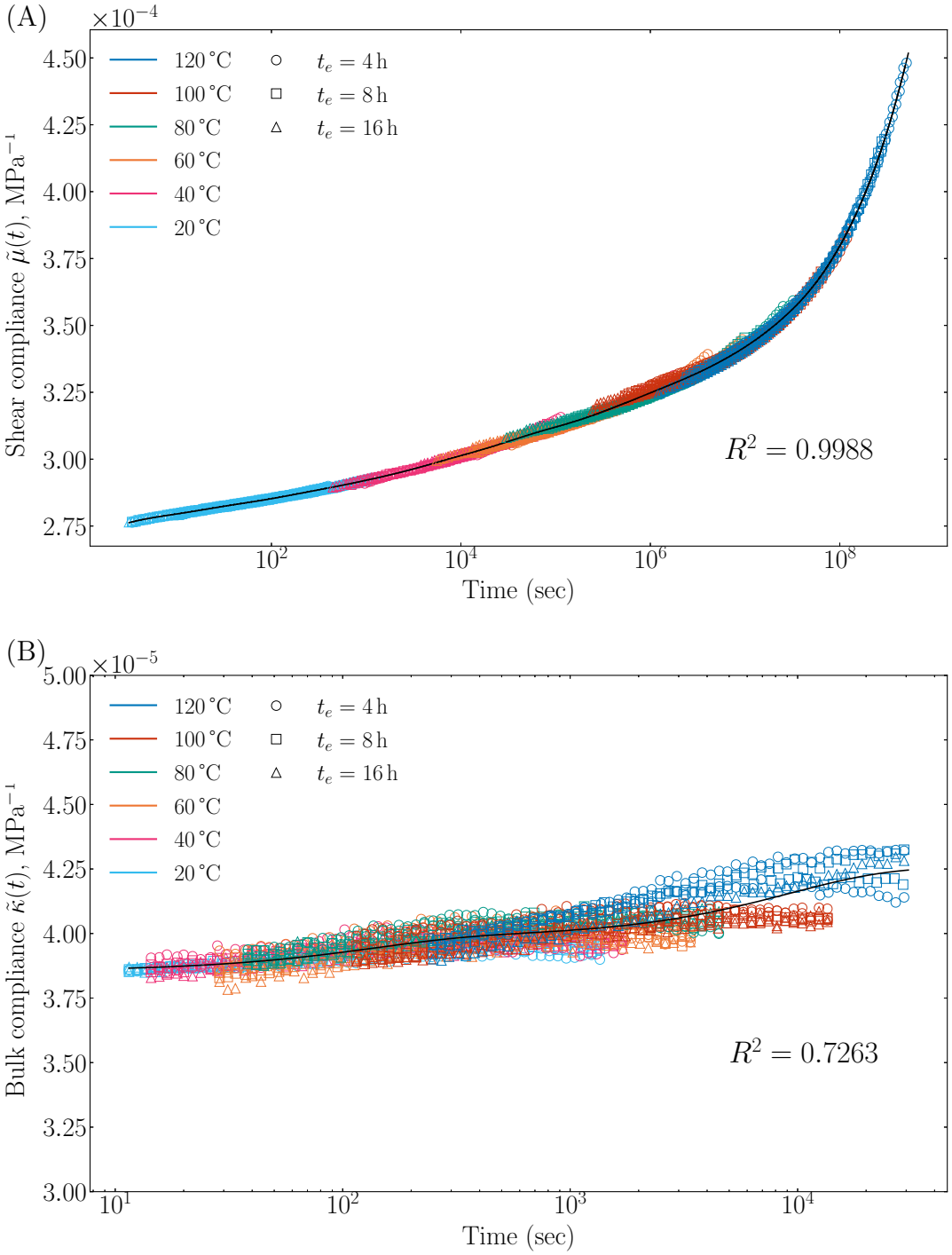

Figure 7.5 The *master curve* constructed by experimental data with the estimated shift factors and the prediction using the identified parameters; (A) Shear compliance, (B) Bulk compliance. The coefficient of determination R^2 was computed to evaluate the prediction accuracy, which are 0.9988 and 0.7263 for the shear and bulk compliance, respectively.

between experimental data and the prediction, with the R^2 value of 0.9988. The shear viscoelastic behavior exhibits a significant time-dependence, with shear compliance increasing from $2.76 \times 10^{-4}\,\mathrm{MPa}^{-1}$ at $3.16 \times 10^{-1}\,\mathrm{s}$ to $4.51 \times 10^{-4}\,\mathrm{MPa}^{-1}$ at $5.29 \times 10^{8}\,\mathrm{s}$ ($\uparrow$ 63.4%). Bulk compliance results also demonstrate concordance between experimental data and predictions, with the R^2 value of 0.7263, which is acceptable considering the order of magnitude difference between bulk and shear compliance (approximately one tenth) and the effect of experimental error on the measurements. It should be noted that the bulk compliance increased marginally with time, increasing from $3.77 \times 10^{-5}\,\mathrm{MPa}^{-1}$ to $4.34 \times 10^{-5}\,\mathrm{MPa}^{-1}$ ($\uparrow$ 15.1%) in the period 10 s to 3.06×10^{4} s. These observations are consistent with other experimental results in the literature (Qvale and Ravi-Chandar, 2004).

7.6.2 Shift factors model parameters

The KAHR-t_e model was used to evaluate the obtained shift factors for the shear behavior of PC. Table 7.3 lists the identified model parameters, where ζ, b, τ_α and β_α are material constants and c_0 and c_1 are temperature-dependent. Two exponential functions were chosen to represent the temperature-dependence of parameters c_0 and c_1 which are expressed as

$$c_0(T) = \gamma_0 + \gamma_1 \exp[\gamma_2 (T - T^{\mathrm{ref}})], \tag{7.36a}$$

$$c_1(T) = \eta_0 + \eta_1 \exp[\eta_2 (T - T^{\mathrm{ref}})]. \tag{7.36b}$$

The obtained parameters c_0 and c_1 at each temperature and the prediction by Equation (7.36) are plotted in Figure 7.6.

The comparison between the obtained shift factors and the model prediction using the estimated parameters is represented in Figure 7.7. It demonstrates that the predictions agree very well with the experimental data, except for the results of the second test at 40 °C (Test #4). This discrepancy could result from errors in the estimation of shift factors based on experimental data. It is noteworthy that the variation in results between the two tests at each temperature accounts for the accumulated physical aging effect at room temperature. Note that the interval between two characterization tests at each elevated temperature is approximately 661 ± 36 h, which is relatively small. Therefore, the room temperature effect

Table 7.3: Estimated KAHR-t_e model parameters. All parameters are unitless.

ζ	b	τ_α	β_α	c_0			c_1		
				γ_0	γ_1	γ_2	η_0	η_1	η_2
0.956	2.31	158	0.517	0.538	0.159	-2.19×10^{-2}	-220	234	-4.40×10^{-4}

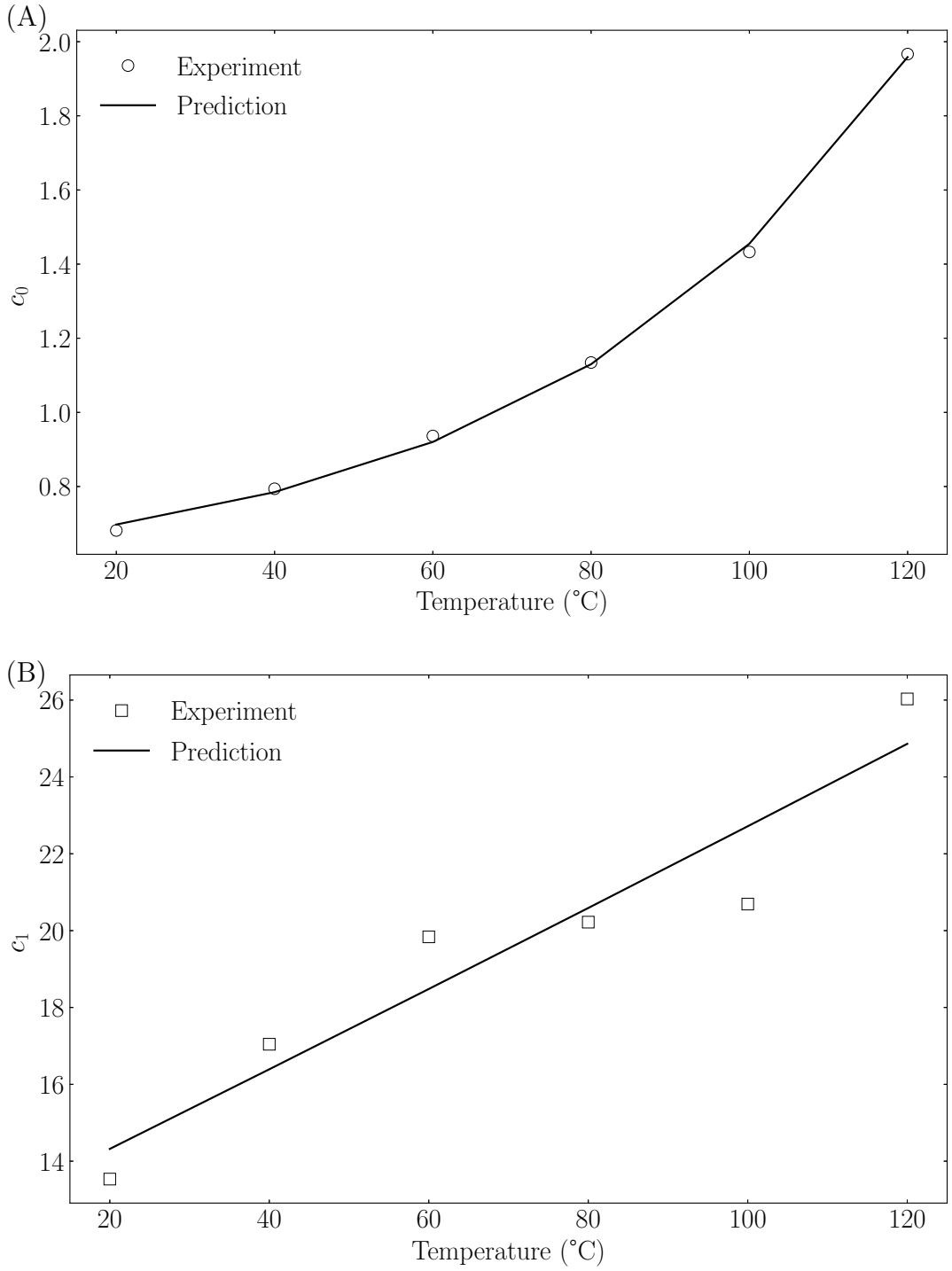

Figure 7.6 Estimated KAHR-t_e model temperature-dependent parameters with respect to temperatures for shear behavior and the prediction by Equation 7.36; (A) c_0, (B) c_1. The parameter c_0 shows an exponential relationship with temperature, while c_1 is approximately linear.

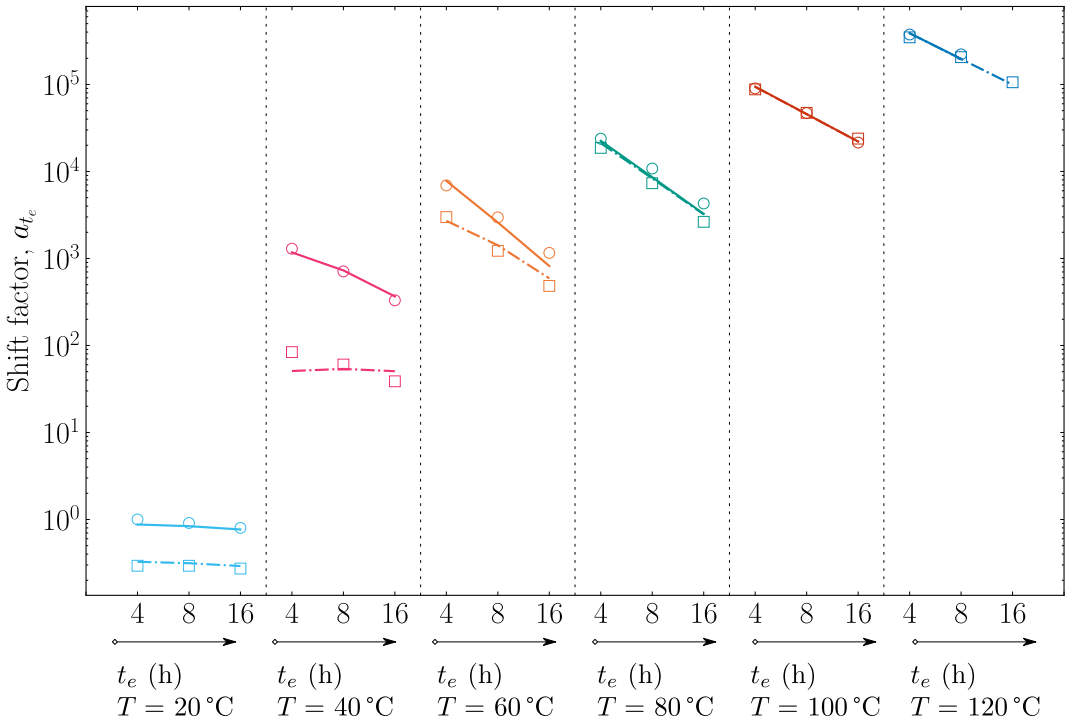

Figure 7.7 Comparison between the shift factors estimated from experiments and the prediction using KAHR-t_e model. ∘ denotes the shift factors of the first test performed at each temperature (Test #1, #3, ..., #11), while □ stands for the results of second tests (Test #2, #4, ..., #12). The solid and the dash-dotted lines are the estimated shift factor by HAHR-t_e model using the identified parameters for the first and second tests, respectively. The predicted shift factors with identified KAHR-t_e model agree well with estimated values from experiments. The aging effect of PC at room temperature becomes less significant as the characterization test temperature increases.

between two tests at each elevated temperature is assumed to be identical. For relatively low temperatures, e.g., 40 °C and 60 °C, the accumulated effect of physical aging at room temperature has a significant effect on the material's properties at the investigation temperature. In comparison, the accumulated physical aging effects were less pronounced at higher temperatures. At 120 °C, the shift factors were nearly identical in both tests, measuring of 4.03×10^5 and 2.44×10^5 after aging 4 hours and 8 hours in the first test, and 4.04×10^5 and 2.43×10^5 in the second one.

The shift factors for bulk compliance were modeled by the WLF equation. The obtained shift factors and the WLF equation prediction are plotted in Figure 7.8. Due to the fact that the shift factor of bulk compliance is comparatively small, the simulation using the WLF equation is approximately linear and contains some error. Additionally, this result indicates that the bulk behavior of PC is temperature dependent, which is consistent with previous

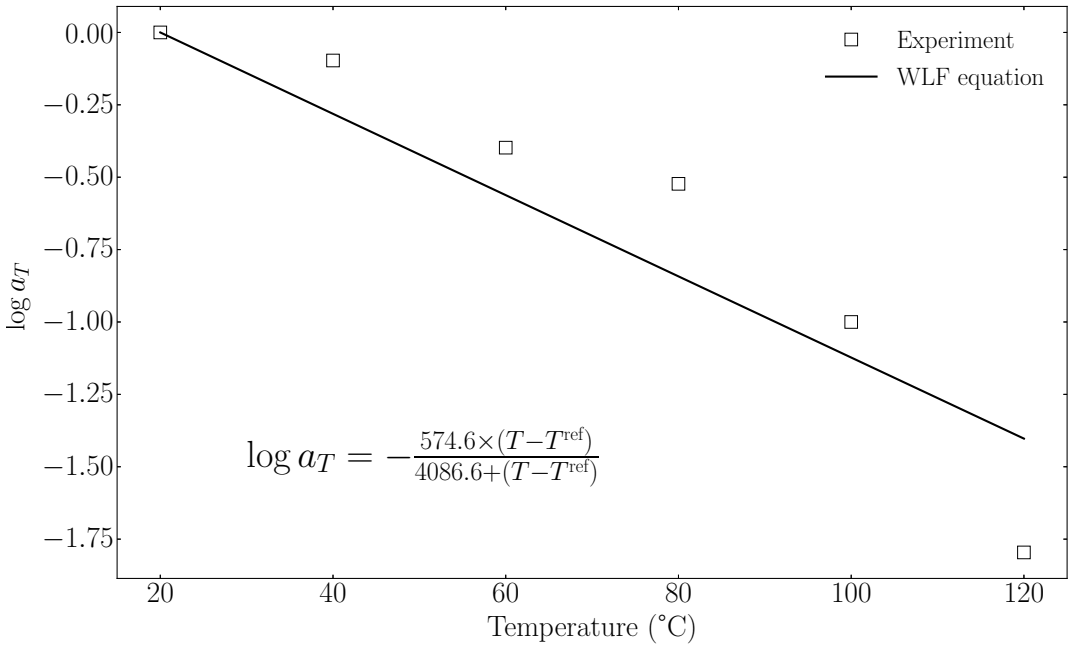

Figure 7.8 Comparison between the estimated shift factors from experiments and the prediction with identified WLF equation of the bulk compliance of PC. The shift factors have small values, and their logarithmic values are approximately linear with temperature over the temperature range examined.

research findings (Qvale and Ravi-Chandar, 2004). However, the exact shift factors data for bulk behavior of PC was not reported, limiting the comparison between the results in our work and the literature data.

7.6.3 Discussion

It is interesting to note that temperature and physical aging time have a competitive effect on the mechanical properties of PC. In general, increasing the temperature makes the material more compliant, while increasing the physical aging time makes it stiffer. Additionally, elevated temperatures accelerate the physical aging process. As illustrated in Figure 7.3, after 16 hours of aging at 100 °C, the material will be stiffer than after 4 hours of aging at 80 °C. Thus, when investigating the effect of temperature on the mechanical properties of PC, it is necessary to consider the effect of physical aging. Additionally, in the development of polymers or polymer composites that are capable of operating at elevated temperatures, the effects of temperature and physical aging must be considered concurrently to accurately predict the mechanical properties of materials subjected to a complex thermal history.

Temperature and physical aging have a variety of effects on the properties of polymer mate-

rials. In comparison to the shear property, the bulk behavior is less affected by temperature and physical aging. The effect of physical aging on the bulk behavior is comparatively small and could neglected whereas the effect of temperature is readily apparent over longer time scales. As a result, certain assumptions about the bulk modulus or Poisson's ratio of polymers remaining constant at elevated temperatures are inappropriate for applications requiring a high degree of prediction accuracy. However, the investigation in this paper is based on PC; for other materials, additional tests must be conducted to verify this conclusion. Additionally, because of the order of magnitude of the variation in bulk modulus between different test conditions is quite small, the errors introduced by the measurements in the test may have a significant effect on the results, such as those introduced by the equipment size and strain gauges used in Qvale and Ravi-Chandar (2004), as well as the offset introduced by the installation of extensometer in this work. Therefore, it is strongly recommended that in thermo-mechanical studies of polymer materials, non-contact measurement methods such as Digital Image Correlation (DIC) be used to minimize measurement errors.

7.7 Conclusion

The main contribution of this work was the successful application of a previously proposed Bayesian inference method for determining the viscoelastic parameters in combination with temperature and physical aging effects. The identified viscoelastic constitutive models and related shift factors agree well with experimental data at a variety of temperatures and aging times for PC. Additionally, this work investigated and discussed various effects on the shear and bulk behavior of PC. The shear properties are affected by both temperature and physical aging, whereas the bulk behavior is only affected by temperature and is relatively insignificant in comparison to the shear properties.

While this work focuses on the properties of PC, the approach presented in this work can be applied to other materials to derive more general conclusions about the effects of temperature and aging time on three-dimensional behavior of polymer solids.

Declaration of competing interest

The authors declare that they have no known competing financial interests or personal relationships that could have appeared to influence the work reported in this paper.

Acknowledgments

This research was partially funded by the Natural Sciences and Engineering Research Council (NSERC) of Canada, Discovery Grant RGPIN-06412-2016 and Fonds de Recherche du Québec Nature et technologies (FRQNT), Team Research Project 146219. The authors greatly acknowledge Dr. Qingkai Meng from *Lavergne Inc* for providing PC pellets and Anic Desforges from Department of Chemical Engineering Polytechnique Montréal for assisting the injection molding of PC specimens.

CHAPTER 8 GENERAL DISCUSSION

8.1 Characteristic times of viscoelasticity

8.1.1 Number of characteristic times

This thesis investigated the characteristic times λ_m related to the creep compliances of three different thermoplastics, i.e., PMMA, PP and PC, based on experimental results. Note that the viscoelasticity of the bulk properties is much smaller than that of the shear properties. For the sake of illustration, only the shear compliance characteristic times are discussed here. Table 8.1 lists the experimental time window and the optimal number of characteristic times M for three thermoplastics. Figure 8.1 plots their optimal characteristic times and associated relative compliances. It can be found that the optimal M is nearly identical to the decades of experimental time window, but the distance (in logarithm) between characteristic times is not identical for all three materials. Therefore, the Prony series model with one characteristic time per decade during the experimental time window is the simplest model to precisely represent test data.

In most works of applying classical methods to determine viscoelastic parameters, the characteristic time has been *a priori* fixed as logarithm equidistant and one per decade (Courtois, Hirsekorn, *et al.*, 2019; Crochon, 2014). It should be noted that this choice is inappropriate according to the previous conclusions. When the characteristic time is freely distributed, one characteristic time per decade is the optimal choice. However, a fixed logarithmic equidistant per decade may fall short of the required precision. Therefore, if a classical approach is required in some special cases, 1.5 or 2 characteristic times per decade is suggested to balance

Table 8.1: Comparison between experimental time windows and optimal characteristic times for three thermoplastic. $t_{\min}$ and $t_{\max}$ represent the lower and upper limits of the experimental time window, respectively. The experimental time window for PMMA and PP is directly determined from experiments, while the experimental time window for PC is determined using the structured master curve for 573 hours physical aging at 20 °C. The optimal characteristic times M is nearly identical to the elapsed decades of experimental time window for three thermoplastics.

Material	$t_{\min}$ (s)	$t_{\max}$ (s)	Elapsed decades	Optimal M
PMMA	1	3.4×10^3	3.5	3
PP	1	3.4×10^3	3.5	4
PC	3.2×10^{-1}	5.3×10^8	9.2	9

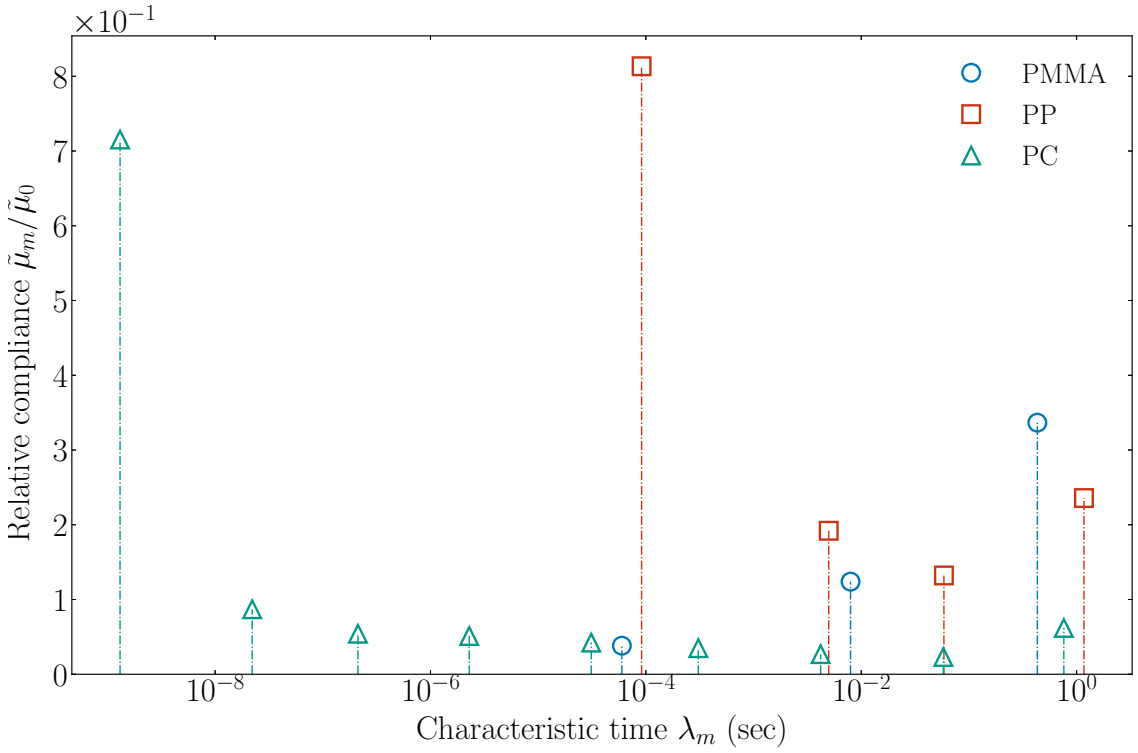

Figure 8.1 Optimal characteristic times identified from experimental data for PMMA, PP and PC. The relative compliance is defined as the ratio of the compliance $\tilde{\mu}_m$ corresponding to each characteristic time λ_m to the elastic compliance $\tilde{\mu}_0$. Characteristic times are distributed nearly one per decade; the distance between each characteristic time is not the same.

the model complexity and prediction accuracy.

8.1.2 Nature of characteristic times

The determination of the characteristic times for viscoelastic solids in most works, including this thesis, is based on an approximation theory viewpoint, where identifying the parameters of the Prony series model approximates the kernel function $\mathbf{C}(t)$ or $\mathbf{S}(t)$ of the material using non-negative exponential sum functions. Thus, the characteristic time represents the base of the exponential and the function.

However, from a physicochemical point of view, the characteristic times of the polymer have a clear physical meaning. Viscoelasticity manifests itself as a delayed response of the molecular chain structure to external stresses (Ferry, 1980). Therefore, the characteristic time of a polymer should be determined by the physicochemical properties of the polymer, including type of molecule, the molecular weight, the configuration of the molecular chain, etc.

Likhtman and McLeish (2002) have proposed a quantitative model at the molecular chain scale to estimate the viscoelasticity of entangled polymer melts. In this model, the structure and dynamics of single molecular chains are modeled based on the classical reptation theory (De Gennes, 1971), yielding a quantitative model with a clear physical meaning, without any non-physical adjustable parameters. The characteristic times are computed from the number of monomers in each molecular chain, molecular weight, temperature, etc. This model agrees well with experimental data on polystyrene.

However, no clear physical model for glassy polymers has been established. Because the molecular chains lack sufficient thermal energy to move freely in a glassy state, they face more significant restrictions than in the molten state (Ferry, 1980). As a result, the classical reptation theory is invalid. Therefore, developing a physical model of viscoelasticity for glassy polymers based on molecular dynamics continues to be an open and challenging problem. Furthermore, establishing a quantitative correlation between the characteristic times and the physicochemical properties of polymer solids is of considerable interest.

8.2 Bayesian framework based identification method

8.2.1 Assumption

An essential assumption in the Bayesian framework based approach proposed in this thesis is that the experimental error is independent during a test. In practice, the error ϵ_i is probably not independent of ϵ_{i+1}. However, it should be noted that the point estimates, e.g., the MAP estimate used in this thesis, are quite robust to the dependence of errors (Varin *et al.*, 2011). Therefore, the method proposed in this thesis is applicable to the actual situation.

However, if it is desired to generalize more information about the viscoelastic parameters via their posterior distribution from experimental results, the assumption of independent errors should be taken into account. Therefore, the proposed Bayesian method can also be improved by releasing this assumption for future exploring the Bayesian analysis on parameters.

8.2.2 Limitation

The proposed Bayesian framework based method is a robust and automated method for determining the optimal number of three-dimensional viscoelastic parameters. However, when compared to classical identification methods, this approach features the limitation of high computational cost. The classical approach here refers to fixing the characteristic time *a priori* and solving the identification problem for Equation (2.26) using a derivative

optimization method, such as the one proposed by Lévesque *et al.* (2008).

The relatively high computational cost of the Bayesian approach is mainly due to the fact that it is solved differently than the classical approach. In the classical method, the parameters are solved iteratively by calculating the residual between the experimental data and the model prediction. The calculation stops when a stopping criterion is met. Usually, the stopping criterion chosen is the number of iterations, the tolerance between the experimental data and the model prediction, or the change in the parameter between two iterations. However, the idea of the Bayesian approach is to estimate the posterior distribution of the parameters by MCMC simulations, which is more computationally demanding than finding point estimate. After the sampling convergence, statistical analysis and point estimation are then performed using the posterior distribution. Thus, the sampling convergence criterion, i.e., the stopping rule, is critical for the Bayesian method's efficiency. Several MCMC sampling convergence criteria have been proposed to address this (Brooks and Gelman, 1998; Gelman and Rubin, 1992; Gelman *et al.*, 2013).

This thesis chooses the number of iterations as the convergence criterion for MCMC sampling. This choice has limitations. When using Bayesian methods to determine the optimal number of parameters for a Prony series model, models with different parameter numbers (from 1 to M) need to be computed in sequence. The number of sampling iterations required varies according to the complexity of the model, but it is impossible to preview the required number before the simulation. Therefore, a constant iteration number is chosen for all models during the identification. To ensure that the sampling converges for the model with a large number of parameters, a relatively large iteration number, e.g., 10 000, was conservatively used in this research, resulting in a high cost of time required for the entire parameter identification.

Therefore, selecting suitable convergence criteria and investigating more advanced sampling methods to accelerate convergence are of considerable interest for the future research about improving the Bayesian framework method in viscoelastic constitutive theory identification.

8.2.3 Extensibility

One of the advantages of the Bayesian framework based parameter identification method is that it can easily be extended to handle more complex constitutive models and to incorporate prior knowledge about the parameters. For example, in this thesis, the method for determining the viscoelastic parameters was initially developed for the material at room temperature. Within the same framework and only changing the likelihood function, the method can be extended to identify parameters for a more complex model that includes viscoelasticity and the effect of temperature and physical aging.

Moreover, the Bayesian method can also be extended by altering the prior function. Extensions can be implemented in a variety of aspects, such as:

1. Updating the knowledge of material. Once the viscoelastic parameters of a material is identified with the Bayesian method, the distribution of its parameters or the point estimate of the distribution can be obtained. This information can be used as a prior function for identifying similar materials, accelerating the identification process.

2. Incorporating the physicochemical properties of the material. If a physicochemical model can be developed for polymer solids, it could be used as a prior function to provide more physical meaning to the identified parameters.

Therefore, while the Bayesian approach has limitations such as a high computational cost, it also has significant advantages and the potential to be a potent numerical tool for other researchers or engineers interested in developing and characterizing novel viscoelastic solids.

CHAPTER 9 CONCLUSION AND RECOMMENDATIONS

This thesis developed a numerical predictive tool for the long-term mechanical properties of thermoplastics. A robust and automated method based on the Bayesian framework was proposed to identify the three-dimensional viscoelastic parameters of thermoplastic solids under different temperature and physical aging conditions. Mechanical tests experimentally validated the proposed method on three thermoplastics under varying conditions.

A Bayesian framework-based method was initially proposed to identify the three-dimensional viscoelastic parameters of thermoplastics at room temperature. The ill-posedness of the Prony series model identification problem was addressed through MCMC simulations. With the proposed method, identifying the viscoelastic parameters does not require *a priori* fixing of the characterization time. Moreover, the optimal number of parameters for the Prony series can be derived by this method. The viscoelastic parameters are identified from three-dimensional experimental data and experimentally validated on independent data for two different thermoplastics, PMMA and PP. The excellent agreement between the DIC measurements and the FEM simulations performed through the identified parameters demonstrated the robustness and adequacy of the method at room temperature.

Then, three-dimensional non-isothermal physical aging tests on PC specimens were conducted at room temperature (20 °C), 40 °C, 60 °C, 80 °C, 100 °C, and 120 °C, respectively. Axial and transverse strains were measured with a biaxial extensometer during these tests. The sources of measurement errors of the extensometer were analyzed. A robust and straightforward procedure was proposed to eliminate the temperature-induced and penetration drifts of axial and transverse measurements with the biaxial extensometer during the thermo-mechanical testing. Experimental results at 120 °C demonstrated the reproducibility and reliability of the proposed experimental methodology.

Finally, the previously proposed method was successfully extended to simultaneously identify viscoelastic, temperature, and physical aging-related 3D model parameters from generated non-isothermal physical aging test data on PC specimens. The identified viscoelastic constitutive models and related shift factors agree well with experimental data under various temperatures and physical aging conditions for PC. The effects of temperature and physical aging on the bulk and shear behavior of PC were investigated. Temperature and physical aging both affect shear properties, whereas bulk behavior is only affected by temperature and is relatively insignificant when compared to shear properties.

In overall, the developed Bayesian framework-based method is capable of predicting the

long-term mechanical properties of thermoplastics under a variety of test conditions. Other researchers and engineers can use this numerical tool to develop and characterize novel viscoelastic materials, as well as to investigate the effects of temperature and physical aging on the mechanical properties of the materials.

Recommendations for future studies

The previous conclusions result in the following recommendations.

- **Improve the performance of MCMC simulations**

  The computational cost of MCMC simulations limits the efficiency of the proposed Bayesian based identification method. Therefore, it is of interest to improve the performance of MCMC simulations by selecting the advanced sampling methods to accelerate the convergence or altering the convergence criterion to a more appropriate one.

- **Investigate other types of viscoelastic constitutive model**

  The Prony series model was used in this thesis. Other types of thermodynamically consistent viscoelastic constitutive models exist, e.g., fractional order models (Lion, 1997). The proposed identification method can be applied to these models by altering the function in the likelihood function. Comparing different viscoelastic models in studying viscoelastic materials and structures is interesting.

- **Measure strains with DIC at elevated temperatures**

  When using an extensometer to measure strain in a specimen, there are errors caused by installing the extensometer that is difficult to eliminate. Therefore, it is necessary to use DIC for measurement at high temperatures if high accuracy is required. In addition, comparing the results of DIC and extensometer measurements in a test in the environmental chamber can be used to validate the correction of the extensometer drifts in this work.

- **Generate a database for viscoelastic solids**

  An essential feature of the Bayesian approach is its ability to incorporate new information from test results after each experimental test. This feature enables the establishment of a database for collecting and analyzing the information about the viscoelastic parameters of polymers to aid in the development of novel polymers.

- **Extend the predictive numerical tool to composites**

This thesis focused on neat thermoplastics. However, the proposed method can be extended to predict the long-term mechanical properties of composites, when a homogenization model is included. The development of such a predictive numerical tool to assist in developing and designing novel composites is of considerable interest.

REFERENCES

An, D., Kim, N. H., and Choi, J.-H. (2015). Practical options for selecting data-driven or physics-based prognostics algorithms with reviews. *Reliability Engineering & System Safety*, *133*, 223–236. doi: 10.1016/j.ress.2014.09.014

Andrews, R., and Tobolsky, A. (1951). Elastoviscous properties of polyisobutylene. iv. relaxation time spectrum and calculation of bulk viscosity. *Journal of Polymer Science*, *7*(2-3), 221–242. doi: 10.1002/pol.1951.120070210

Andrieu, C., De Freitas, N., Doucet, A., and Jordan, M. I. (2003). An introduction to mcmc for machine learning. *Machine learning*, *50*(1-2), 5–43.

Biot, M. A. (1954, nov). Theory of Stress Strain Relations in Anisotropic Viscoelasticity and Relaxation Phenomena. *Journal of Applied Physics*, *25*(11), 1385–1391. doi: 10.1063/1.1721573

Bishop, C. M. (2006). *Pattern recognition and machine learning (information science and statistics)*. Secaucus, NJ, USA: Springer-Verlag New York, Inc.

Bouleau, N. (1991). Interprétation probabiliste de la viscoélasticité linéaire. *Mechanics Research Communications*, *19*, 16–20.

Bouleau, N. (1999). Visco-elasticité et Processus de Lévy. *Potential Analysis*, *11*(3), 289–302. doi: 10.1023/A:1008696219448

Bradshaw, R., and Brinson, L. C. (1997a). Physical aging in polymers and polymer composites: An analysis and method for time-aging time superposition. *Polymer Engineering & Science*, *37*(1), 31–44. doi: 10.1002/pen.11643

Bradshaw, R., and Brinson, L. C. (1997b, 07). Recovering nonisothermal physical aging shift factors via continuous test data: Theory and experimental results. *Journal of Engineering Materials and Technology*, *119*(3), 233-241. doi: 10.1115/1.2812250

Bradshaw, R., and Brinson, L. C. (1999). A continuous test data method to determine a reference curve and shift rate for isothermal physical aging. *Polymer Engineering & Science*, *39*(2), 211–235. doi: 10.1002/pen.11409

Brinson, L. C., and Gates, T. S. (1995). Effects of physical aging on long term creep of polymers and polymer matrix composites. *International Journal of Solids and Structures*, *32*(6-7), 827–846. doi: 10.1016/0020-7683(94)00163-Q

Brooks, S. P., and Gelman, A. (1998). General methods for monitoring convergence of iterative simulations. *Journal of computational and graphical statistics*, *7*(4), 434–455. doi: 10.1080/10618600.1998.10474787

Caruthers, J. M., Adolf, D. B., Chambers, R. S., and Shrikhande, P. (2004). A thermodynamically consistent, nonlinear viscoelastic approach for modeling glassy polymers. *Polymer*, *45*(13), 4577–4597. doi: 10.1016/j.polymer.2004.04.021

Christensen, R. (2012). *Theory of viscoelasticity: an introduction*. Elsevier.

Claverie, P., Denis, A., and Yeramian, E. (1989). The representation of functions through the combined use of integral transforms and padé approximants: Padé-laplace analysis of functions as sums of exponentials. *Computer Physics Reports*, *9*(5), 247–299. doi: 10.1016/0167-7977(89)90025-7

Correlated, S. (2010). *Vic-3d help manual. correlated solutions.*

Courtois, A., Hirsekorn, M., Benavente, M., Jaillon, A., Marcin, L., Ruiz, E., and Lévesque, M. (2019). Viscoelastic behavior of an epoxy resin during cure below the glass transition temperature: Characterization and modeling. *Journal of Composite Materials*, *53*(2), 155–171. doi: 10.1177/0021998318781226

Courtois, A., Marcin, L., Benavente, M., Ruiz, E., and Lévesque, M. (2019). Numerical multiscale homogenization approach for linearly viscoelastic 3d interlock woven composites. *International Journal of Solids and Structures*, *163*, 61–74. doi: 10.1016/j.ijsolstr.2018.12.018

Crochon, T. (2014). *Modeling in the viscoelastic behavior of polyimide matrix at elevated temperature* (Unpublished doctoral dissertation). École Polytechnique de Montréal.

Crochon, T., Li, C., and Lévesque, M. (2015). On time–temperature-dependent viscoelastic behavior of an amorphous polyimide. *Mechanics of Time-Dependent Materials*, *19*(3), 305–324. doi: 10.1007/s11043-015-9265-9

Crochon, T., Schönherr, T., Li, C., and Lévesque, M. (2010). On finite-element implementation strategies of schapery-type constitutive theories. *Mechanics of Time-Dependent Materials*, *14*(4), 359–387. doi: 10.1007/s11043-010-9115-8

Cunat, C. (2001). The dnlr approach and relaxation phenomena. part i–historical account and dnlr formalism. *Mechanics of Time-Dependent Materials*, *5*(1), 39–65.

Davies, A., and Anderssen, R. S. (1997). Sampling localization in determining the relaxation spectrum. *Journal of Non-Newtonian Fluid Mechanics*, *73*(1-2), 163–179. doi: 10.1016/S0377-0257(97)00056-6

De Gennes, P.-G. (1971). Reptation of a polymer chain in the presence of fixed obstacles. *The journal of chemical physics*, *55*(2), 572–579. doi: 10.1063/1.1675789

Deonovic, B., and J Smith, B. (2018). *Mamba: Markov chain monte carlo (mcmc) for bayesian analysis in julia.* `https://github.com/brian-j-smith/Mamba.jl`. GitHub.

Drozdov, A. D. (2000). Viscoelastoplasticity of amorphous glassy polymers. *European polymer journal*, *36*(10), 2063–2074. doi: 10.1016/S0014-3057(00)00010-0

Duane, S., Kennedy, A. D., Pendleton, B. J., and Roweth, D. (1987). Hybrid monte carlo. *Physics letters B*, *195*(2), 216–222. doi: 10.1016/0370-2693(87)91197-X

Emri, I., and Prodan, T. (2006). A measuring system for bulk and shear characterization of polymers. *Experimental mechanics*, *46*(4), 429–439. doi: 10.1007/s11340-006-8528-4

Emri, I., and Tschoegl, N. (1993). Generating line spectra from experimental responses. part i: Relaxation modulus and creep compliance. *Rheologica Acta*, *32*(3), 311–322. doi: 10.1007/BF00434195

Emri, I., and Tschoegl, N. (1994). Generating line spectra from experimental responses. part iv: Application to experimental data. *Rheologica acta*, *33*(1), 60–70. doi: 10.1007/BF00453464

Emri, I., and Tschoegl, N. (1995). Determination of mechanical spectra from experimental responses. *International journal of solids and structures*, *32*(6-7), 817–826. doi: 10.1016/0020-7683(94)00162-P

Ferry, J. D. (1980). *Viscoelastic properties of polymers*. John Wiley & Sons. doi: 10.1149/1.2428174

Freund, J. B., and Ewoldt, R. H. (2015). Quantitative rheological model selection: Good fits versus credible models using bayesian inference. *Journal of Rheology*, *59*(3), 667–701. doi: 10.1122/1.4915299

Gelman, A., and Rubin, D. B. (1992). Inference from iterative simulation using multiple sequences. *Statistical science*, *7*(4), 457–472. doi: 10.1214/ss/1177011136

Gelman, A., Stern, H. S., Carlin, J. B., Dunson, D. B., Vehtari, A., and Rubin, D. B. (2013). *Bayesian data analysis*. Chapman and Hall/CRC. doi: 10.1201/b16018

Geman, S., and Geman, D. (1984). Stochastic relaxation, gibbs distributions, and the bayesian restoration of images. *IEEE Transactions on pattern analysis and machine intelligence*(6), 721–741. doi: 10.1109/TPAMI.1984.4767596

Gerlach, S., and Matzenmiller, A. (2005). Comparison of numerical methods for identification of viscoelastic line spectra from static test data. *International journal for numerical methods in engineering*, *63*(3), 428–454. doi: 10.1002/nme.1161

Gill, P. E., Murray, W., and Wright, M. H. (2019). *Practical optimization*. SIAM. doi: 10.1137/1.9781611975604

Grant, B., Stone, H., Withers, P., and Preuss, M. (2009). High-temperature strain field measurement using digital image correlation. *The Journal of Strain Analysis for Engineering Design*, *44*(4), 263–271. doi: 10.1243/03093247JSA478

Grassia, L., and D'Amore, A. (2009). On the interplay between viscoelasticity and structural relaxation in glassy amorphous polymers. *Journal of Polymer Science Part B: Polymer Physics*, *47*(7), 724–739. doi: 10.1002/polb.21675

Grassia, L., and D'Amore, A. (2006). Constitutive law describing the phenomenology of subyield mechanically stimulated glasses. *Physical Review E*, *74*(2), 021504. doi: 10.1103/PhysRevE.74.021504

Grédiac, M., and Hild, F. (2012). *Full-field measurements and identification in solid mechanics*. John Wiley & Sons. doi: 10.1002/9781118578469

Guo, Y., and Bradshaw, R. D. (2007). Isothermal physical aging characterization of polyether-ether-ketone (peek) and polyphenylene sulfide (pps) films by creep and stress relaxation. *Mechanics of Time-Dependent Materials*, *11*(1), 61–89. doi: 10.1007/s11043-007-9032-7

Guo, Y., and Bradshaw, R. D. (2009). Long-term creep of polyphenylene sulfide (pps) subjected to complex thermal histories: The effects of nonisothermal physical aging. *Polymer*, *50*(16), 4048–4055. doi: 10.1016/j.polymer.2009.06.046

Guo, Y., Wang, N., Bradshaw, R. D., and Brinson, L. C. (2009). Modeling mechanical aging shift factors in glassy polymers during nonisothermal physical aging. i. experiments and kahr-ate model prediction. *Journal of Polymer Science Part B: Polymer Physics*, *47*(3), 340–352. doi: 10.1002/polb.21643

Haario, H., von Hertzen, R., Karttunen, A. T., and Jorkama, M. (2014). Identification of the viscoelastic parameters of a polymer model by the aid of a mcmc method. *Mechanics Research Communications*, *61*, 1–6. doi: 10.1016/j.mechrescom.2014.07.002

Halvorson, H. R. (1992). [3] padé-laplace algorithm for sums of exponentials: Selecting appropriate exponential model and initial estimates for exponential fitting. In *Methods in enzymology* (Vol. 210, pp. 54–67). Elsevier. doi: 10.1016/0076-6879(92)10005-X

Hansen, S. (2008). Estimation of the relaxation spectrum from dynamic experiments using bayesian analysis and a new regularization constraint. *Rheologica Acta*, *47*(2), 169–178. doi: 10.1007/s00397-007-0225-4

Hastings, W. K. (1970). Monte carlo sampling methods using markov chains and their applications. *Biometrika*, *57*(1), 97–109. doi: 10.1093/biomet/57.1.97

He, T., Liu, L., and Makeev, A. (2018). Uncertainty analysis in composite material properties characterization using digital image correlation and finite element model updating. *Composite Structures*, *184*, 337–351. doi: 10.1016/j.compstruct.2017.10.009

Hernández, W., Castello, D., Roitman, N., and Magluta, C. (2017). Thermorheologically simple materials: A bayesian framework for model calibration and validation. *Journal of Sound and Vibration*, *402*, 14–30. doi: 10.1016/j.jsv.2017.05.005

Holmström, K., and Petersson, J. (2002). A review of the parameter estimation problem of fitting positive exponential sums to empirical data. *Applied Mathematics and Computation*, *126*(1), 31–61. doi: 10.1016/S0096-3003(00)00138-7

Hutchinson, J. M. (1995). Physical aging of polymers. *Progress in Polymer Science*, *20*(4), 703–760. doi: 10.1016/0079-6700(94)00001-I

Istratov, A. A., and Vyvenko, O. F. (1999). Exponential analysis in physical phenomena. *Review of Scientific Instruments*, *70*(2), 1233–1257. doi: 10.1063/1.1149581

Jalocha, D., Constantinescu, A., and Neviere, R. (2015). Revisiting the identification of generalized maxwell models from experimental results. *International Journal of Solids and Structures*, *67*, 169–181. doi: 10.1016/j.ijsolstr.2015.04.018

Jensen, E. A. (2002). Determination of discrete relaxation spectra using simulated annealing. *Journal of non-newtonian fluid mechanics*, *107*(1-3), 1–11. doi: 10.1016/S0377-0257(02)00110-6

Kaipio, J., and Somersalo, E. (2006). *Statistical and computational inverse problems* (Vol. 160). Springer Science & Business Media. doi: 10.1007/b138659

Kaschta, J., and Schwarzl, F. (1994a). Calculation of discrete retardation spectra from creep data-ii. analysis of measured creep curves. *Rheologica acta*, *33*(6), 530–541. doi: 10.1007/BF00366337

Kaschta, J., and Schwarzl, R. R. (1994b). Calculation of discrete retardation spectra from creep data-i. method. *Rheologica Acta*, *33*(6), 517–529. doi: 10.1007/BF00366336

Knauss, W. G., and Emri, I. (1981). Non-linear viscoelasticity based on free volume consideration. In *Computational methods in nonlinear structural and solid mechanics* (pp. 123–128). Elsevier. doi: 10.1016/0045-7949(81)90116-4

Knauss, W. G., Emri, I., and Lu, H. (2008). Handbook of experimental solid mechanics. In (pp. 49–95). Boston, MA: Springer New York. doi: 10.1007/978-0-387-30877-7_3

Kovacs, A. J., Aklonis, J. J., Hutchinson, J. M., and Ramos, A. R. (1979). Isobaric volume and enthalpy recovery of glasses. ii. a transparent multiparameter theory. *Journal of Polymer Science: Polymer Physics Edition*, *17*(7), 1097–1162. doi: 10.1002/pol.1979.180170701

Kovacs, A. J., Stratton, R. A., and Ferry, J. D. (1963). Dynamic mechanical properties of polyvinyl acetate in shear in the glass transition temperature range. *The Journal of Physical Chemistry*, *67*(1), 152–161. doi: 10.1021/j100795a037

Krein, M., and Nudelman, A. (1998). An interpolation problem in the class of stieltjes functions and its connection with other problems. *Integral Equations and Operator Theory*, *30*(3), 251–278. doi: 10.1007/BF01195584

Lanczos, C. (1988). *Applied analysis*. Courier Corporation. doi: 10.1063/1.3060402

Levenberg, K. (1944). A method for the solution of certain non-linear problems in least squares. *Quarterly of applied mathematics*, *2*(2), 164–168. doi: 10.1090/qam/10666

Lévesque, M., Derrien, K., Baptiste, D., and Gilchrist, M. D. (2008). On the development and parameter identification of schapery-type constitutive theories. *Mechanics of Time-Dependent Materials*, *12*(2), 95–127. doi: 10.1007/s11043-008-9052-y

Lévesque, M., Gilchrist, M. D., Bouleau, N., Derrien, K., and Baptiste, D. (2007). Numerical inversion of the laplace–carson transform applied to homogenization of randomly reinforced linear viscoelastic media. *Computational mechanics*, *40*(4), 771–789. doi: 10.1007/s00466-006-0138-6

Likhtman, A. E., and McLeish, T. C. (2002). Quantitative theory for linear dynamics of linear entangled polymers. *Macromolecules*, *35*(16), 6332–6343. doi: 10.1021/ma0200219

Lion, A. (1997). On the thermodynamics of fractional damping elements. *Continuum Mechanics and Thermodynamics*, *9*(2), 83–96. doi: 10.1007/s001610050057

Liu, Y. (2001, oct). Approximation by Dirichlet Series with Nonnegative Coefficients. *Journal of Approximation Theory*, *112*(2), 226–234. doi: 10.1006/JATH.2001.3589

Lomellini, P. (1992). Viscosity-temperature relationships of a polycarbonate melt: Williams-landel-ferry versus arrhenius behaviour. *Die Makromolekulare Chemie*, *193*(1), 69–79.

Lu, H., Zhang, X., and Knauss, W. (1997). Uniaxial, shear, and poisson relaxation and their conversion to bulk relaxation: studies on poly (methyl methacrylate). *Polymer composites*, *18*(2), 211–222. doi: 10.1002/pc.10275

Luk-Cyr, J., Crochon, T., Li, C., and Lévesque, M. (2013). Interconversion of linearly viscoelastic material functions expressed as prony series: a closure. *Mechanics of Time-Dependent Materials*, *17*(1), 53–82. doi: 10.1007/s11043-012-9176-y

Marquardt, D. W. (1963). An algorithm for least-squares estimation of nonlinear parameters. *Journal of the society for Industrial and Applied Mathematics*, *11*(2), 431–441. doi: 10.1137/0111030

McKenna, G. B. (2003). Mechanical rejuvenation in polymer glasses: fact or fallacy? *Journal of Physics: Condensed Matter*, *15*(11), S737. doi: 10.1088/0953-8984/15/11/301

McKenna, G. B., Leterrier, Y., and Schultheisz, C. R. (1995). The evolution of material properties during physical aging. *Polymer Engineering & Science*, *35*(5), 403–410. doi: 10.1002/pen.760350505

Metropolis, N., Rosenbluth, A. W., Rosenbluth, M. N., Teller, A. H., and Teller, E. (1953). Equation of state calculations by fast computing machines. *The journal of chemical physics*, *21*(6), 1087–1092. doi: 10.1063/1.1699114

Meyer, H., Mangin, P.-M., and Ferry, J. D. (1965). Dynamic mechanical properties of poly (n-butyl methacrylate) near its glass transition temperature.(j. polymer sci., a3, 1785–1792, 1965). *Journal of Polymer Science Part A: General Papers*, *3*(11), 4000–4000. doi: 10.1002/pol.1965.100031135

Murphy, K. P. (2012). *Machine learning: A probabilistic perspective*. The MIT Press.

O'connell, P., and McKenna, G. (1997). Large deformation response of polycarbonate: Time-temperature, time-aging time, and time-strain superposition. *Polymer Engineering & Science*, *37*(9), 1485–1495. doi: 10.1002/pen.11797

O'Connell, P., and McKenna, G. (2002). The non-linear viscoelastic response of polycarbonate in torsion: An investigation of time-temperature and time-strain superposition. *Mechanics of Time-Dependent Materials*, *6*(3), 207–229.

Painter, P. C., and Coleman, M. M. (1994). *Fundamentals of polymer science: an introductory text*. Technomic. doi: 10.1201/9780203755211

Qaiser, A. A., and Price, J. (2011). Estimation of long-term creep behavior of polycarbonate by stress-time superposition and effects of physical aging. *Mechanics of Time-Dependent Materials*, *15*(1), 41–50. doi: 10.1007/s11043-010-9124-7

Qvale, D., and Ravi-Chandar, K. (2004). Viscoelastic characterization of polymers under multiaxial compression. *Mechanics of time-dependent materials*, *8*(3), 193–214. doi: 10.1023/B:MTDM.0000046749.79406.f5

Rataj, M., Malesa, M., Kujawińska, M., Wawer, P., Seweryn, K., Malowany, K., *et al.* (2015). 3d dic tests of mirrors for the single-mirror small-size telescope of cta. *Experimental Astronomy*, *39*(3), 513–525. doi: 10.1007/s10686-015-9455-0

Reu, P. L., Miller, T. J., Sutton, M., and Wang, Y. (2009). *Uncertainty quantification for digital image correlation.* (Tech. Rep.). doi: 10.1007/978-1-4614-4235-6_43

Roberts, G. O., and Rosenthal, J. S. (2009). Examples of adaptive mcmc. *Journal of Computational and Graphical Statistics*, *18*(2), 349–367. doi: 10.1198/jcgs.2009.06134

Ruhe, A. (1980). Fitting empirical data by positive sums of exponentials. *SIAM Journal on Scientific and Statistical Computing*, *1*(4), 481–498. doi: 10.1137/0901035

Sanahuja, J., and Toulemonde, C. (2011). Numerical homogenization of concrete microstructures without explicit meshes. *Cement and Concrete Research*, *41*(12), 1320–1329. doi: 10.1016/j.cemconres.2011.03.023

Sane, S., and Knauss, W. G. (2001). The time-dependent bulk response of poly (methyl methacrylate). *Mechanics of Time-Dependent Materials*, *5*(4), 293–324. doi: 10.1023/A:1012517421899

Schapery, R. A. (1962). *A simple collocation method for fitting viscoelastic models to experimental data* (Tech. Rep.).

Schapery, R. A. (1964). Application of thermodynamics to thermomechanical, fracture, and birefringent phenomena in viscoelastic media. *Journal of Applied Physics*, *35*(5), 1451–1465. doi: 10.1063/1.1713649

Schapery, R. A. (1970). On a thermodynamic constitutive theory and its application to various nonlinear materials. In *Thermoinelasticity* (pp. 259–285). Springer. doi: 10.1007/978-3-7091-8244-4_16

Schapery, R. A. (1974). Viscoelastic behavior and analysis of composite materials. *Mechanics of composite materials*.

Schwarz, G. (1978). Estimating the dimension of a model. *The annals of statistics*, 461–464. doi: 10.1214/aos/1176344136

Sorvari, J., and Hämäläinen, J. (2010). Time integration in linear viscoelasticity-a comparative study. *Mechanics of Time-Dependent Materials*, *14*(3), 307–328. doi: 10.1007/s11043-010-9108-7

Struik, L. C. E. (1977). *Physical aging in amorphous polymers and other materials*. Citeseer.

Struik, L. C. E. (1988). Dependence of relaxation times of glassy polymers on their specific volume. *Polymer*, *29*(8), 1347–1353. doi: 10.1016/0032-3861(88)90296-0

Sullivan, J., Blais, E., and Houston, D. (1993). Physical aging in the creep behavior of thermosetting and thermoplastic composites. *Composites Science and Technology*, *47*(4), 389–403. doi: 10.1016/0266-3538(93)90008-5

Tabiai, I., Tkachev, G., Diehl, P., Frey, S., Ertl, T., Therriault, D., and Lévesque, M. (2019). Hybrid image processing approach for autonomous crack area detection and tracking using local digital image correlation results applied to single-fiber interfacial debonding. *Engineering Fracture Mechanics*, *216*, 106485. doi: 10.1016/j.engfracmech.2019.106485

Taylor, R. L., Pister, K. S., and Goudreau, G. L. (1970). Thermomechanical analysis of viscoelastic solids. *International Journal for Numerical Methods in Engineering*, *2*(1), 45–59. doi: 10.1002/nme.1620020106

Tierney, L. (1994). Markov chains for exploring posterior distributions. *the Annals of Statistics*, 1701–1728. doi: 10.1214/aos/1176325750

Tscharnuter, D., Jerabek, M., Major, Z., and Lang, R. W. (2011a). On the determination of the relaxation modulus of pp compounds from arbitrary strain histories. *Mechanics of Time-Dependent Materials*, *15*(1), 1–14. doi: 10.1007/s11043-010-9119-4

Tscharnuter, D., Jerabek, M., Major, Z., and Lang, R. W. (2011b). Time-dependent poisson's ratio of polypropylene compounds for various strain histories. *Mechanics of time-dependent materials*, *15*(1), 15–28. doi: 10.1007/s11043-010-9121-x

Tschoegl, N. W., Knauss, W. G., and Emri, I. (2002). Poisson's ratio in linear viscoelasticity–a critical review. *Mechanics of Time-Dependent Materials*, *6*(1), 3–51. doi: 10.1023/A:1014411503170

Valeri, G., Koohbor, B., Kidane, A., and Sutton, M. A. (2017). Determining the tensile response of materials at high temperature using dic and the virtual fields method. *Optics and Lasers in Engineering*, *91*, 53–61. doi: 10.1016/j.optlaseng.2016.11.004

Van Krevelen, D. W., and Te Nijenhuis, K. (2009). *Properties of polymers: their correlation with chemical structure; their numerical estimation and prediction from additive group contributions*. Elsevier.

Varah, J. M. (1985). On fitting exponentials by nonlinear least squares. *SIAM journal on scientific and statistical computing*, *6*(1), 30–44. doi: 10.1137/0906003

Varin, C., Reid, N., and Firth, D. (2011). An overview of composite likelihood methods. *Statistica Sinica*, 5–42.

White, J. R. (2006). Polymer ageing: physics, chemistry or engineering? time to reflect. *Comptes Rendus Chimie*, *9*(11-12), 1396–1408. doi: 10.1016/j.crci.2006.07.008

Williams, M. L., Landel, R. F., and Ferry, J. D. (1955). The temperature dependence of relaxation mechanisms in amorphous polymers and other glass-forming liquids. *Journal of the American Chemical society*, *77*(14), 3701–3707. doi: 10.1021/ja01619a008

Womack, W. (2020a). *Temperature sensitivity compensation* (Tech. Rep.). Epsilon Technology Corp.

Womack, W. (2020b). *Understanding thermal drift* (Tech. Rep.). Epsilon Technology Corp.

Womack, W. (2020c). *Understanding warmup drift* (Tech. Rep.). Epsilon Technology Corp.

Yeramian, E., and Claverie, P. (1987). Analysis of multiexponential functions without a hypothesis as to the number of components. *Nature*, *326*(6109), 169. doi: 10.1038/326169a0

Yue, L. (2020). *Viscobayes.* `https://github.com/yuelingyu/ViscoBayes`. GitHub.

Yue, L., Heuzey, M.-C., Jalbert, J., and Lévesque, M. (2021). On the tri-dimensional constitutive theory identification of linearly viscoelastic solids based on bayesian framework. *International Journal of Solids and Structures*, *230*, 111157. doi: 10.1016/j.ijsolstr.2021.111157

Yue, L., Heuzey, M.-C., Jalbert, J., and Lévesque, M. (2022). On the thermo-mechanical testing of polymeric materials: A case of characterizing temperature and physical aging effects of polycarbonate. *Submitted to Experimental Mechanics*.